

AD-A115 404 CALIFORNIA INST OF TECH PASADENA

F/6 20/4

STUDY OF THE EFFECT OF FREE-STREAM TURBULENCE UPON DISTURBANCES--ETC(U)

NAS7-100

NL

UNCLASSIFIED

AFWAL-TR-82-3002

1. a. 1
b. 2
c. 3
d. 4
e. 5
f. 6
g. 7
h. 8
i. 9
j. 10
k. 11
l. 12
m. 13
n. 14
o. 15
p. 16
q. 17
r. 18
s. 19
t. 20
u. 21
v. 22
w. 23
x. 24
y. 25
z. 26
aa. 27
ab. 28
ac. 29
ad. 30
ae. 31
af. 32
ag. 33
ah. 34
ai. 35
aj. 36
ak. 37
al. 38
am. 39
an. 40
ao. 41
ap. 42
aq. 43
ar. 44
as. 45
at. 46
au. 47
av. 48
aw. 49
ax. 50
ay. 51
az. 52
ba. 53
bb. 54
bc. 55
bd. 56
be. 57
bf. 58
bg. 59
bh. 60
bi. 61
bj. 62
bk. 63
bl. 64
bm. 65
bn. 66
bo. 67
bp. 68
bq. 69
br. 70
bs. 71
bt. 72
bu. 73
bv. 74
bw. 75
bx. 76
by. 77
bz. 78
ca. 79
cb. 80
cc. 81
cd. 82
ce. 83
cf. 84
cg. 85
ch. 86
ci. 87
cj. 88
ck. 89
cl. 90
cm. 91
cn. 92
co. 93
cp. 94
cq. 95
cr. 96
cs. 97
ct. 98
cu. 99
cv. 100
cw. 101
cx. 102
cy. 103
cz. 104
da. 105
db. 106
dc. 107
dd. 108
de. 109
df. 110
dg. 111
dh. 112
di. 113
dj. 114
dk. 115
dl. 116
dm. 117
dn. 118
do. 119
dp. 120
dq. 121
dr. 122
ds. 123
dt. 124
du. 125
dv. 126
dw. 127
dx. 128
dy. 129
dz. 130
ea. 131
eb. 132
ec. 133
ed. 134
ee. 135
ef. 136
eg. 137
eh. 138
ei. 139
ej. 140
ek. 141
el. 142
em. 143
en. 144
eo. 145
ep. 146
eq. 147
er. 148
es. 149
et. 150
eu. 151
ev. 152
ew. 153
ex. 154
ey. 155
ez. 156
fa. 157
fb. 158
fc. 159
fd. 160
fe. 161
ff. 162
fg. 163
fh. 164
fi. 165
fj. 166
fk. 167
fl. 168
fm. 169
fn. 170
fo. 171
fp. 172
fq. 173
fr. 174
fs. 175
ft. 176
fu. 177
fv. 178
fw. 179
fx. 180
fy. 181
fz. 182
ga. 183
gb. 184
gc. 185
gd. 186
ge. 187
gf. 188
gg. 189
gh. 190
gi. 191
gj. 192
gk. 193
gl. 194
gm. 195
gn. 196
go. 197
gp. 198
gq. 199
gr. 200
gs. 201
gt. 202
gu. 203
gv. 204
gw. 205
gx. 206
gy. 207
gz. 208
ha. 209
hb. 210
hc. 211
hd. 212
he. 213
hf. 214
hg. 215
hh. 216
hi. 217
hj. 218
hk. 219
hl. 220
hm. 221
hn. 222
ho. 223
hp. 224
hq. 225
hr. 226
hs. 227
ht. 228
hu. 229
hv. 230
hw. 231
hx. 232
hy. 233
hz. 234
ia. 235
ib. 236
ic. 237
id. 238
ie. 239
if. 240
ig. 241
ih. 242
ii. 243
ij. 244
ik. 245
il. 246
im. 247
in. 248
io. 249
ip. 250
iq. 251
ir. 252
is. 253
it. 254
iu. 255
iv. 256
iw. 257
ix. 258
iy. 259
iz. 260
ja. 261
jb. 262
jc. 263
jd. 264
je. 265
jf. 266
jg. 267
jh. 268
ji. 269
jj. 270
jk. 271
jl. 272
jm. 273
jn. 274
jo. 275
jp. 276
jq. 277
jr. 278
js. 279
jt. 280
ju. 281
jv. 282
jw. 283
jx. 284
jy. 285
jz. 286
ka. 287
kb. 288
kc. 289
kd. 290
ke. 291
kf. 292
kg. 293
kh. 294
ki. 295
kj. 296
kk. 297
kl. 298
km. 299
kn. 300
ko. 301
kp. 302
kq. 303
kr. 304
ks. 305
kt. 306
ku. 307
kv. 308
kw. 309
kx. 310
ky. 311
kz. 312
la. 313
lb. 314
lc. 315
ld. 316
le. 317
lf. 318
lg. 319
lh. 320
li. 321
lj. 322
lk. 323
ll. 324
lm. 325
ln. 326
lo. 327
lp. 328
lq. 329
lr. 330
ls. 331
lt. 332
lu. 333
lv. 334
lw. 335
lx. 336
ly. 337
lz. 338
ma. 339
mb. 340
mc. 341
md. 342
me. 343
mf. 344
mg. 345
mh. 346
mi. 347
mj. 348
mk. 349
ml. 350
mm. 351
mn. 352
mo. 353
mp. 354
mq. 355
mr. 356
ms. 357
mt. 358
mu. 359
mv. 360
mw. 361
mx. 362
my. 363
mz. 364
na. 365
nb. 366
nc. 367
nd. 368
ne. 369
nf. 370
ng. 371
nh. 372
ni. 373
nj. 374
nk. 375
nl. 376
nm. 377
nn. 378
no. 379
np. 380
nq. 381
nr. 382
ns. 383
nt. 384
nu. 385
nv. 386
nw. 387
nx. 388
ny. 389
nz. 390
oa. 391
ob. 392
oc. 393
od. 394
oe. 395
of. 396
og. 397
oh. 398
oi. 399
oj. 400
ok. 401
ol. 402
om. 403
on. 404
oo. 405
op. 406
oq. 407
or. 408
os. 409
ot. 410
ou. 411
ov. 412
ow. 413
ox. 414
oy. 415
oz. 416
pa. 417
pb. 418
pc. 419
pd. 420
pe. 421
pf. 422
pg. 423
ph. 424
pi. 425
pj. 426
pk. 427
pl. 428
pm. 429
pn. 430
po. 431
pp. 432
pq. 433
pr. 434
ps. 435
pt. 436
pu. 437
pv. 438
pw. 439
px. 440
py. 441
pz. 442
qa. 443
qb. 444
qc. 445
qd. 446
qe. 447
qf. 448
qg. 449
qh. 450
qi. 451
qj. 452
qk. 453
ql. 454
qm. 455
qn. 456
qo. 457
qp. 458
qq. 459
qr. 460
qs. 461
qt. 462
qu. 463
qv. 464
qw. 465
qx. 466
qy. 467
qz. 468
ra. 469
rb. 470
rc. 471
rd. 472
re. 473
rf. 474
rg. 475
rh. 476
ri. 477
rj. 478
rk. 479
rl. 480
rm. 481
rn. 482
ro. 483
rp. 484
rq. 485
rr. 486
rs. 487
rt. 488
ru. 489
rv. 490
rw. 491
rx. 492
ry. 493
rz. 494
sa. 495
sb. 496
sc. 497
sd. 498
se. 499
sf. 500
sg. 501
sh. 502
si. 503
sj. 504
sk. 505
sl. 506
sm. 507
sn. 508
so. 509
sp. 510
sq. 511
sr. 512
ss. 513
st. 514
su. 515
sv. 516
sw. 517
sx. 518
sy. 519
sz. 520
ta. 521
tb. 522

END
DATE
FILMED
7-82
DTIC

AFWAL-TR-82-3002

2

TITLE STUDY OF THE EFFECT OF FREE-STREAM TURBULENCE UPON DISTURBANCES IN THE
PRE-TRANSITIONAL LAMINAR BOUNDARY LAYER (Part I); LAMINAR BOUNDARY
LAYER DISTORTION BY SURFACE ROUGHNESS; EFFECT UPON STABILITY (Part II)

CONTRACTOR'S NAME Jet Propulsion Laboratory
CONTRACTOR'S ADDRESS California Institute of Technology
4800 Oak Grove Drive
Pasadena, California 91109

APRIL 1982

REPORT FOR PERIOD December 1978 - September 1981



APPROVED FOR PUBLIC RELEASE: DISTRIBUTION UNLIMITED

FLIGHT DYNAMICS LABORATORY
AIR FORCE WRIGHT AERONAUTICAL LABORATORIES
AIR FORCE SYSTEMS COMMAND
WRIGHT-PATTERSON AIR FORCE BASE, OHIO 45433

DTIC
ELECTE
JUN 9 1982
S D
E

82 06 09 086

AD A 115404

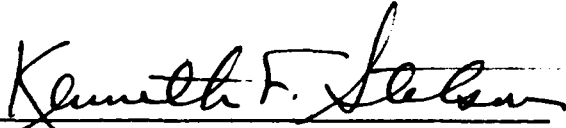
DTIC FILE COPY

NOTICE

When Government drawings, specifications, or other data are used for any purpose other than in connection with a definitely related Government procurement operation, the United States Government thereby incurs no responsibility nor any obligation whatsoever; and the fact that the government may have formulated, furnished, or in any way supplied the said drawings, specifications, or other data, is not to be regarded by implication or otherwise as in any manner licensing the holder or any other person or corporation, or conveying any rights or permission to manufacture use, or sell any patented invention that may in any way be related thereto.

This report has been reviewed by the Office of Public Affairs (ASD/PA) and is releasable to the National Technical Information Service (NTIS). At NTIS, it will be available to the general public, including foreign nations.

This technical report has been reviewed and is approved for publication.

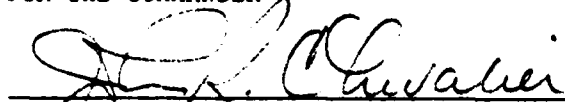


KENNETH F. STETSON
AEROSPACE ENGINEER



J.C. BOISON, CHIEF, HIGH SPEED
AERO PERFORMANCE BRANCH

FOR THE COMMANDER



JOHN R. CHEVALIER, COL, USAF
CHIEF, AEROMECHANICS DIVISION

"If your address has changed, if you wish to be removed from our mailing list, or if the addressee is no longer employed by your organization please notify AFWAL/FIMG, W-PAFB, OH 45433 to help us maintain a current mailing list".

Copies of this report should not be returned unless return is required by security considerations, contractual obligations, or notice on a specific document.

Unclassified

SECURITY CLASSIFICATION OF THIS PAGE (When Data Entered)

REPORT DOCUMENTATION PAGE		READ INSTRUCTIONS BEFORE COMPLETING FORM
1. REPORT NUMBER AFWAL-TR-82-3002	2. GOVT ACCESSION NO. AD A115 404	3. RECIPIENT'S CATALOG NUMBER
4. TITLE (and Subtitle) STUDY OF THE EFFECT OF FREE-STREAM TURBULENCE UPON DISTURBANCES IN THE PRE-TRANSITIONAL LAMINAR BOUNDARY LAYER (Part I); LAMINAR BOUNDARY LAYER DISTORTION BY SURFACE ROUGHNESS; EFFECT UPON STABILITY (Part II)		5. TYPE OF REPORT & PERIOD COVERED FINAL REPORT Dec 1978 - Sept 1981
		6. PERFORMING ORG. REPORT NUMBER
7. AUTHOR(s) James M. Kendall		8. CONTRACT OR GRANT NUMBER(s) NASA Contract NAS7-100
9. PERFORMING ORGANIZATION NAME AND ADDRESS Jet Propulsion Laboratory California Institute of Technology 4800 Oak Grove Drive, Pasadena, CA 91109		10. PROGRAM ELEMENT, PROJECT, TASK AREA & WORK UNIT NUMBERS Project 2307 Task 2307N4 Work Unit 2307N434
11. CONTROLLING OFFICE NAME AND ADDRESS Flight Dynamics Laboratory Air Force Wright Aeronautical Laboratories Wright-Patterson Air Force Base, Ohio 45433		12. REPORT DATE April 1982
14. MONITORING AGENCY NAME & ADDRESS (if different from Controlling Office)		13. NUMBER OF PAGES 71
		15. SECURITY CLASS. (of this report) Unclassified
15a. DECLASSIFICATION/DOWNGRADING SCHEDULE		
16. DISTRIBUTION STATEMENT (of this Report) Approved for public release; distribution unlimited		
17. DISTRIBUTION STATEMENT (of the abstract entered in Block 20, if different from Report)		
18. SUPPLEMENTARY NOTES		
19. KEY WORDS (Continue on reverse side if necessary and identify by block number) Boundary Layer Stability Boundary Layer Transition Free-Stream Turbulence Surface Roughness		
20. ABSTRACT (Continue on reverse side if necessary and identify by block number) Part I: Hot wire anemometry has been employed to determine certain characteristics of the turbulence in the free-stream of a low-speed, low-turbulence wind tunnel and to study the influence of such turbulence upon the fluctuations within a flat-plate boundary layer. A technique was employed which provided information concerning the propagation speed of the disturbances and this was used as a means of classification as to type or cause. It was found that Tollmien-Schlichting waves did not possess significant energy until a Reynolds number considerably		

DD FORM 1473

1 JAN 73

EDITION OF 1 NOV 65 IS OBSOLETE

Unclassified

SECURITY CLASSIFICATION OF THIS PAGE (When Data Entered)

Unclassified

SECURITY CLASSIFICATION OF THIS PAGE(When Data Entered)

higher than that of the theoretical neutral point was attained and that the subsequent growth exceeded the prediction of linear analysis.

Part II: Distributed roughness present upon an aerodynamic surface alters the laminar boundary layer mean velocity profile such as to increase the instability presented here of the profile distortion for the case of small roughness in a Blasius boundary layer. The roughnesses tested include a single protuberance at Reynolds numbers below 50, the interaction between two such elements, the interaction between one element and a multitude of others, and the distortion due to distributed roughness.

Unclassified

SECURITY CLASSIFICATION OF THIS PAGE(When Data Entered)

FOREWARD

This document presents the results of two experimental investigations relating to boundary layer transition to turbulence. The studies were carried out at the California Institute of Technology, Jet Propulsion Laboratory. This report is the final report for Work Unit 2307N434.

Accession For	
NTIS GRA&I	<input checked="checked" type="checkbox"/>
DTIC TAB	<input type="checkbox"/>
Unannounced	<input type="checkbox"/>
Justification	
By _____	
Distribution/ _____	
Availability Codes	
Dist	Avail and/or Special
A	



TABLE OF CONTENTS

SECTION		PAGE
	PART I: FREE-STREAM TURBULENCE	
I	INTRODUCTION	1
II	EQUIPMENT AND TECHNIQUES	2
III	RESULTS	
	1. Free Stream Fluctuations	6
	2. Broadband Fluctuation Development in the Layer	7
	3. Narrowband Fluctuation Development in the Layer	8
	4. Phase Measurements; Disturbance Propagation Speed	10
	5. T-S Wave Growth	12
	6. Conclusions	13
	REFERENCES	15
	PART II: SURFACE ROUGHNESS	
I	INTRODUCTION	49
II	EQUIPMENT AND TECHNIQUES	51
III	RESULTS	
	1. Types of Result; Format of Presentation	53
	2. Single-Element Results	53
	3. Multiple-Grit Interaction Measurements	55
	4. Distributed Roughness Measurements	56
	5. Stability of Distorted Profiles	58
	6. Conclusions	59
	REFERENCES	60

LIST OF ILLUSTRATIONS

FIGURE		PAGE
PART I: FREE-STREAM TURBULENCE		
1	Pressure Distribution in Tunnel	17
2	Test of Dual-Sensor Probe	18
3	Example of Eigenfunction, $R = 600$, $F \times 10^4 = 0.6$	19
4	Wave Speed C_{ph_x} Versus Obliqueness Angle	20
5	Broadband Fluctuation Amplitude in Tunnel Stream	21
6	Narrowband Fluctuation Amplitude in Tunnel Stream	22
7	Free-Stream Fluctuation Spectra	23
8	Free-Stream Narrowband Fluctuation Amplitude for Constant Dimensionless Frequency Versus Tunnel Velocity	24
9a	Broadband Fluctuation Amplitude in Layer for $R = 460$	25
9b	Broadband Fluctuation Amplitude in Layer for $R = 532$	26
9c	Broadband Fluctuation Amplitude in Layer for $R = 594$	27
9d	Broadband Fluctuation Amplitude in Layer for $R = 651$	28
10	Peak Broadband Fluctuation Amplitude Versus x	29
11	Fluctuation Spectra in Layer at Location of Peak Fluctuation with Grid Present and Absent	30
12	Normalized Fluctuation Spectra in Free-Stream and in Layer	31
13a	Narrowband Fluctuation Amplitude in Layer for Two Dimensionless Frequencies	32
13b	Narrowband Fluctuation Amplitude in Layer for Three Dimensionless Frequencies	33
14a	Narrowband Fluctuation Amplitude in Layer for $R = 460$	34
14b	Narrowband Fluctuation Amplitude in Layer for $R = 532$	35
14c	Narrowband Fluctuation Amplitude in Layer for $R = 594$	36
14d	Narrowband Fluctuation Amplitude in Layer for $R = 651$	37

LIST OF ILLUSTRATIONS (CONTINUED)

FIGURE		PAGE
15a	Narrowband Fluctuation Amplitude in Layer for $R = 592$	38
15b	Narrowband Fluctuation Amplitude in Layer for $R = 632$	39
15c	Narrowband Fluctuation Amplitude in Layer for $R = 670$	40
15d	Narrowband Fluctuation Amplitude in Layer for $R = 707$	41
15e	Narrowband Fluctuation Amplitude in Layer for $R = 742$	42
15f	Narrowband Fluctuation Amplitude in Layer for $R = 775$	43
16	Narrowband Fluctuation Amplitude in Layer with Grid Present and Absent	44
17	Measured Phase Difference at Several Stations Through the Layer	45
18	Measured Phase Difference at Vertical Location Near T-S Peak for Several x-Stations	46
19a	Theoretical and Measured Narrowband Fluctuation Amplitude Versus R for $F \times 10^4 = 0.8$	47
19b	Theoretical and Measured Narrowband Fluctuation Amplitude Versus R for $F \times 10^4 = 1.0$	48

PART II: SURFACE ROUGHNESS

1	Vertical Profiles of Velocity Defect at Lateral Centerline Behind a Single Roughness Element	62
2	Lateral Variation of Velocity Defect at Four Stations Behind a Single Roughness Element. Measurements Made at Height of Peak Defect. Baselines Are Zero Defect	63
3	Streamwise Variation of Peak Velocity Defect in Near-Wake Behind a Single Roughness Element. Measurements made at Lateral Centerline. Blasius Velocity at $y = k$ is Indicated by Arrow	64
4	Streamwise Variation of Peak Velocity Defect Magnitude in Far-Wake Behind a Single Roughness Element. Negative Defect Occurred on Lateral Centerline; Positive Defects Appeared on Each Side of Centerline for $x/k > 50$	65

LIST OF ILLUSTRATIONS (CONCLUDED)

FIGURE		PAGE
5	Iso-Defect Contours at a Station 80 Roughness-Heights Behind a Single Element. Positions of Measurement Denoted by Small + Symbols. Element Shown to Scale in Gray	66
6	Lateral Variation of Velocity Defect Due to a Single Roughness Element Amid a Field of Other Elements (Circles), and Same Results in Absence of Field (Squares)	67
7	Velocity Defect Induced by Flow Over a Forward-Facing Step of Small Height Located at $x = x_s$	68
8	Velocity Profiles Above Distributed Roughness (Triangles) and Above Smooth Surface (Circles) at Same Station. Blasius Profile is Shown	69
9	Velocity Defect Due to Distributed Roughness Corresponding to Data of Fig. 8. Curve has been Fitted to Data in Region $\eta > 1.5$	70
10	Velocity Defect Downstream of Distributed Roughness (#80 Abrasive) and an Analytic Representation Intended for Use in Stability Analysis	71

NOMENCLATURE

A	Disturbance amplitude at a particular frequency
C_{ph_x}	x-component of phase speed
D	Steady component of perturbation velocity due to presence of roughness
F	Dimensionless frequency, $2\pi f\gamma/U_o^2$
f	Dimensional circular frequency
k	Characteristic roughness height
p	Static pressure
q	Dynamic pressure, $\rho U_o^2/2$
R	Square root of x-Reynolds number
Re_k	Reynolds number based upon velocity $U(k)$ at height $y = k$
u'	Fluctuation amplitude
$u(\eta)$	Local velocity in layer
U_o	Free-stream velocity
$U(k)$	Velocity at top of roughness element
x	Distance from plate leading edge
Δx	Distance behind roughness element
x_k	x-location of roughness element
y	Distance normal to plate surface
η	Blasius coordinate, yR/x
λ_x	x-component of disturbance wavelength
ν	Kinematic viscosity
ρ	Density
ϕ_m	Measured phase-difference of dual-sensor probe

PART I: STUDY OF THE EFFECT OF FREE-STREAM TURBULENCE UPON
DISTURBANCES IN THE PRE-TRANSITIONAL LAMINAR BOUNDARY LAYER

SECTION I

INTRODUCTION

It is widely accepted that Tollmien-Schlichting (T-S) amplification plays a principal role in the physical process of boundary layer transition to turbulence. Accordingly, much work has gone into the development of the linear theory in order to describe the effects upon wave growth of pressure gradient, heat transfer, cross-flow, non-parallel flow, etc., and computer programs which incorporate these developments are in current use. However, instability amplification is but one aspect of the transition problem, an equally important part being that referred to as the receptivity problem. There, it is sought to understand the origin of those flow fluctuations which subsequently become amplified within the layer, thereby attaining the level of nonlinearity and breakdown to turbulence.

The receptivity of a boundary layer to fluctuation sources arising from sound, vibration, free-stream turbulence, and other sources needs much clarification. The stated objective of the present work was to measure the influence of free-stream turbulence upon a Blasius boundary layer, with particular emphasis upon determining the location within the layer T-S waves are first detectable for the case of a weakly turbulent stream. This information is expected to amount to a first step in describing the mechanism by which these waves become excited. A central problem in this investigation was to be able to distinguish T-S waves from those other motions of the layer, such as the ones due to a passive response of the layer to the external vorticity and pressure fields, which contribute to amplification only in an indirect manner.

This problem was approached by recognizing that each of the various motions believed to be important has a characteristic speed of propagation which differs substantially from that of the others. Therefore, separation of the various types of fluctuations has been carried out on the basis of phase speed, and reasonable success obtained. It is this aspect of the present work which, as much as any other, distinguishes it from previous experiments.

No attempt will be made here to describe the available literature. Experimental results are contained in Refs. 1 - 15, and theoretical ones in 16 - 20. Of particular note, compilations of the data on the measured location of transition in response to a variation of the turbulence level are given in Refs. 10, 11, and 13. Experiments which are especially relevant to the present investigation are those of Klebanoff, as yet unpublished, of Arnal and Juillen²¹, and of Reshotko and Leventhal²². Klebanoff's work concerned an attempt to distinguish T-S waves from other motions as in the present study, but a different approach was taken. Also, he carried out measurements on the turbulence length-scale as a further means of identification of fluctuation type and source. The experiment by Arnal and Juillen contains spectral results on free-stream and boundary layer fluctuations in the presence of two different turbulence-producing grids, and without a grid. The experiment by Reshotko and Leventhal contains information on low frequency fluctuations and the growth within the layer of these.

SECTION II

EQUIPMENT AND TECHNIQUES

The experiment was conducted in a low-turbulence wind tunnel 2.0 m long by 0.35 m wide by 0.60 m high over the velocity range 8.5 to 18.0 m/sec. The test plate, 1.5 m-long by 0.60 m-wide, was configured with a semi-elliptical leading edge and was constructed of acrylic plastic in order to provide an optical-quality surface finish. All measurements were carried out between the stations $x = 0.3$ m and 0.6 m, measured from the leading edge. The plate was mounted vertically between the floor and ceiling of the tunnel, and midway between the sidewalls. The latter were adjusted in divergence to provide a static pressure which was everywhere equal to that of the room. Fig. 1 presents pressure measurements obtained upon the sidewall opposite the working surface of the plate and upon the ceiling of the tunnel, no taps having been provided on the plate itself. The datum of the figure which is singularly low was influenced by the proximity of a blade-like strut upon which a probe was supported. The strut, in turn, was carried by a three-axis traverse mechanism, installed beneath the test section, which provided 0.0025-cm resolution and commensurate rigidity. A cover-plate placed about the strut prevented airflow into or out of the test section.

A turbulence-producing grid was substituted for the last turbulence-damping screen in many of the tests. The grid consisted of a planar array of 0.635-cm diam. rods aligned vertically and spaced laterally on 5.0-cm centers across the 1.8-m x 1.8-m cross-section of the upstream end of the contraction section. The latter provided a 15.4 : 1 reduction in area along a 2.2-m length. The grid was removed or replaced as appropriate during each test in which its effect upon the flow was to be examined, an action requiring only a few seconds and which assured maximum equality in all other test conditions.

Most aspects of the experiment were carried out under computer control, including the steering of the traverse, the sequencing of the data acquisition, the acquisition itself, the data reduction and display, and the data storage. A dedicated minicomputer, an Interdata Mod. 70, incorporated dual 10-bit analog-to-digital (ADC) converters through which all data, except those of static pressure, were obtained. Two main programs handled most of the data analysis. The first accomplished signal analysis to obtain the mean and variance of time-series data, and, as described below, provided mean velocity and rms fluctuation level results. The other, based upon an FFT routine, performed spectral analysis, and provided phase-difference and coherence information from dual time-series data streams.

All flow measurements except those of static pressure were made by means of hot-wire anemometry. The probe employed throughout the experiment incorporated two sensors, each 0.06-cm long. The two wires were separated in the streamwise dimension for the purpose of phase measurement, to be described later. Measurements other than those of phase were made by use of the forward element only. The wires were heated by constant-temperature anemometry circuits for those measurements in which the signal was large in comparison with the electronic noise, and by constant-current circuitry where the minimum-

attainable noise level was necessary, as was the case for free-stream measurements in the absence of the grid.

The signals were amplified and filtered in accordance with need. Where the mean velocity and the fluctuation level were to be measured simultaneously, as within the layer, the signal of the forward sensor was applied to a dc-amplifier whose unfiltered output was connected to an ADC, and was also applied to an ac-amplifier and filter whose output was connected to a second ADC. The gains of the two amplifiers were set individually to match the voltage range of the ADC's. The filter high cut-off frequency was set such as to minimize aliasing, and the low cut-off frequency was set to 0.3 Hz. For measurement of the phase relation between the two sensors, each signal was ac-amplified and filtered as described, except that in most cases the low cut-off frequency was set to 13 Hz in order to eliminate the large, low-frequency, components and to maximize thereby the dynamic range of the measurement.

The wires were calibrated upon emplacement well outside the boundary layer by varying the tunnel speed in stepwise fashion from zero to a suitable maximum. The dc-amplified signal was digitized for 12 - 15 values of speed, and the resulting values were represented as a polynomial function of velocity by means of a least-squares routine. During subsequent measurement of the mean and fluctuating velocities, the dc-signal yielded the mean velocity at any flow condition through the stored analytic relation, and the variance of the ac-signal, together with the relative electronic amplification and the derivative of the voltage-velocity relation at the prevailing velocity, yielded the rms fluctuation level.

In addition to frequency analysis by the FFT method, it was convenient in many cases to employ an analog narrow-band filter to follow the development of fluctuations of a specific frequency. A General Radio Mod. 1564A Sound and Vibration Analyzer, which may be described as a tuned amplifier for which the band-pass is proportional to the center frequency, served this function. The band-width was set to one-third octave, and the electronic gain at the center frequency was incorporated in the data-reduction program.

The aforementioned dual-sensor probe was used in measuring the x-component of the propagation or convection speed of flow fluctuations as a means for classifying the latter as to type or cause. The two wires of the probe were separated in the stream direction by a distance 1.02 cm, were offset in the lateral direction by 0.1 cm, and were aligned in the direction normal to the plate to be equidistant from the surface. The lateral offset, determined by test, prevented the wake of the forward element from influencing the aft one.

The dual time-series, obtained by digitization of the amplified and filtered signals at a 1.0-kHz rate, were transformed simultaneously in complex form using block lengths set to values between 128 and 1024 for various tests. From the transforms were computed the real autopower of each signal and the complex crosspower of the two, and these were summed in turn to form the averages. At the conclusion, the averages of the autopower of each signal, the coherence, and the phase difference of the two signals were determined. These quantities are defined as follows:

$$G_{11} = S_1 S_1^* \quad \text{Autopower 1.}$$

$$G_{22} = S_2 S_2^* \quad \text{Autopower 2.}$$

$$G_{12} = S_1 S_2^* \quad \text{Crosspower.}$$

$$\gamma^2 = \frac{G_{12} G_{12}^*}{G_{11} G_{22}} \quad \text{Coherence.}$$

$$\varphi_m = \tan^{-1} \frac{\text{Im}(S_1)}{\text{Re}(S_1)} - \tan^{-1} \frac{\text{Im}(S_2)}{\text{Re}(S_2)} \quad \text{Phase Diff.,}$$

where S_1 and S_2 are the averages of the transforms of the two series, and the $*$ symbol denotes the complex conjugate.

One aspect of the ensemble averaging which bears explanation concerns the general process by which the phase angle is determined. As each transform is computed in turn, the complex crosspower for each frequency is added vectorially to the cumulative sum. For signals of high coherence, the phase vectors computed sequentially lay in nearly equal directions, and thus were additive. For the case of low coherence, as at high frequencies where electronic noise was not always small or where the persistence of a fluctuation was short in comparison with the transit time from one sensor to the other, the vectors lay in random directions and tended to cancel. Although the coherence is a direct measure of this randomness, the smoothness with frequency of the results also serves this purpose well. Accordingly, coherence results will not be presented, and information derived from phase results will be limited to frequencies below 300 Hz, approximately.

The relation between the measured phase angle and the phase speed of waves moving past the probe is most readily apparent for the case in which there exists a unique relation between the wave number and the wave speed, as for T-S waves. For a given family of waves, the x-component of the wavelength λ_x is given by

$$\lambda_x = \frac{2\pi L_x}{\varphi_m(f)},$$

where L_x is the axial spacing of the sensors (the lateral offset being neglected), f is the frequency of wave passage, and where the average of the measured phase difference $\varphi_m(f)$ has no ambiguity, i.e., there exists not more than one wavelength within the sensor spacing L_x . The x-component of phase speed is then

$$C_{ph_x}(\lambda_x) = \frac{2\pi f L_x}{\varphi_m(f) U_0}$$

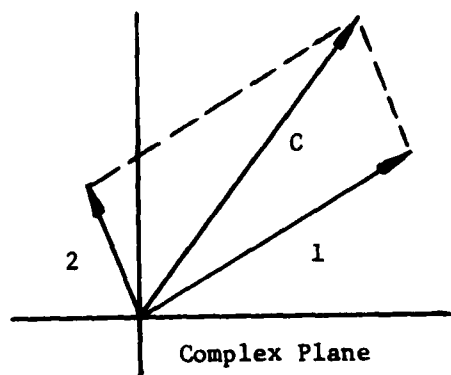
That is, the propagation speed of waves of a given class may be determined from

the phase measurement. The case in which multiple types of waves are present is considered subsequently.

Two-dimensional T-S waves were employed to test the accuracy of the technique. Such waves were introduced into the boundary layer by affixing an earphone to the reverse side of the plate at a station $x = 0.3$ m. Four 1.0-mm orifices spaced laterally on 2.0-mm centers transmitted the signal to the working side of the plate. The hot-wire probe was placed at 0.6 m and in lateral alignment with the orifice pattern for the interception of 2-D waves. The earphone was excited sinusoidally, and for each of several frequencies throughout the unstable band the amplitude, phase difference, and coherence were recorded at a number of positions through the thickness of the layer. The angles were converted to phase speed as above, and were set into ratio with the theoretical result obtained from Gaster's series method. These results are presented in Fig. 2. and indicate that the performance was good except near the location within the layer where the eigenfunction vanished, approximately $\eta = 3.6$ for the frequencies and Reynolds number tested here. A sample eigenfunction is shown for reference in Fig. 3. Further, it was possible to vary the amplitude of the most unstable waves over a 33 dB range without affecting the phase difference. The background fluctuations of the layer established the lower limit, and non-linearity of the waves set the upper limit. Waves at the lower limit were much weaker than those discernable by eye on an oscilloscope.

Because 3-D T-S waves are also important in general, computation was made of the dependence of C_{ph} upon the wave angle, ψ . Fig. 4 shows the results for several values of the dimensionless frequency, $F = 2\pi f\gamma/U_o^2$, for a typical Reynolds number. Because waves steeper than 60° are not expected to be important in the present experiment, it is apparent that wave obliquity does not produce a large error in the inferred wave speed.

Interpretation of the phase angle results in terms of a disturbance propagation speed is straightforward only when there exists a single family of disturbances. However, it remains possible to derive valuable information when two wave families are present, as when T-S waves and ones travelling at the stream speed, i.e., ones driven by free-stream turbulence, coexist within the layer. Consider a possible outcome of a phase measurement as shown in the



sketch for a single, arbitrary, frequency. The crosspower vector labelled C is that of the composite signal, as sensed by the probe for the case of linear fluctuations. On account of linearity, this vector may be decomposed into the components 1 and 2 which represent the contributions due to the two families. It is essential in performing the decomposition that the two phase angles be known a priori, and this was the case for the experiments to be described. Use is made of the decomposition in determining wave growth in Section III.

SECTION III

RESULTS

1. FREE-STREAM FLUCTUATIONS

It became apparent at the outset of the experiment that the stream contained a great deal of fluctuation energy at frequencies far below those of importance to T-S amplification, and that the measurement of such energy posed two problems. First, the level measured by means of the hot-wire depended strongly upon the low-frequency cut-off of the amplification system. For example, the level determined in the absence of the turbulence-producing grid using a commercial amplifier with a specification of 1.0 Hz amounted to less than two-thirds of that determined by use of the custom circuit employed for all results presented. An implication of this is that comparison of results from the literature on the basis of free-stream fluctuation level requires care unless the bandwidth of the measurement is known in each case. Second, a problem unique to the present tunnel is that heat from the motor entered the tunnel intake and raised the apparent free-stream fluctuation level by approximately 25 percent over a period of four hours. Correction of this problem was not attempted.

Based upon the discovery of the importance of the fan inlet conditions, the tunnel configuration was modified for the remainder of the experiment by installing 5.0-cm hexagonal-cell honeycomb within the 0.9-m diam. fan inlet, and by preceding this with the turbulence-damping screen which had been removed from the tunnel for installation of the grid. The free-stream rms signal amplitude in the grid-absent case then diminished approximately two-fold with respect to the prior level. It is believed that the screen and honeycomb reduced the level of turbulence ingested from the room, thereby rendering the fan lift more constant. The improvement pertained mostly to low frequencies, and the spectrum in the T-S frequency band was not altered greatly.

Figure 5 presents the axial distribution of the broadband rms fluctuation measured at a location 5.0 cm from the plate surface with the grid both present and absent, as obtained during alternate forward and aft traverses of the probe. The scatter is attributable to the averaging of a small number of ensembles. In related measurements it was found that the rms amplitude was approximately independent of the distance from the plate, except within and near the boundary layer, and also was approximately independent of wind speed. Therefore, the levels given within Fig. 5 typify the broadband fluctuation levels imposed upon the boundary layer throughout the experiment.

The axial variation of the fluctuation amplitude for the particular dimensionless frequency, $F = 2\pi f y / U_o^2 = 1.0 \times 10^{-4}$, lying near the upper limit of the range important to T-S amplification, is given in Fig. 6. The minor increase of level with x is not believed to be significant, and the result is taken to indicate that turbulence decay was insignificant within the frequency range of interest in the present experiment.

Figure 7 displays one-dimensional spectra measured 5.0 cm from the plate for the grid-present and -absent cases. The reference level of the ordinate is

arbitrary, but the two curves are shown with correct relative placement. The spectral features of the lower curve are apparently due to electronic noise within the low-level signal; the frequencies and magnitudes of the features did not depend upon wind speed. Two important results are evident. First, the extreme steepness with which the grid-absent spectrum rises at low frequency explains why the low-frequency performance of the electronic instrumentation affected the apparent fluctuation level determined here, and probably in other experiments, as well. Second, whereas introducing the grid increased the free-stream fluctuation amplitude by approximately fifty percent, i.e., from 0.07 percent to 0.11 percent, according to Fig. 5 and to other data not shown, the intensity within the T-S frequency band increased by approximately 20 dB, i.e., by ten-fold in amplitude. The frequency range of unstable T-S waves extended from 75 to 250 Hz, approximately, for the range of Reynolds numbers of the present experiment.

One specification of the free-stream turbulence which is of particular interest in connection with the effect of unit Reynolds number upon transition is the variation of intensity with wind speed. It was stated above that the broadband level was independent of speed, but, because this result pertained mostly to frequencies far below those of T-S amplification, measurements were made with the grid installed for frequencies within the T-S range. Fig. 8 gives the variation with tunnel speed of the rms amplitude within three one-third octave bands covering much of the T-S range of importance. Here, the frequency of analysis was adjusted in accordance with changes in windspeed such as to maintain the dimensionless frequency constant. It is to be noted that the analyzer bandwidth was automatically maintained proportional to the center frequency, as is appropriate for rendering the results dimensionless.

It may be seen that the fluctuation levels for velocities below 10.0 m/sec varied in opposition to those at higher speeds. It is believed that the low speed behavior is a peculiarity of the facility and of the grid, whereas the higher speed results may be more typical. The Reynolds number of flow past the grid rods was less than 400 at the lower speeds, a range in which the wake of a cylinder becomes Reynolds-number dependent. The fluctuation variation evident above this speed would be expected to produce a unit-Reynolds-number effect upon transition consistent with results from the literature, but this matter was not investigated.

2. BROADBAND FLUCTUATION DEVELOPMENT IN THE LAYER

The broadband fluctuations measured within the layer for the frequency range 0.3 Hz to 300 Hz are presented for four x-stations in Figs. 9a - 9d. Grid-present and grid-absent data are given in each case, together with the mean velocity profiles which were obtained concurrently. η (ETA in the figure) is the Blasius coordinate. It will be shown subsequently that the x-range of the survey spanned the region within which T-S amplification commenced.

The general shapes of the fluctuation profiles of the figure resemble each other, and also are in close conformity with results of similar nature given by Klebanoff (unpublished), Arnal and Juillen²¹, and by Reshotko and Leventhal²². All found that the profile peaks occurred at $\eta = 2.3$, and the present results reproduce this accurately. Moreover, Klebanoff had shown that the

characteristic shape of the profile was explainable in terms of the Blasius profile according to a thickening/thinning motion of the layer, which he referred to as "breathing".

The values of the peak fluctuation levels of the curves, obtained by fairing the data in the vicinity of the crests, are given in Fig. 10. It is apparent that the fluctuations grew stronger at a modest rate during their downstream course, a result known from both the Klebanoff and the Reshotko and Leventhal studies.

It is important to note in the figure that the fluctuation amplitude within the layer tripled in response to the installation of the grid, whereas the stream level increased not more than fifty percent, according to Fig. 5. A satisfactory explanation of this high degree of receptivity is not available, but it may be offered that the layer response was not in linear ratio on account of the free-stream fluctuations having been composed of differing types of motion in the grid-present and -absent cases. The free-stream measurements described thus far were not adequate to distinguish such a difference, but results presented below support this assertion.

As a further observation, although the fluctuations within the layer in the grid-present case exceeded seven percent, a level which is known to produce nonlinearity for the vortical fluctuations which precede transition, nonlinearity may not have been significant here on account of the long wavelengths involved. The slow and orderly growth of the low-frequency components provides assurance on this matter. However, the low frequency waves almost certainly affect the formation and growth of the T-S components.

3. NARROWBAND FLUCTUATION DEVELOPMENT IN THE LAYER

An observation believed to be of importance was immediately apparent upon starting those measurements which were conducted by the use of the one-third octave analog filter. In contrast to the wideband hot-wire signal, which appeared to be steady in time when viewed by means of an oscilloscope, the filtered signal was highly non-stationary, especially when the probe was placed within the layer and the filter tuned to the T-S frequency range. Here, the filter appeared to have been excited by pulses contained within the hot-wire signal occurring at time intervals amounting, on the average, to several times the exponential decay time of the filter. Attempt has not yet been made to quantify this observation.

Before describing the spatial variation of boundary layer fluctuations within the T-S region, it is appropriate to show representative spectra covering a more complete frequency range. Fig. 11 presents grid-present and -absent spectra obtained at the location of the wideband amplitude peak for a Reynolds number at which T-S amplification was unimportant. As in Fig. 7, the relative placement of the curves is correct, but the reference level is arbitrary. Through comparison with Fig. 7, it is evident that each signal contained relatively less high frequency than was present in the stream, a result noted by Arnal and Juillen²¹, and that the additional fluctuation introduced by the grid was proportionately less here than in the stream. Fig. 12 presents normalized spectra measured at various values of η , showing a

relative decline of high frequency energy as the probe was set deeper within the layer. Included there are the values of the relative electronic gain utilized in placing the curves at the levels shown in the figure.

Measurements were made, with the grid installed, of the fluctuation distribution within the layer for various values of the dimensionless frequency spanning a major portion of the T-S amplification range. Figs. 13a,b present amplitude profiles and concurrently-measured mean velocities for an x-station at which T-S wave amplitudes were observed to be unimportant. The profile for the lowest frequency, $Fx10^4 = 0.2$, appears to be qualitatively similar to the broad-band results of Fig. 9, except that the peak was located at a value of $\eta = 3.3$, and the ratio of peak to free-stream amplitudes was much less than that inferred from Figs. 5 and 10. With increase of $Fx10^4$ toward 1.0, the profiles became concave upward in the wall region and the location of the peak moved progressively to greater values of η , reaching 4.5, for which $U(\eta)/U_0 = 0.97$. Also, the ratio of peak to free-stream amplitudes diminished greatly with increase of frequency. Whereas the very low frequencies, i.e., those which contributed most heavily to the free-stream level, induced motions fairly deep within the layer and which were 60-fold, approximately, greater in amplitude than those of the stream, the fluctuations within the T-S frequency range induced much weaker ones in the layer, and these remained much closer to the edge of the layer.

The most significant result contained within Figs. 13a,b is that the layer was caused by the the free-stream turbulence to execute a characteristic motion which contained temporal frequencies for which the layer, at somewhat higher Reynolds numbers, was unstable. However, the amplitude profile of this motion through the layer bears little similarity to that of a T-S wave, as reference to the eigenfunction presented in Fig. 3 indicates. Accordingly, this forced motion is presumed to be unrelated to T-S fluctuations.

T-S waves possessing a frequency near $Fx10^4 = 1.0$ are expected from theory to be among those to appear earliest along the length of the plate. Accordingly, the growth of fluctuations of that frequency was measured for four stations covering the region in which T-S wave growth was expected to commence. Figs. 14a - d present the data for the grid-installed case. Inspection shows that the peak value of the fluctuation amplitude remained nearly constant along the x-direction, in accordance with the free-stream fluctuation amplitude, but in contrast with the broadband fluctuation growth seen in Fig. 10. Also, it may be noted that although the location of the peak, expressed in terms of η , did not change from station to station, the profiles became somewhat fuller with increase of x.

The most important effect contained here is the growth of signal amplitude near the location $\eta = 1.5$, as is most readily apparent in Fig. 14d. This growth is believed to be a consequence of T-S amplification. Reference to Fig. 3 indicates that the location $\eta = 1.5$ is near the amplitude peak of the T-S eigenfunction, and it is there that the disparity in shape between the forced-wave profiles and the eigenfunctions is greatest. Accordingly, that is the location for which T-S waves are most easily distinguished against the background fluctuations. The rate of growth of waves at this location is considered in a later section.

A further study of narrowband wave development was made at increased tunnel speed, with the frequency of analysis having been lowered to $Fx10^4 = 0.8$ in accordance with the increase in maximum Reynolds number. It is to be pointed out that the increase of speed must have been accompanied by a reduction in free-stream fluctuation level, according to Fig. 8. Figs. 15a - f present the profiles obtained for these conditions, and most of the observations offered concerning Figs. 14a - d are relevant here as well. However, there is seen here at the more forward stations a higher relative fluctuation level near the wall than prevailed in the previous figure, a disparity which might have been due to a dependence of the free-stream fluctuation composition upon speed. The onset of wall-region fluctuation growth is again evident. It is seen that the profile shape at the final station differs greatly from those recorded at the earlier stations, and that the maximum amplitude had grown greatly (note the difference in scale). The T-S component appears to have become predominant.

Mention has been made of a possibility that the composition of the free-stream fluctuation differed in the grid-present and -absent cases. Further evidence of this was gained by measuring the layer response in the absence of the grid. Fig. 16 shows that the profile shape differed greatly from that with the grid present, indicating that the forcing mechanism in the two cases must have differed. As a cautionary note, the grid-absent result is believed to contain a small, but non-negligible, contribution due to electronic noise within the weak signal.

4. PHASE MEASUREMENTS; DISTURBANCE PROPAGATION SPEED

As in Section II, the phase measurements obtained by use of the dual-sensor probe may, under certain circumstances, be interpreted in terms of a wave propagation speed for the purpose of classifying disturbances as to type or cause. The relation between phase and speed was given there. Here, however, only phase-difference results are shown, but these are interpreted in terms of fluctuation type according to the corresponding speed whenever possible. The goal in this part of the investigation was to isolate the component of the signal due to T-S waves from the remainder of the fluctuation field, and to record the growth of T-S wave energy.

Two results of significance may be conveyed fully without graphical display. First, when the probe was removed to the free-stream and the tunnel fluctuation level was further increased by the insertion of an additional 6.3-mm rod near the grid such that its wake was incident upon the probe, the phase then recorded was everywhere linearly proportional to frequency, with the inferred convection speed of all wave components equalling that of the stream. This is the result expected for a vorticity field, and it constitutes further evidence of the reliability of the experimental technique.

Second, for the grid-absent case, with the probe positioned at any value of η within the layer and at any x , the phase angle was zero for all frequencies, except for slightly negative values of phase at the lowest frequencies. The definiteness of the vanishing of the phase was taken as evidence that an unidentified class of fluctuations contributed most of the signal energy, because the recognized mechanisms of T-S oscillation and of wave-forcing by the turbulence would have produced non-zero phase angles. When

the probe was placed in the stream and the grid was absent, the quality of the result was poor, as indicated by a low coherence. The phase was then mostly zero except for substantial excursions at several of the spectral features attributed to noise present within the two signals. The vanishing of the phase in both the stream and in the layer constitutes further evidence that the composition of the free-stream fluctuations differed substantially in the grid-present and -absent cases.

One interpretation of the zero-phase result is that the residual fluctuation in the grid-absent case was principally a mass-flow variation induced by unsteady lift of the tunnel fan blades. This type of motion would have been communicated by downstream- and upstream-running acoustic waves, accounting for the vanishing of the phase angle. Clearly, this supposition requires testing before acceptance.

The phase difference for grid-present fluctuations within the layer is presented in Fig. 17 for a Reynolds number at which, apparently, T-S waves had been induced by the stream. The four traces for each location through the layer are exact repetitions of the measurement, and indicate in a general way the reproducibility, or lack thereof, of the results due to the aforementioned non-stationarity of narrowband observations. Two anomalies are evident in the figure: the negative values of angle seen at low frequencies in the upper three curves are as yet unexplained, while the two departures from constant slope seen in the bottom figure are due to electronic noise.

Interpretation here is potentially difficult because it is recognized that the layer may respond simultaneously to the exterior vorticity field, to the aforementioned pressure field, and to the presence of T-S waves. However, the results are seemingly understandable for the regions of the layer near the wall and near the edge, shown as the top and bottom curve sets of the figure, respectively. Near the wall, and neglecting the negative phase values, the phase varies in a manner explainable by assuming the simultaneous presence of two wave types: T-S waves, and those zero-phase ones which predominate in the absence of the grid. Unfortunately, the phase was not measured at the specific location of the eigenfunction peak, and at the next height of measurement the relative T-S contribution had diminished, as seen. The indefiniteness of the phase results evident at the next two stations outward may imply that there existed a mixture of forced waves and of those unidentified motions which make up the characteristic profiles of Figs. 13 and 14. Near to and beyond the edge of the layer the phase variation approaches that of the free-stream vorticity field, as expected.

The development of the phase difference near the wall was followed along x as a means of observing the onset and growth of T-S wave amplitude. Fig. 18 shows the results obtained at $\eta = 1.0$, approximately, for five stations. Again, four repetitions of each measurement were made, but these were averaged and faired for display. Also shown is the phase variation, computed by Gaster's method, which would have prevailed if the T-S component had been predominant. The onset and growth of the T-S component is clearly evident by the departure of the phase angle from zero and by the approach toward the theoretical value. The autopower spectra of each of the two signals, measured concurrently with the crosspower and phase but not presented, revealed a discernable "swelling"

within the T-S frequency range as x was increased. This served as further evidence of T-S amplification, but was not sufficiently distinct on account of its broadness to render it useful in quantifying the growth. Also, although the progression of shape with distance seen in Fig. 18 is not uniform, the downward movement of the center frequency with increase of x is in accordance with the prediction of theory.

5. T-S WAVE GROWTH

Figures 19a,b present the wave growth computed by Gaster's method for two frequencies of importance near the onset of instability, with two wave obliqueness angles being included. In each case the amplitude is expressed logarithmically, and is normalized to that at the lower-branch neutral point.

Experimental wave growth rates have been determined from the results contained in Figs. 14, 15, and 18, and are compared with theory in Figs. 19a,b. For the former two figures, the fluctuation amplitude at a location near $\eta = 1.5$ has been taken to represent the value at any station, and the streamwise variation of this used to indicate growth. In each case, the amplitudes at the upstream stations have been taken as reference values, and the logarithms of the amplitude ratios at subsequent stations are given in the figure. Because no distinct feature appears at the stated value of η for the more forward or reference stations, care is required in the interpretation of the growth results, given below.

Estimate was also made of the wave growth by use of the phase difference results of Fig 18 for the particular frequency $Fx10^4 = 1.0$. Further explanation of the technique described in Section II is necessary. Based upon results presented above, it is assumed that the fluctuations in the wall region are composed of ones with zero phase difference, and of T-S waves, for which the phase is as given in Fig. 18. Further, it is assumed that the growth of the former type within the x -region of interest is negligible and that the constant amplitude is denoted by A_0 . The unknown T-S amplitude is denoted by $A_1(x)$. Because the two angles are known, the ratio of the amplitudes has been determined according to simple trigonometry as:

$$\frac{A_1(x)}{A_0} = \frac{\sin(\varphi_m)}{\sin(\varphi_{ts} - \varphi_m)}$$

where φ_m and φ_{ts} are the measured and T-S phase differences. For presentation, the logarithms of the ratios derived for the several stations were adjusted by the addition of a constant in order to bring the value at the first station to zero, there being no clearly defined reference value, and the slope of the result being the important quantity.

The results within Fig. 19b indicate that the two methods yield similar growth rates, and that this growth apparently did not commence until a station well past the onset of instability was crossed. However, once the growth became detectable against the background components, it proceeded faster than that of a continuous, parallel, wave train, which the theory treats. The excess of growth rate over the theoretical value might have been caused by an inception over the

surface of the plate of new wave packets, which thereby grew in number, in lateral extent, and as in strength, during downstream progression.

6. CONCLUSIONS

For a pre-transitional Blasius boundary layer in a weakly turbulent wind tunnel stream it was found that:

a. The free-stream fluctuations were spatially uniform for frequencies not exceeding those at the upper limit of the T-S range.

b. In the absence of a turbulence-producing grid, most of the fluctuation energy lay at frequencies far below those of importance for T-S amplification. Installing the grid raised the broadband free-stream fluctuation level approximately 50 percent; however, the increase within the T-S frequency range was approximately 10-fold.

c. With the grid present, the wideband fluctuation level was nearly independent of tunnel speed, but the variation within certain constant dimensionless frequency bands was substantial, an observation of importance in the consideration of unit-Reynolds number effects upon transition.

d. With the grid present the free-stream fluctuations were found to be convected at free-stream speed, as expected for a vorticity field. The convection results were indefinite in the grid-absent case. Apparently, the fluctuation composition differed from that in the grid-present case.

e. Within the layer, the normalized profiles of broadband fluctuation amplitude through the layer were nearly equal in shape in the grid-present and -absent cases, but the peak value was approximately three-fold higher with the grid present. In both cases the level increased with x . The profile shape, peak level, and relative growth were in accordance with results obtained by others.

f. The fluctuations within the layer contained proportionately less high frequency energy than those of the stream for both the grid-present and -absent cases.

g. Within the layer, the characteristic fluctuation amplitude profiles for fluctuations falling within the T-S amplification range differed, depending upon whether the grid was present or absent. For the former case, the peak of the profile lay near the outer edge of the layer, and the magnitude was independent of x . However, fluctuation growth was observed to commence near the wall, and this was attributed to T-S amplification. T-S waves were not found within the Reynolds number region of survey in the grid-absent case.

h. Phase-difference measurements were obtained within the layer, and these provided supporting evidence for the existence of T-S waves, as mentioned above. The measurements were interpreted in terms of the relative proportion of the total fluctuation at any location contributed by the T-S wave component.

i. Two independent methods were then employed for determining T-S wave growth, i.e., an amplitude method and a phase method. These yielded a

similar result, showing that the onset of T-S wave growth occurred downstream of the neutral Reynolds number, and that the maximum growth rate exceeded that expected from theory.

j. The results show that fluctuation energy was injected by the free-stream fluctuations into the layer along its length, and that T-S wave formation at the forward stations of the plate was unimportant.

REFERENCES

- 1) B. G. Van der Hegge Zijnen, "Measurements of the Velocity Distribution in the Boundary Layer Along a Plane Surface." Report No. 6, Aero Lab Tech. H.S., Delft, 1924.
- 2) H. L. Dryden, "Effect of Turbulence in Wind Tunnel Measurements." NACA Rept. 342, 1930.
- 3) H. L. Dryden, G. B. Schubauer, W. C. Mock, Jr., and H. K. Skramstad, "Measurements of Intensity and Scale of Wind Tunnel Turbulence and their Relation to the Critical Reynolds Numbers of Spheres". NACA Rept. 581, 1937.
- 4) H. L. Dryden, "Air Flow in the Boundary Layer Near a Plate." NACA Rept. 562, 1936.
- 5) A. A. Hall and G. S. Hislop, "Experiments on the Transition of the Laminar Boundary Layer on a Flat Plate." British ARC Rept. and Mem. 1845, 1938.
- 6) G. B. Schubauer, "The Effect of Turbulence on Transition of the Boundary Layer on an Elliptic Cylinder." Proc. 5th Inter. Congr. Appl. Math, 1938.
- 7) G. S. Hislop, "The Transition of a Laminar Boundary Layer in a Wind Tunnel." Ph.D. Thesis, Cambridge Univ., 1940.
- 8) A. Fage and J. H. Preston, "On Transition from Laminar to Turbulent Flow in the Boundary Layer." Proc. Royal Soc. A., Vol. 178, pp. 201-227, 1941.
- 9) G. Drougge, "An Investigation of the Influence of Turbulence on the Transition Point of an Airfoil." Flygtekniska Forsokunskolen FFA Meddelande 20, Ae-24:4, 1946.
- 10) G. B. Schubauer and H. K. Skramstad, "Laminar Boundary-Layer Oscillations and Transition on a Flat Plate." NACA Rept. 909, 1948.
- 11) H. L. Dryden, "Transition from Laminar to Turbulent Flow in Turbulent Flows and Heat Transfer." (C. C. Lin, ed.), Princeton Univ. Press, Princeton, 1959.
- 12) C. S. Wells, "Effects of Free-Stream Turbulence on Boundary-Layer Transition." AIAA J., Vol. 5, 1972.
- 13) D. J. Hall and J. C. Gibbings, "Influence of Stream Turbulence and Pressure Gradient upon Boundary-Layer Transition." J. Mech. Engineering Sci., Vol. 14, pp. 134-146, 1972.
- 14) G. I. Taylor, "Statistical Theory of Turbulence V. Effect of Turbulence on Boundary Layer." Proc. Royal Soc. A, Vol. 156, pp. 307-317, 1936.

- 15) H. W. Liepmann, "Investigation of Boundary Layer Transition on Concave Walls." NACA Wartime Report 87, 1945.
- 16) W. O. Criminale, "Interaction of the Laminar Boundary Layer with Free-Stream Turbulence." Phys. Fluids, Vol. 10, Part II, pp. S101-S107, 1967.
- 17) W. O. Criminale, "On the Structure of the Laminar Boundary Layer on the Presence of a Fluctuating Free Stream." Proceedings of IUTAM Symposium on Recent Research on Unsteady Boundary Layers. Laval University Press, pp. 940-979, Quebec, 1972.
- 18) H. L. Rogler and E. Reshotke, "Disturbances in a Boundary Layer Introduced by a Low Intensity Array of Vortices," SIAM J. Appl. Math., Vol. 28, pp. 431-462, 1975.
- 19) L. M. Mack, "Transition Prediction and Linear Stability Theory." AGARD Conference Proceedings No. 224, 1977.
- 20) J. C. R. Hunt and J. M. R. Graham, "Free-stream Turbulence Near Plane Boundaries." J. Fluid Mech. 84, part 2, pp. 209-235, 1978.
- 21) D. Arnal and J. C. Juillen, "Contribution Experimentale a l'Etude de la Receptivite d'une Couche Limite Laminaire, a la Turbulence de l'Ecoulement General." O. N. E. R. A. Rapport Technique No.1/5018 AYD, June 1978.
- 22) E. Reshotko and L. Leventhal, "Preliminary Experimental Study of Disturbances in a Laminar Boundary Layer due to Distributed Surface Roughness." AIAA Paper 81-1224, Palo Alto, CA. June 1981.

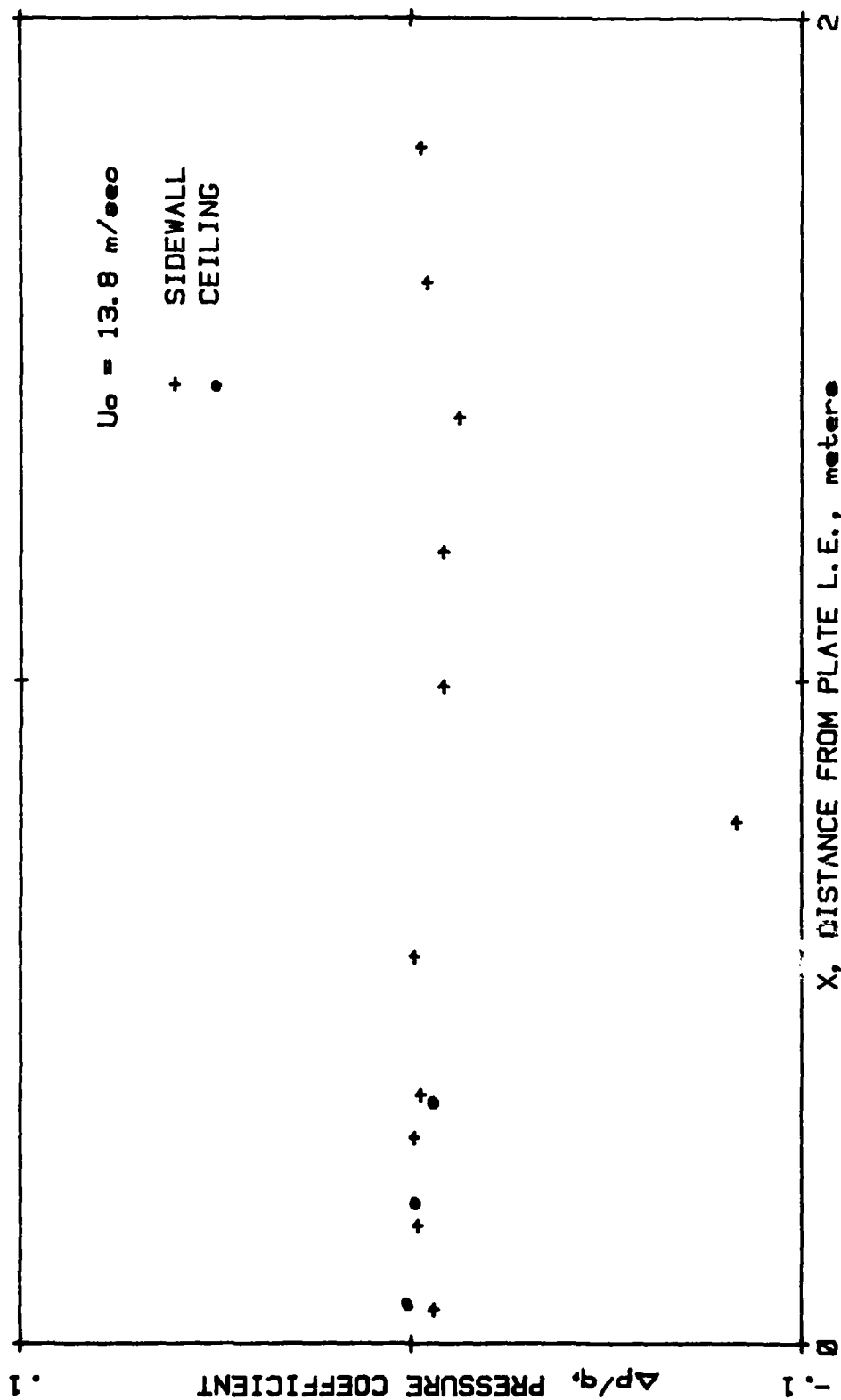


Figure 1. Pressure Distribution in Tunnel

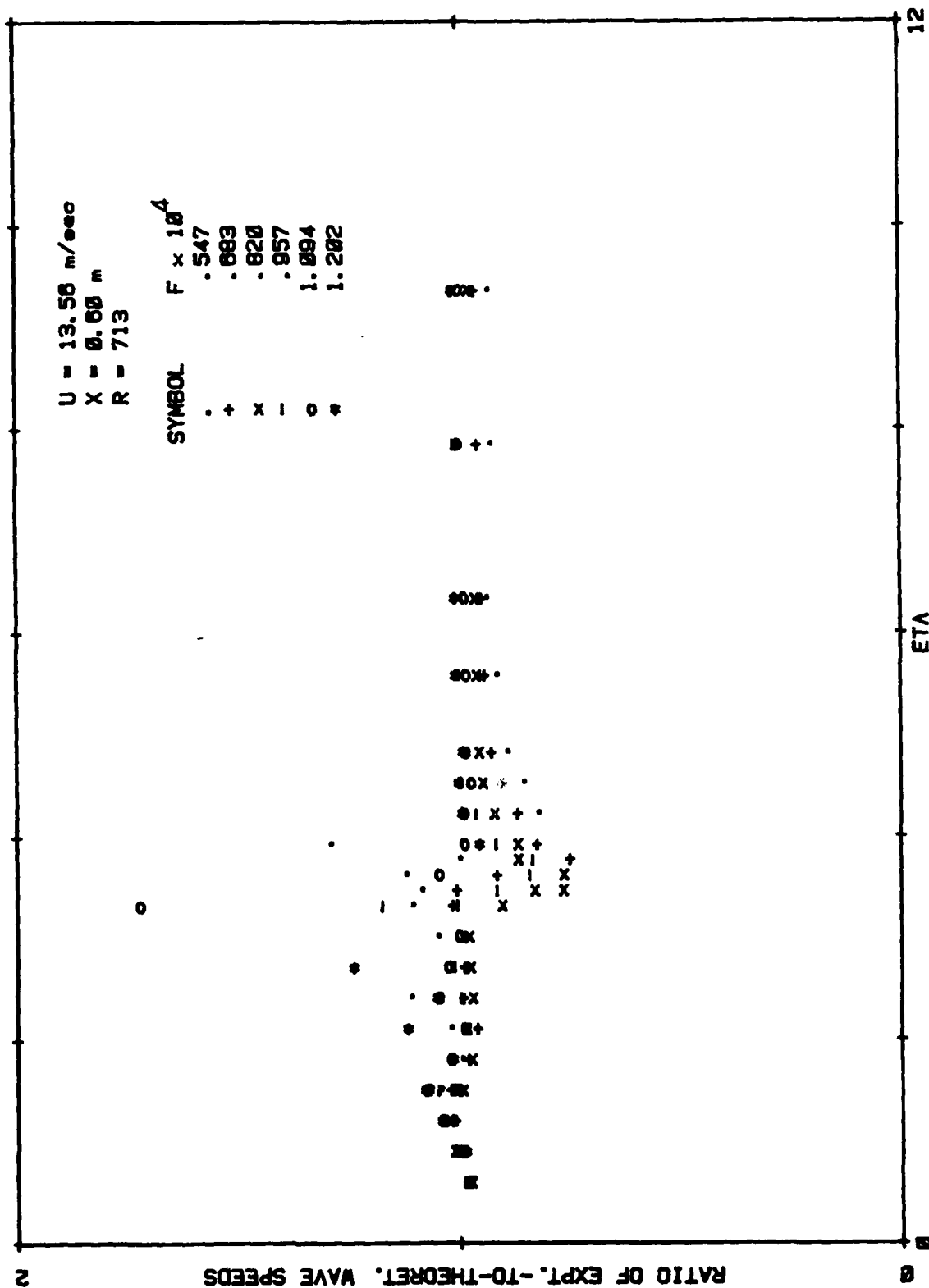


Figure 2. Test of Dual-Sensor Probe

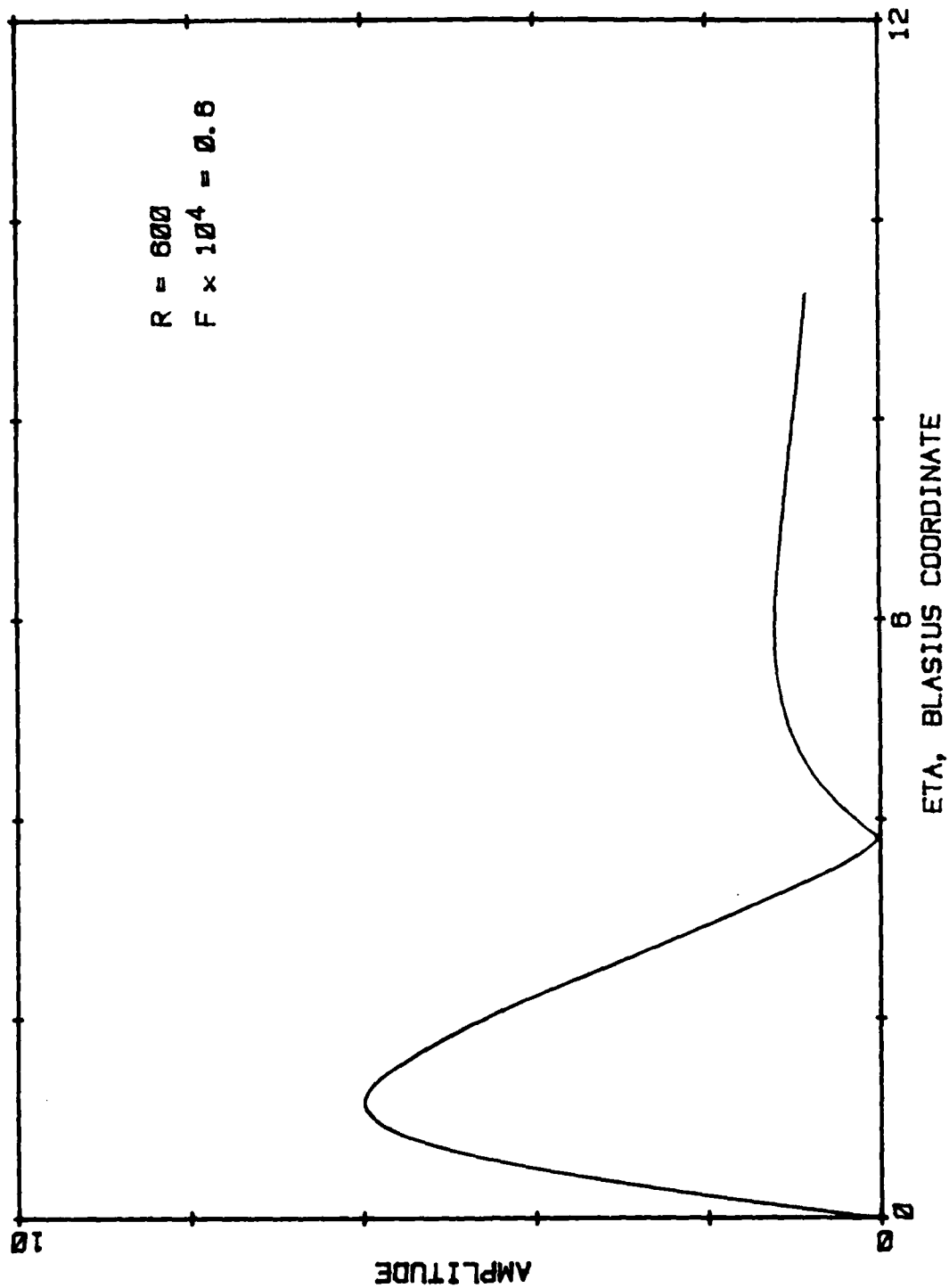


Figure 3. Example of Eigenfunction, $R = 600$, $F \times 10^4 = 0.6$

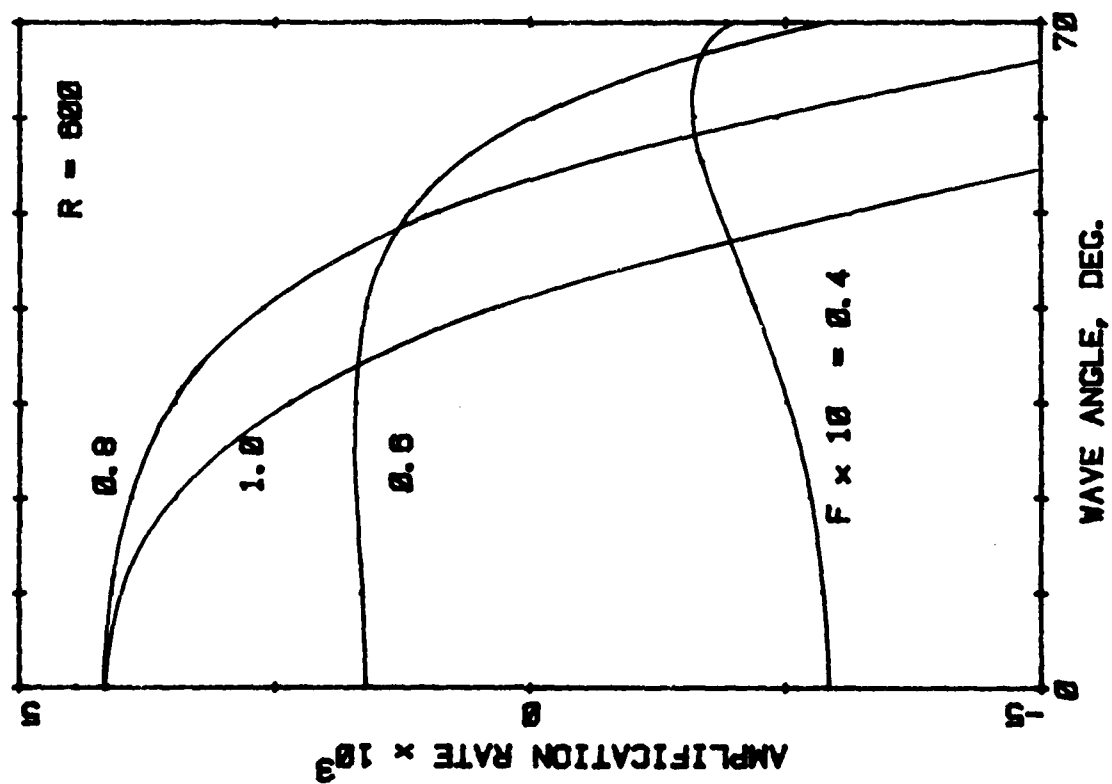
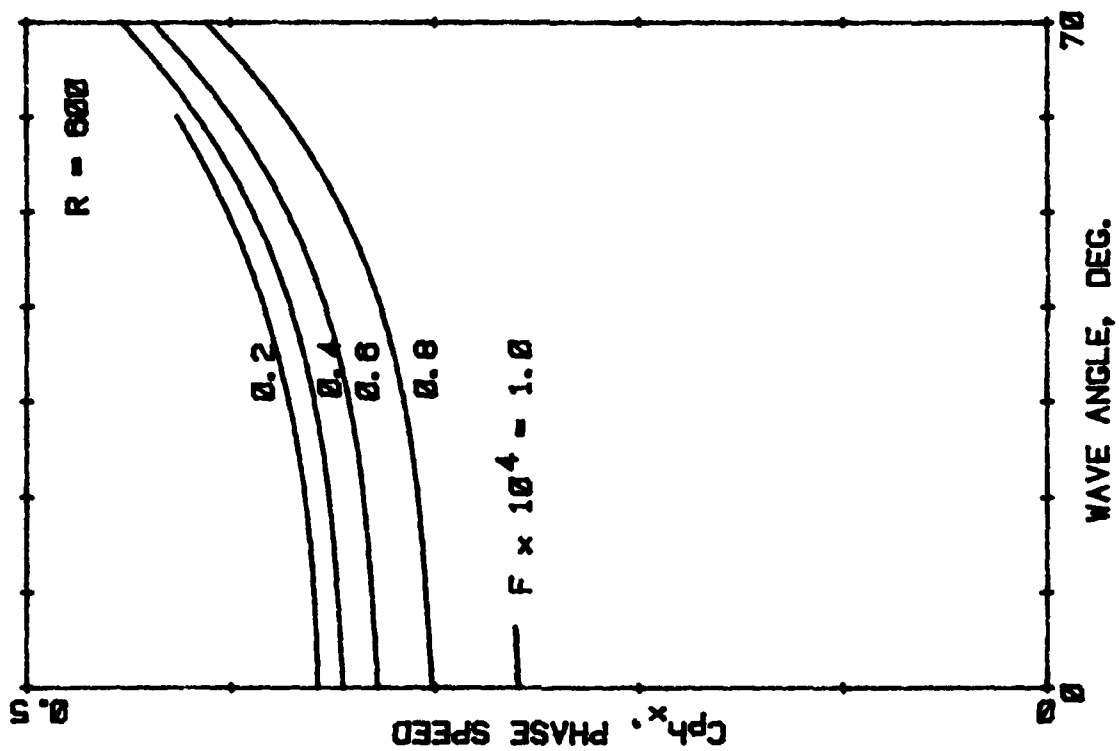


Figure 4. Wave Speed C_{ph_x} Versus Obliqueness Angle

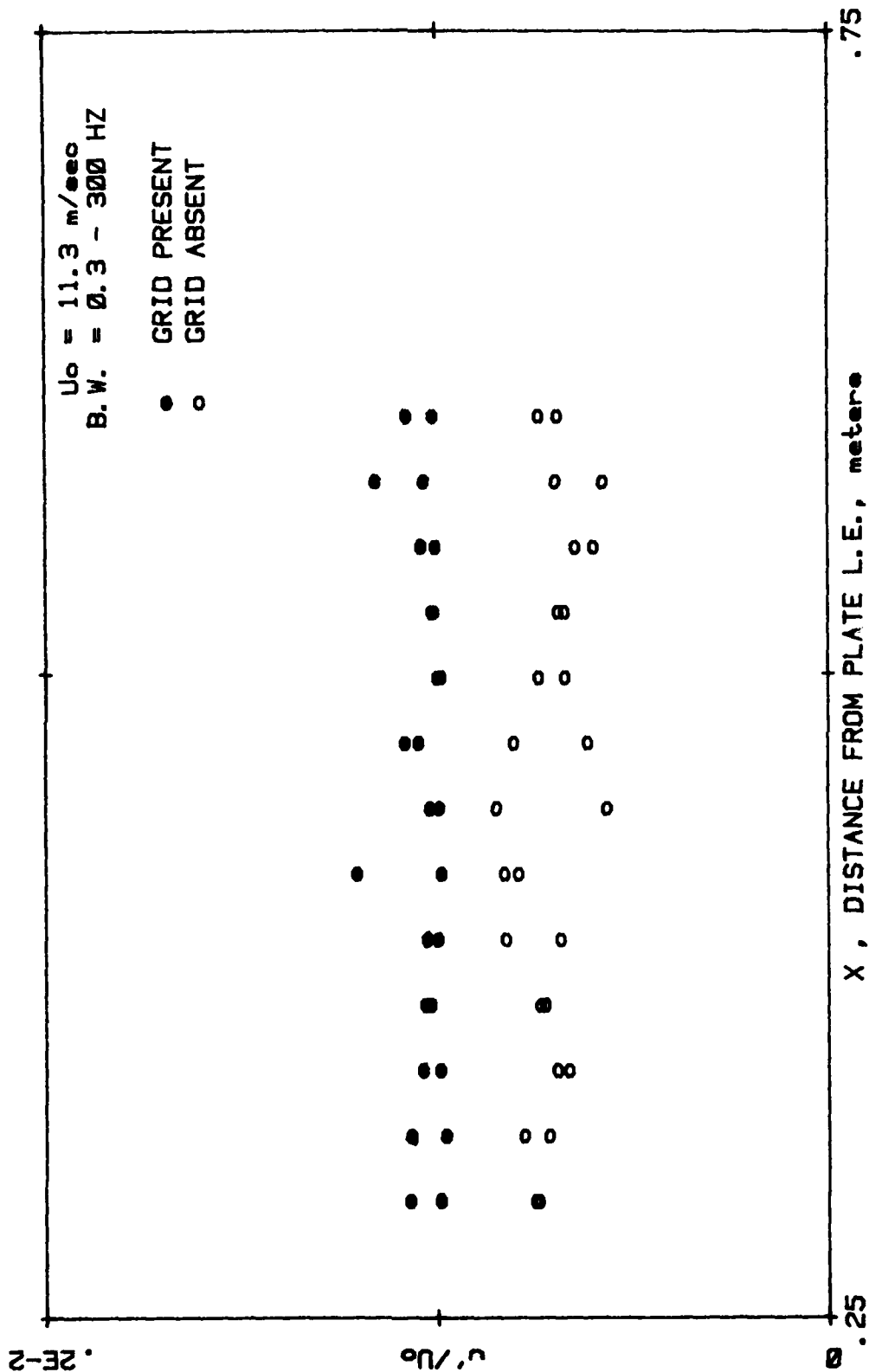


Figure 5. Broadband Fluctuation Amplitude in Tunnel Stream

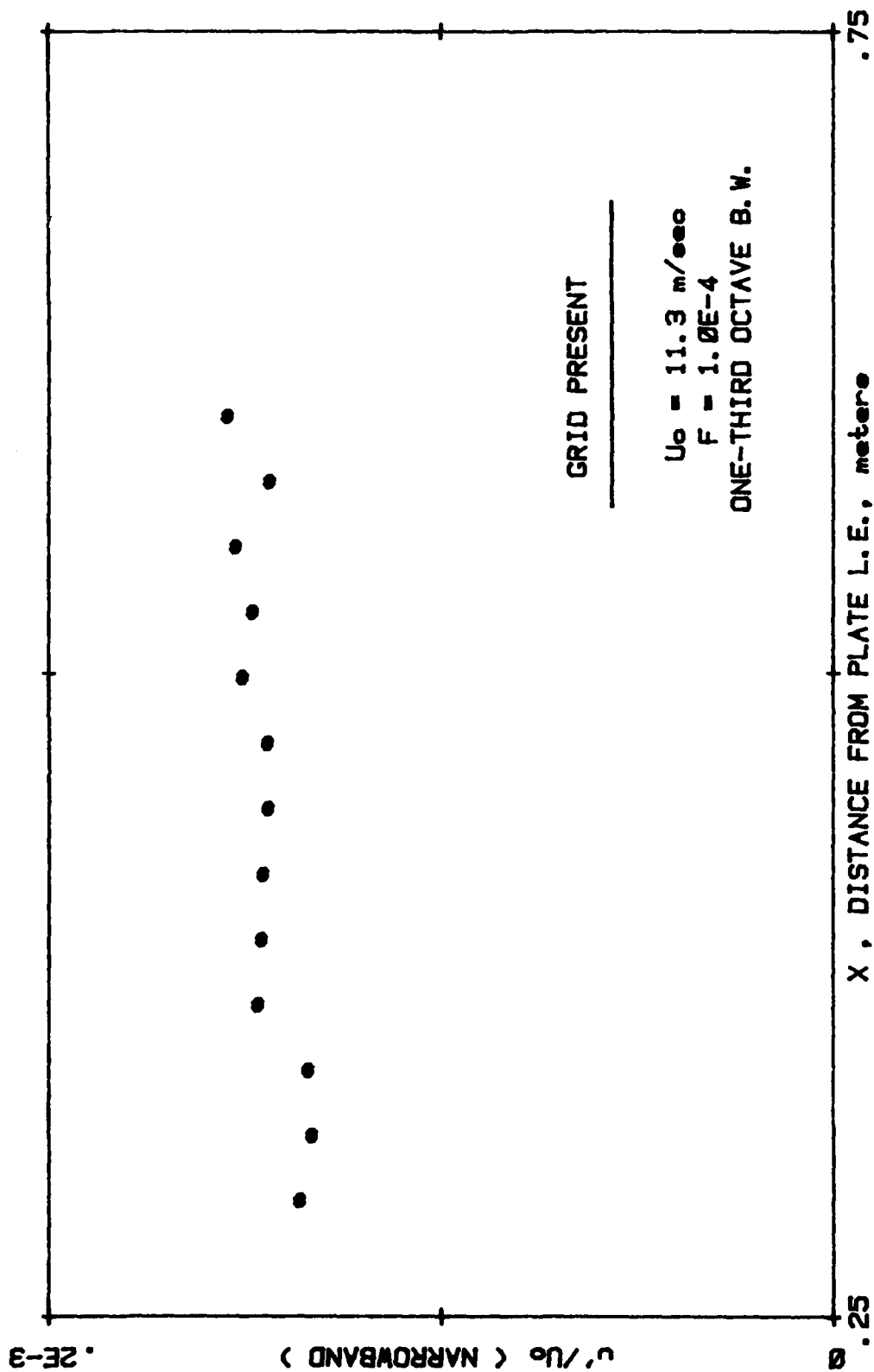


Figure 6. Narrowband Fluctuation Amplitude in Tunnel Stream

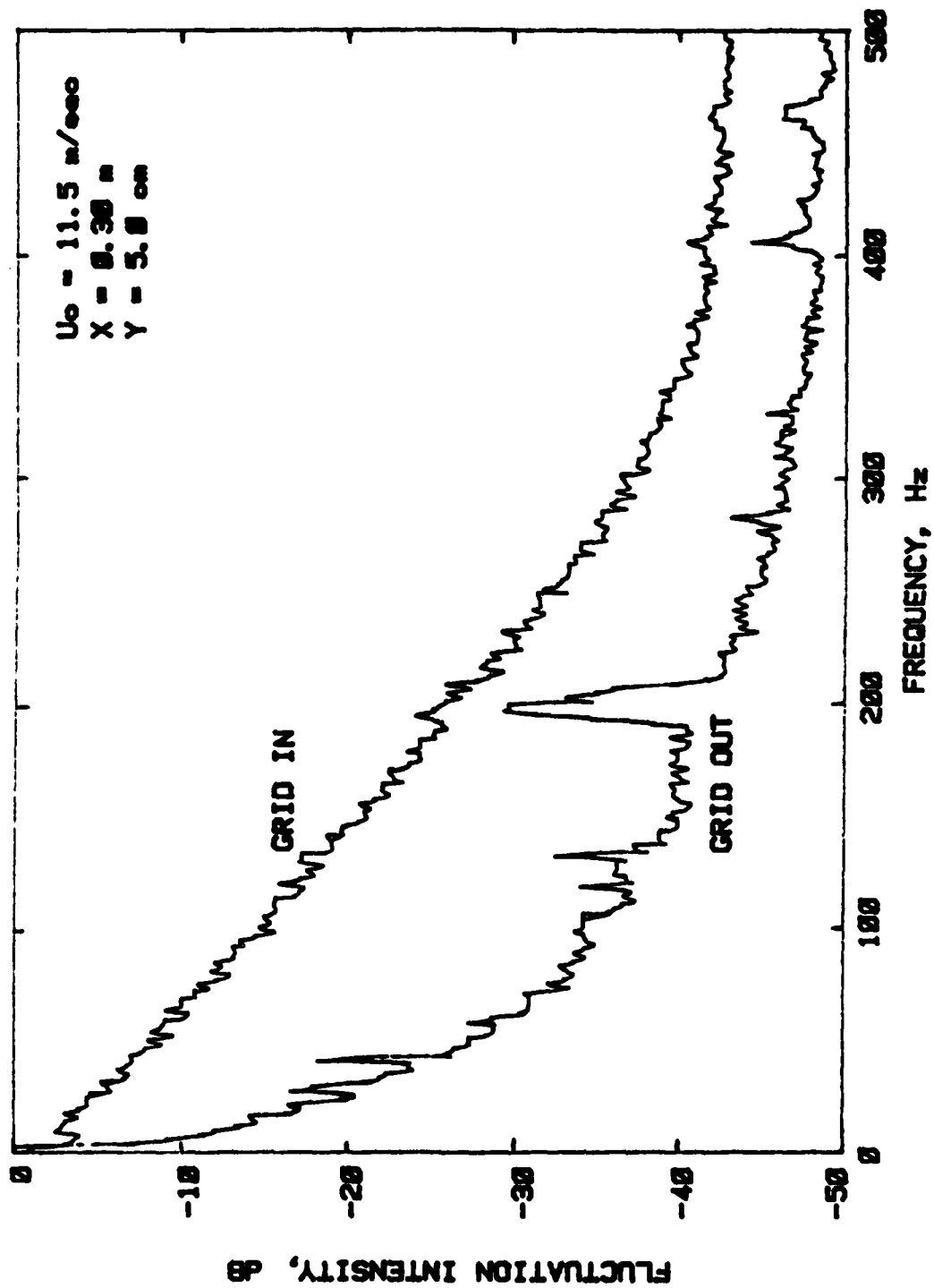


Figure 7. Free-Stream Fluctuation Spectra

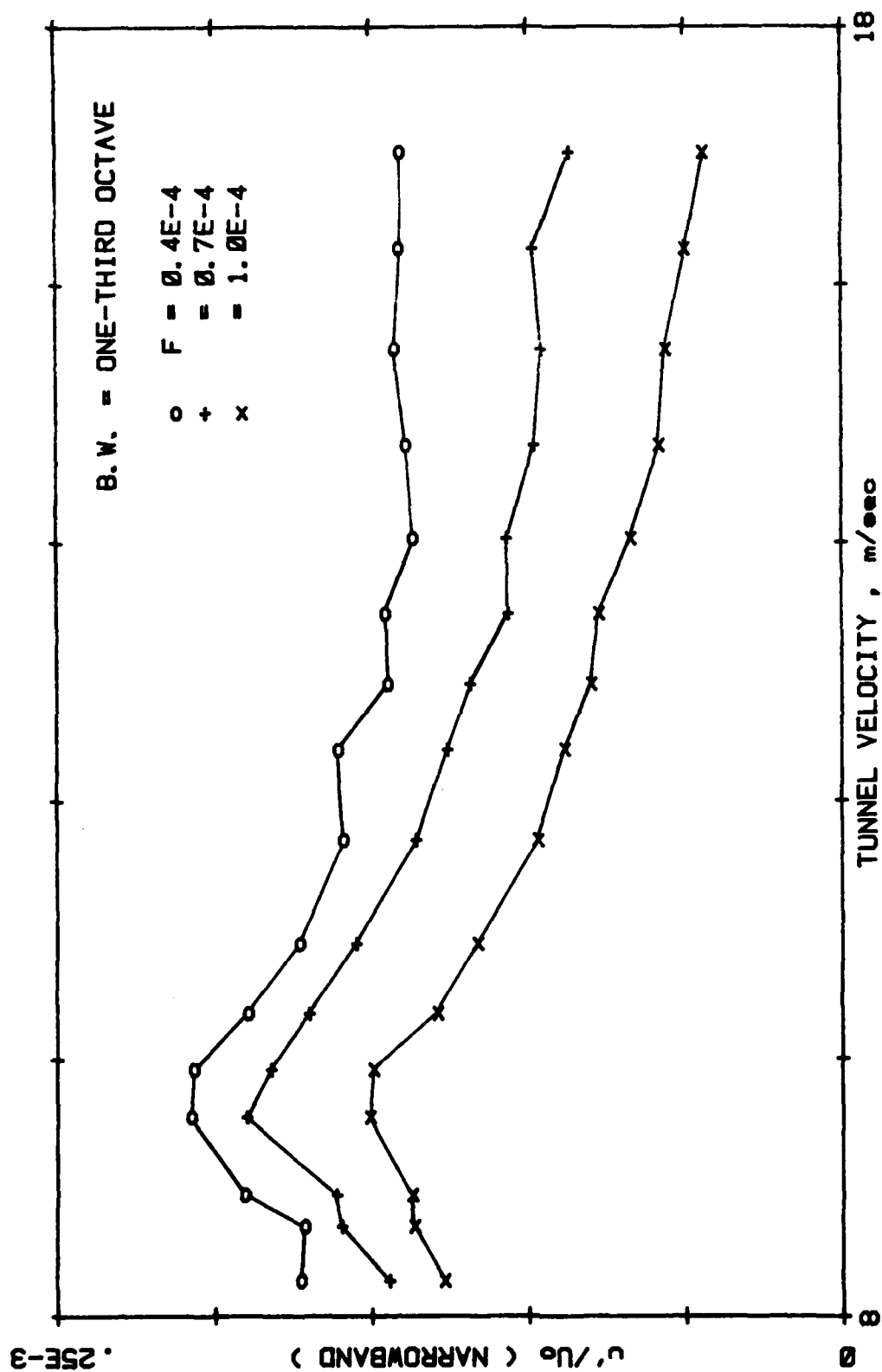


Figure 8. Free-Stream Narrowband Fluctuation Amplitude for Constant Dimensionless Frequency Versus Tunnel Velocity

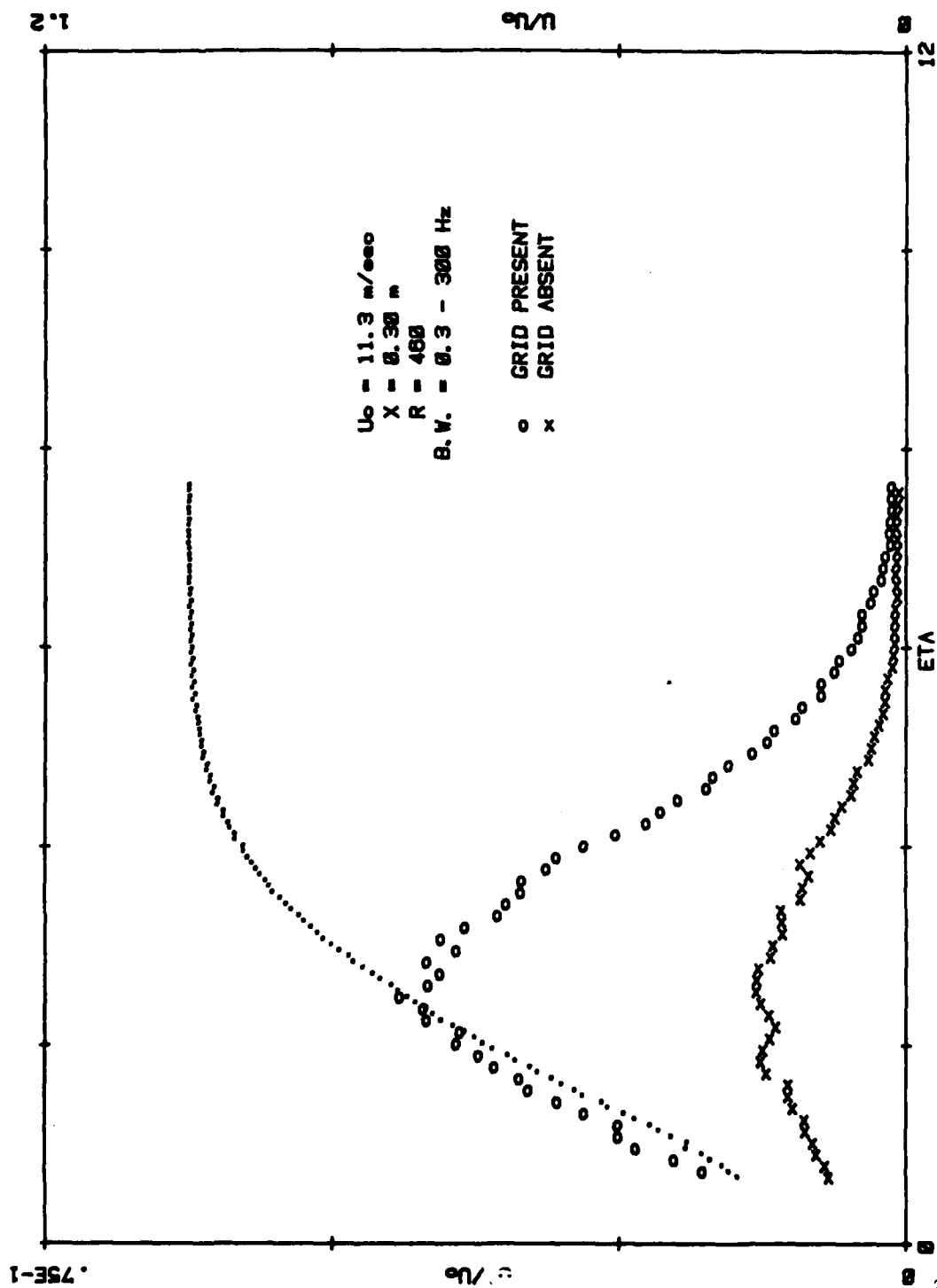


Figure 9a. Broadband Fluctuation Amplitude in Layer for $R = 460$

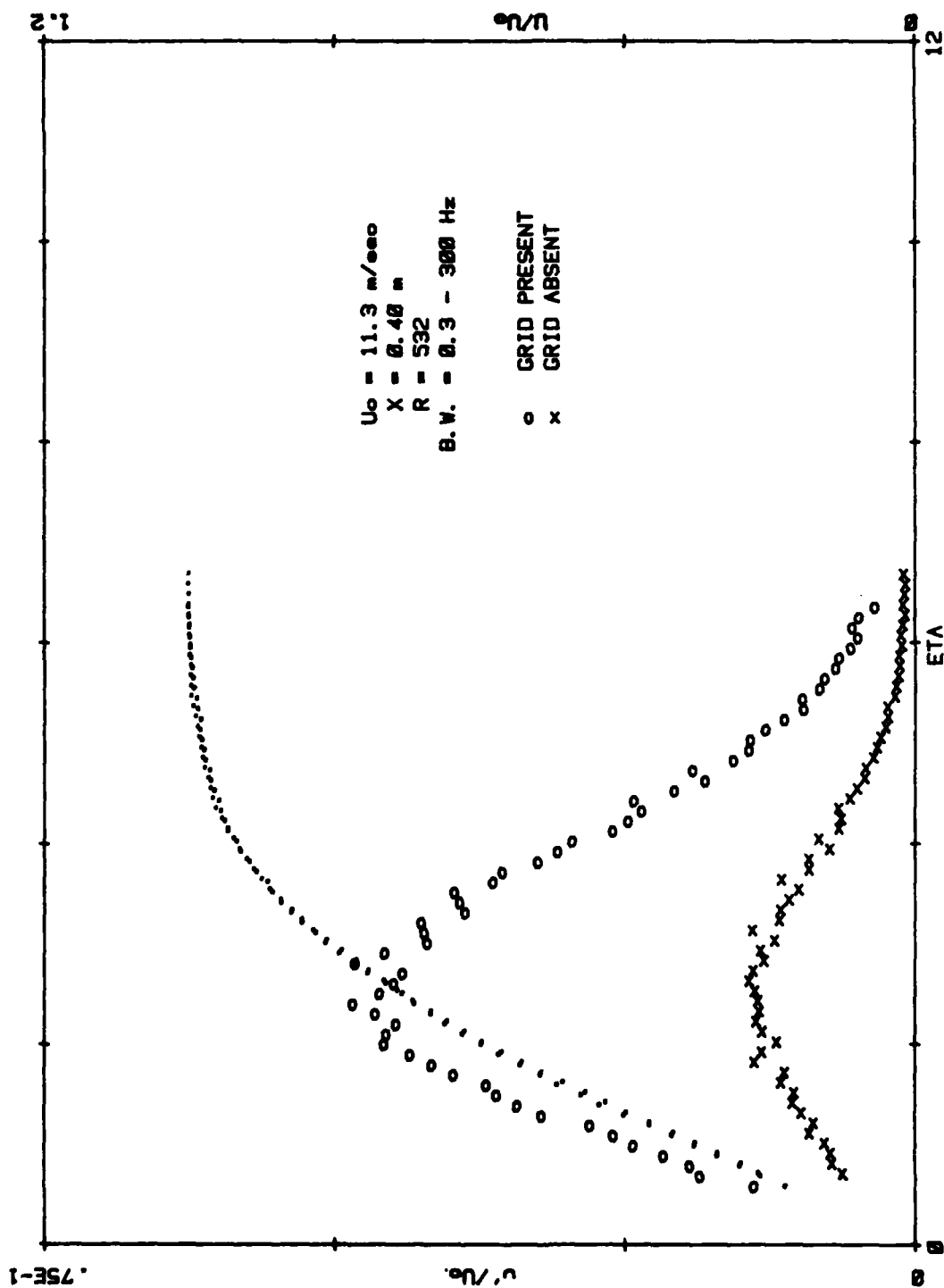


Figure 9b. Broadband Fluctuation Amplitude in Layer for $R = 532$

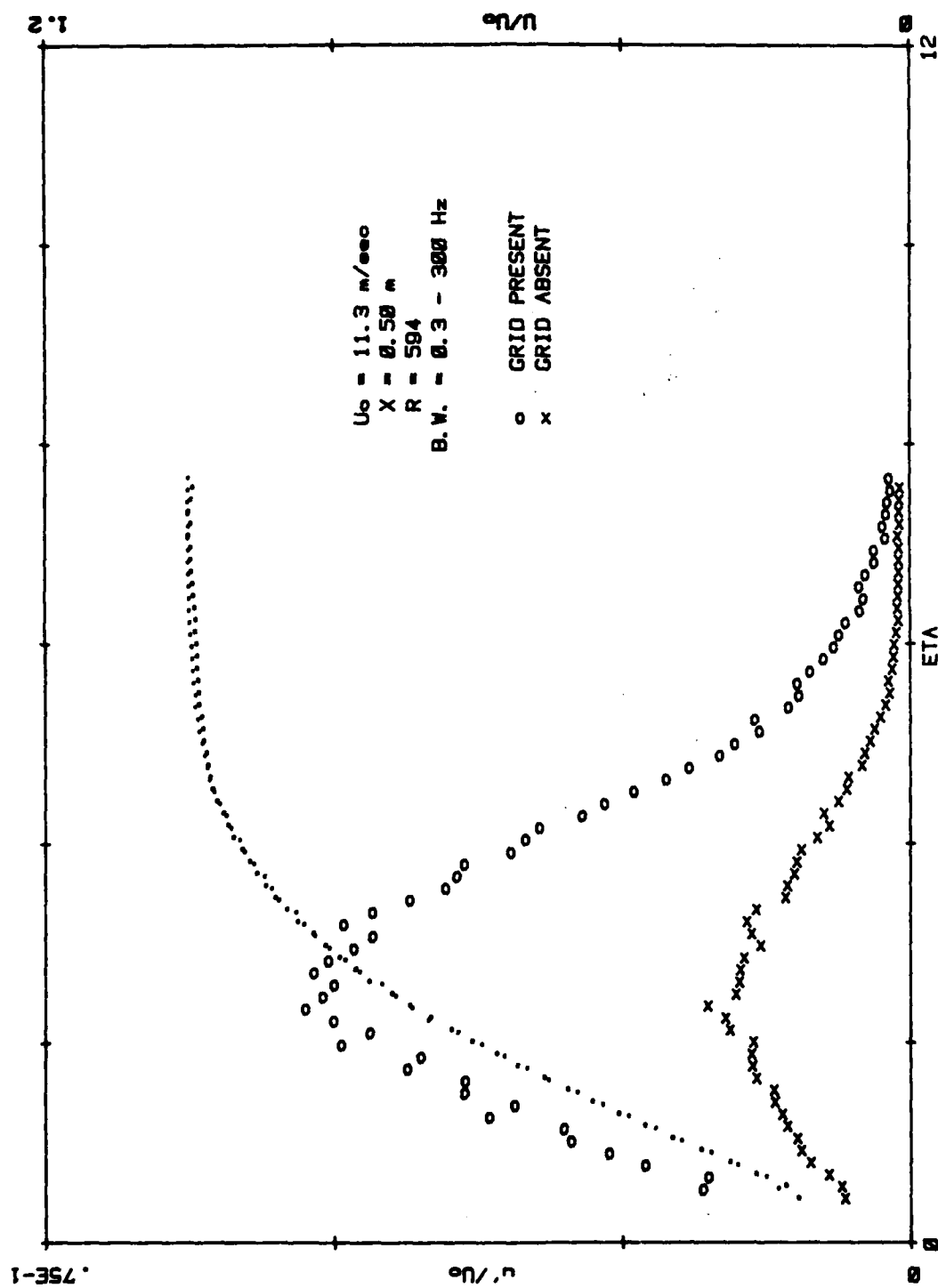


Figure 9c. Broadband Fluctuation Amplitude in Layer for $R = 594$

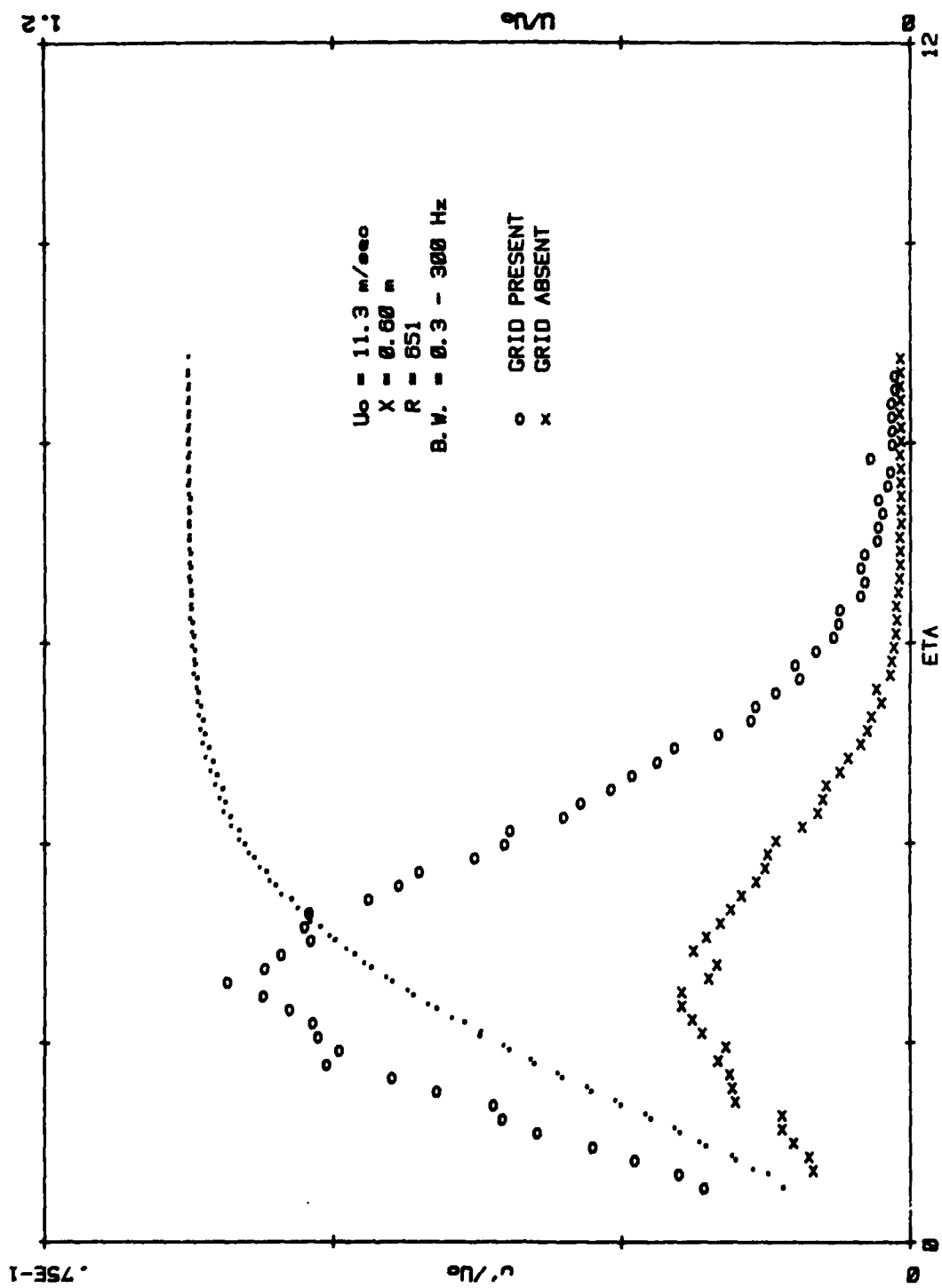


Figure 9d. Broadband Fluctuation Amplitude in Layer for $R = 651$

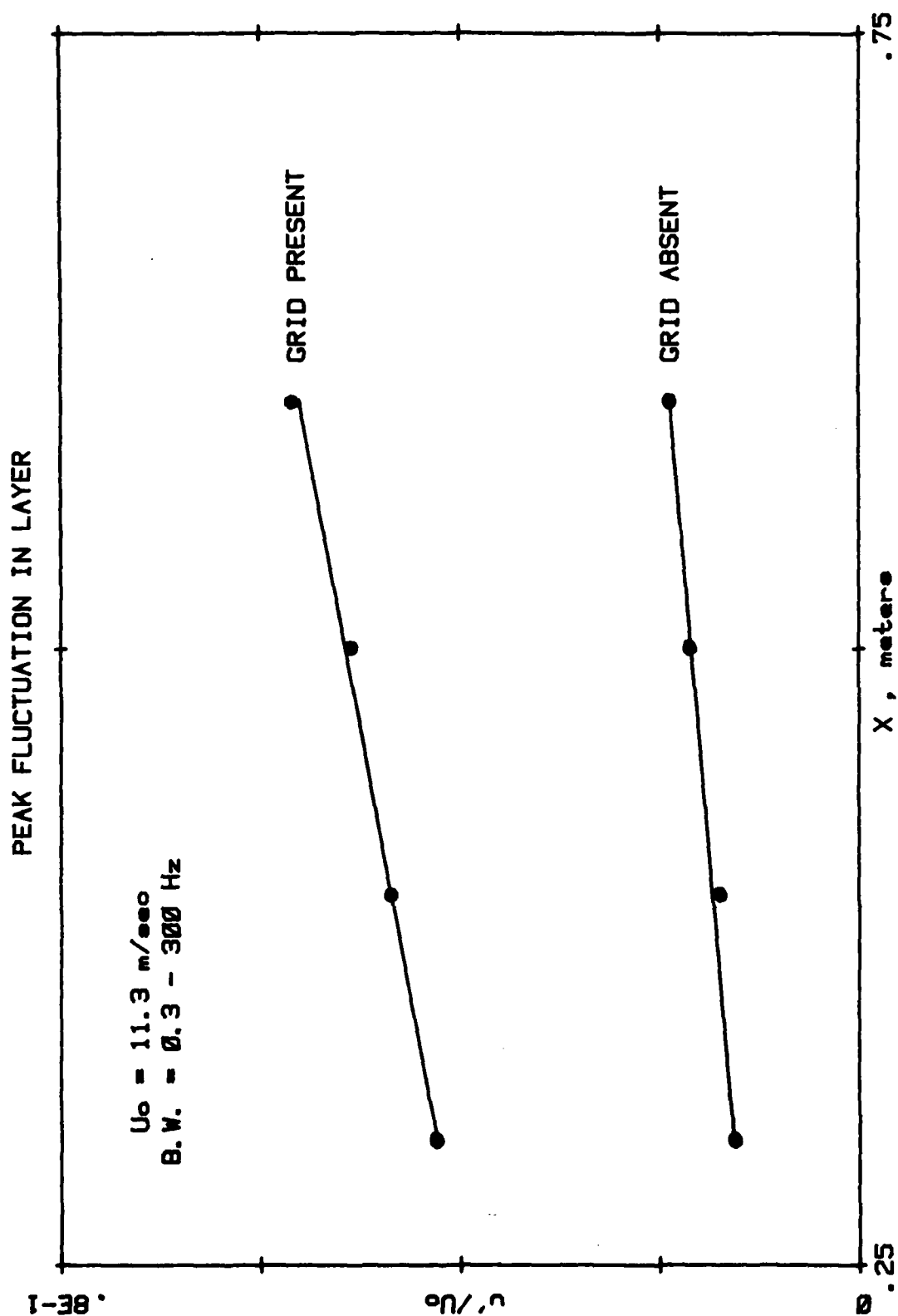


Figure 10. Peak Broadband Fluctuation Amplitude Versus x

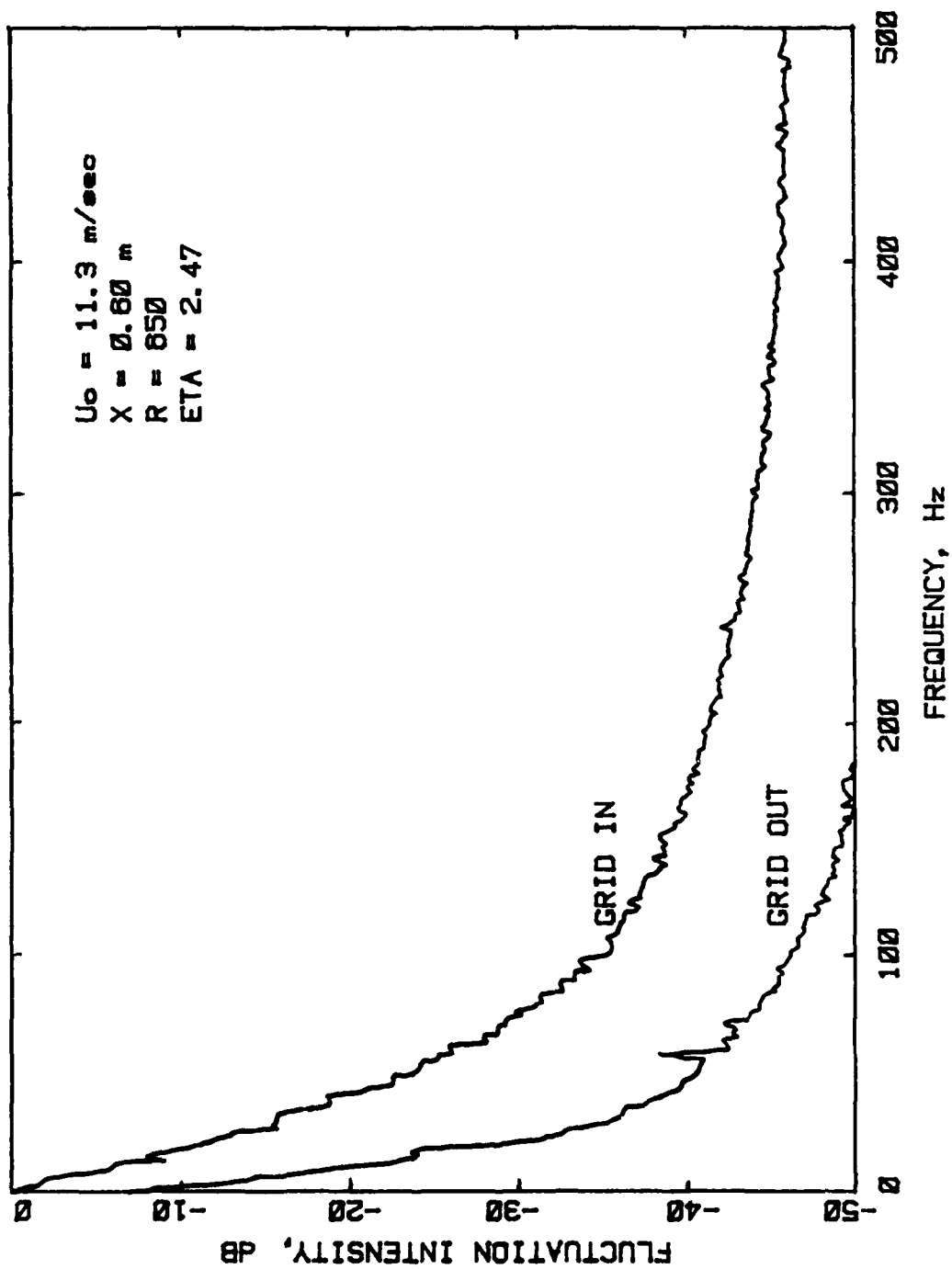


Figure 11. Fluctuation Spectra in Layer at Location of Peak Fluctuation with Grid Present and Absent

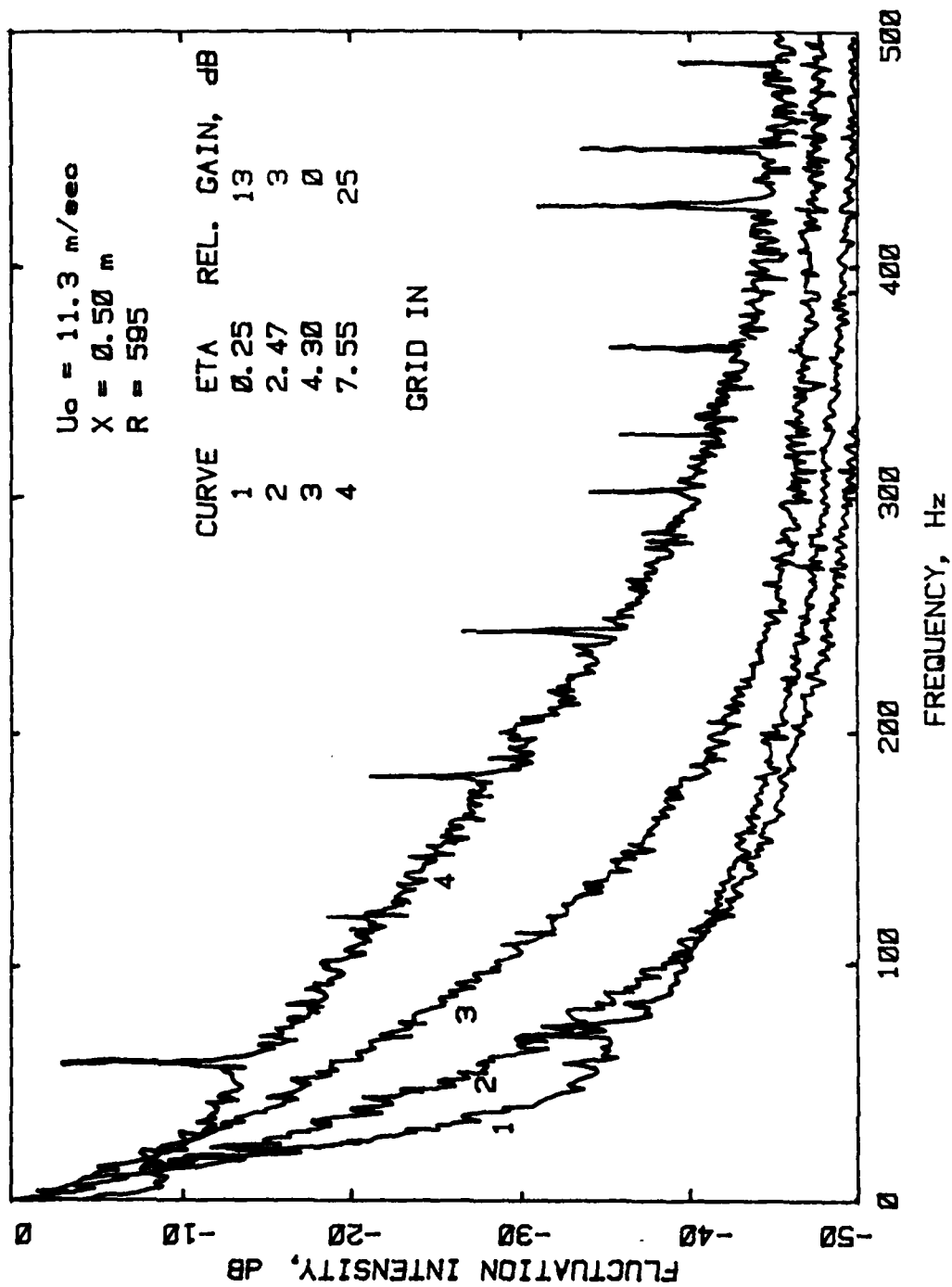


Figure 12. Normalized Fluctuation Spectra in Free-Stream and in Layer

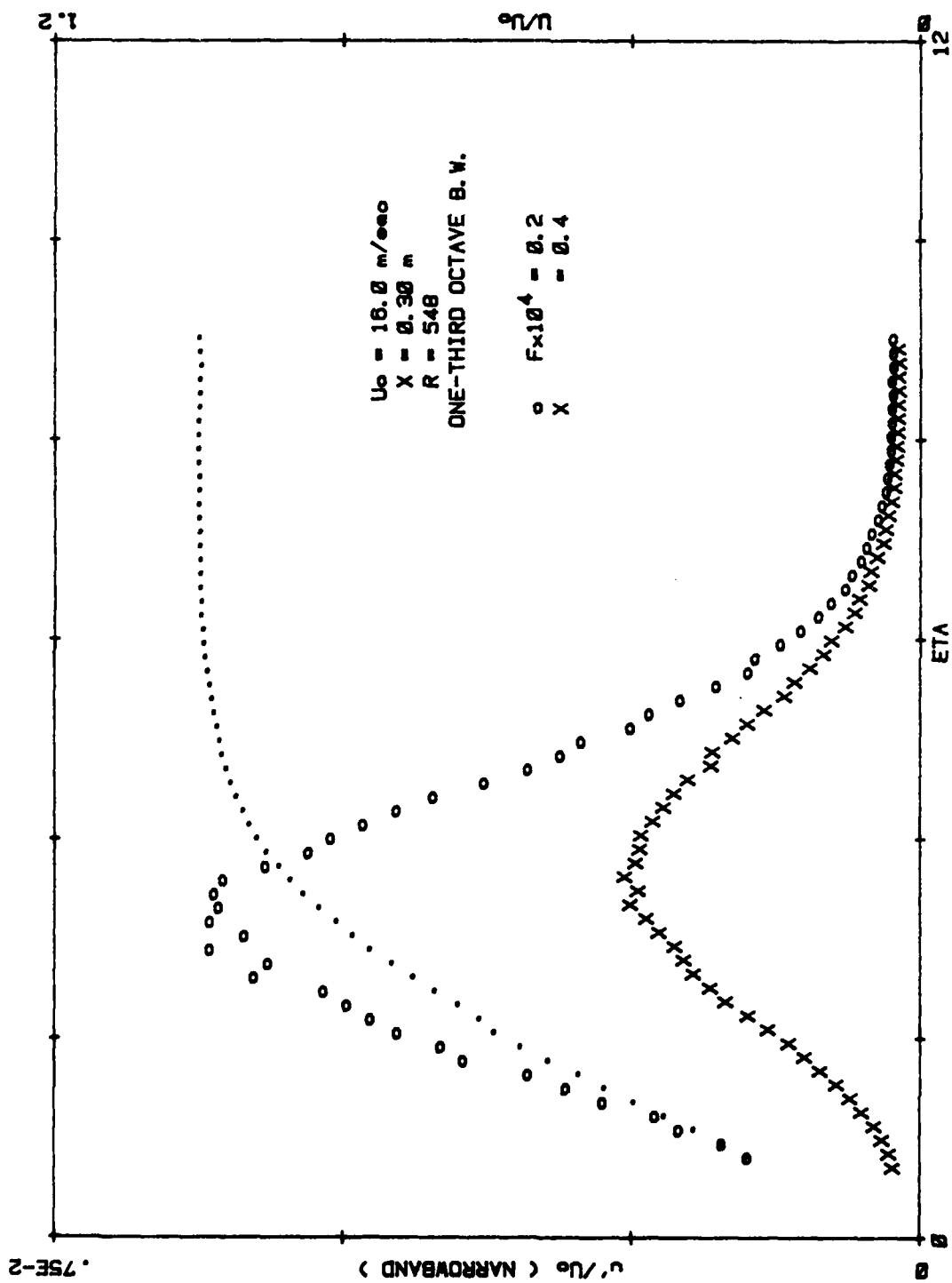


Figure 13a. Narrowband Fluctuation Amplitude in Layer for Two Dimensionless Frequencies

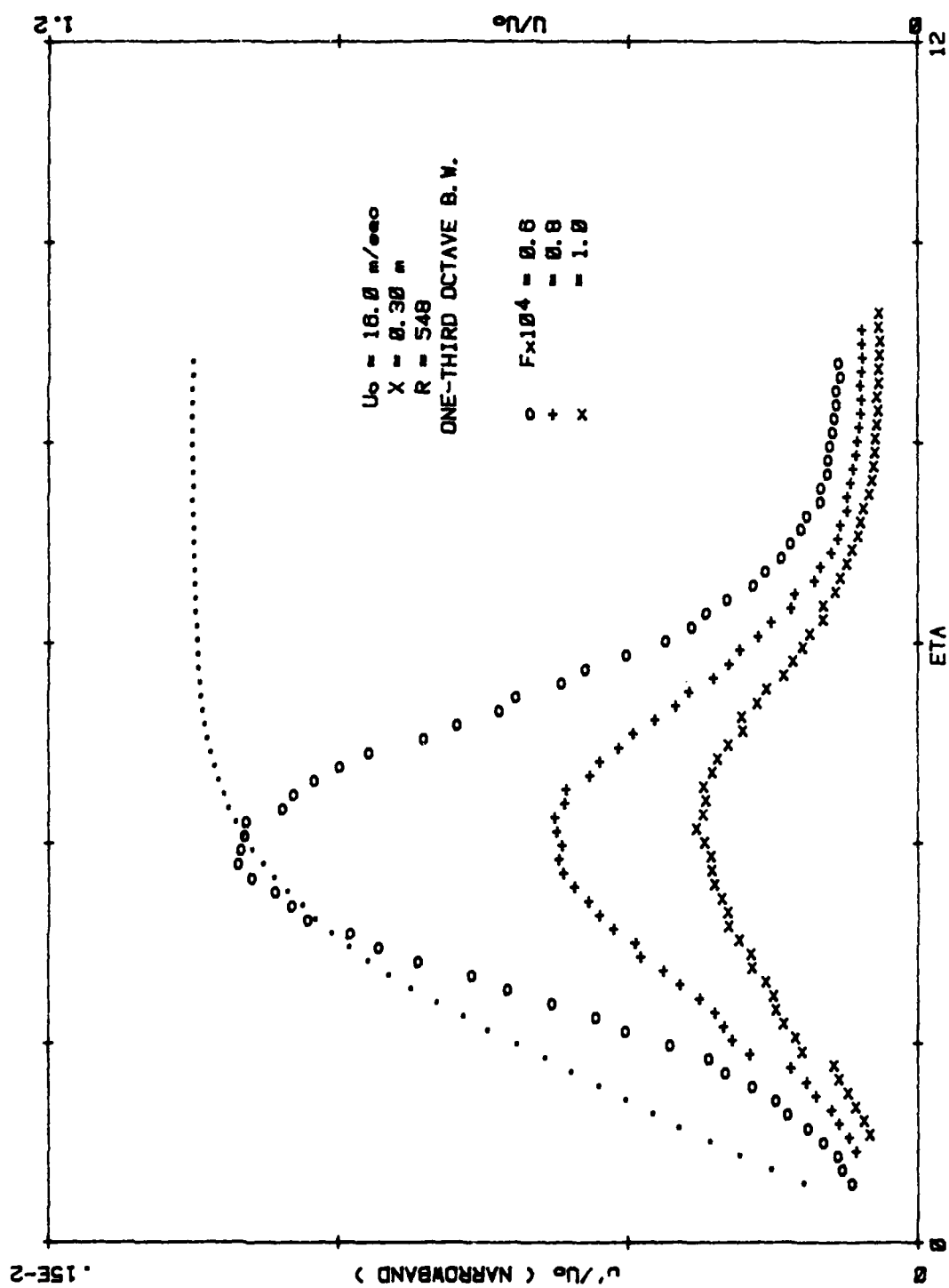


Figure 13b. Narrowband Fluctuation Amplitude in Layer for Three Dimensionless Frequencies

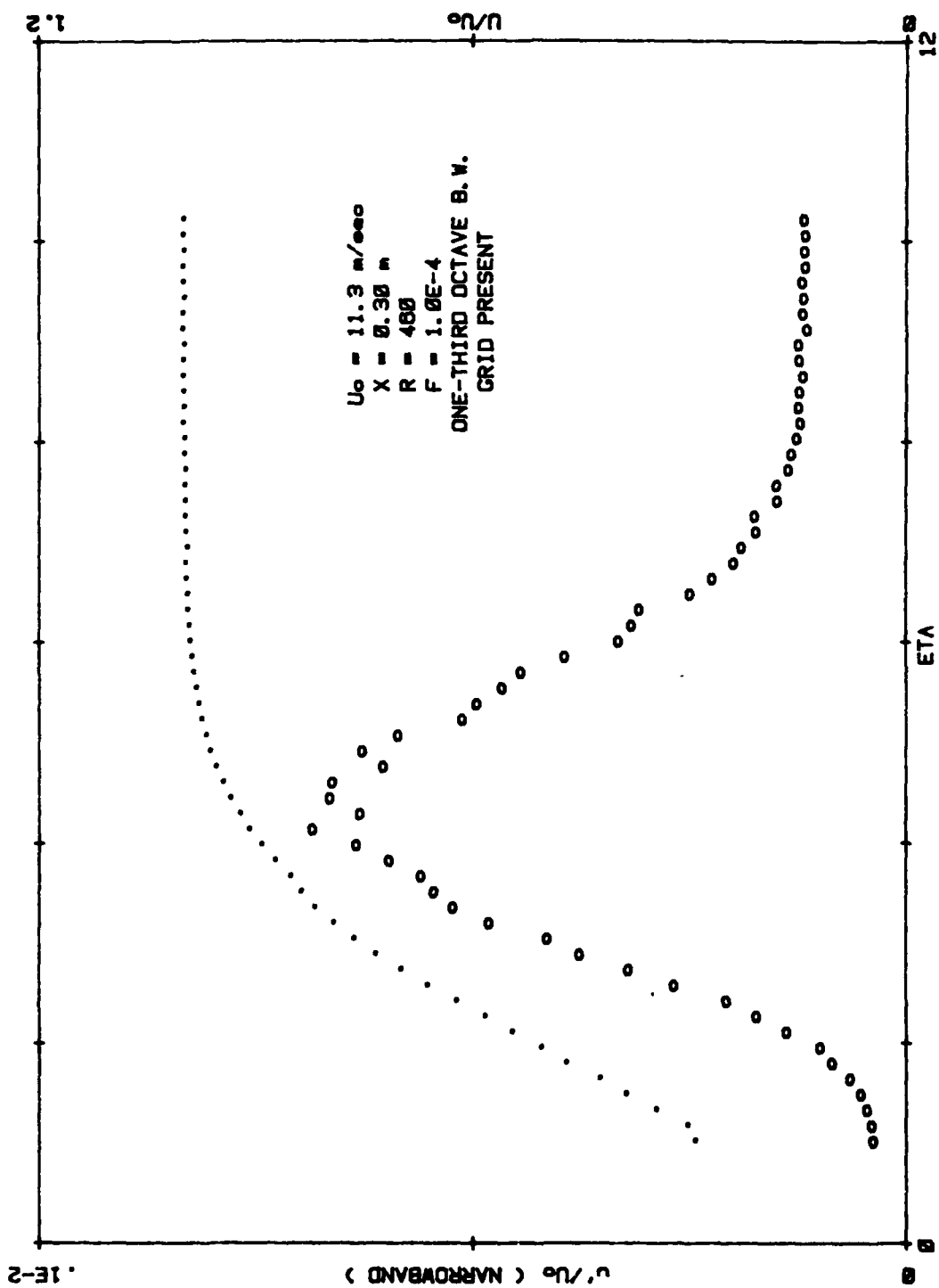


Figure 14a. Narrowband Fluctuation Amplitude in Layer for $R = 460$

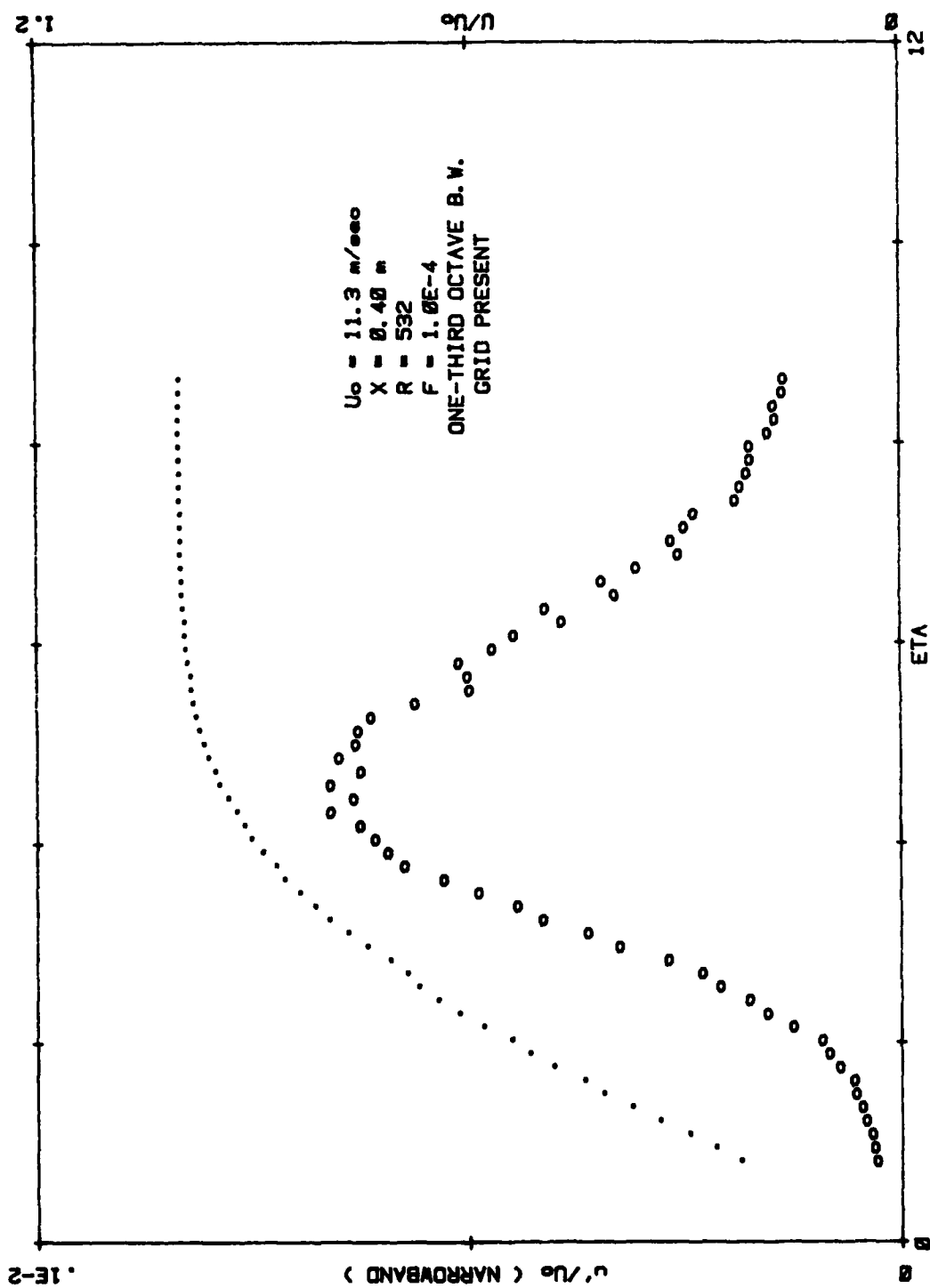


Figure 14b. Narrowband Fluctuation Amplitude in Layer for $R = 532$

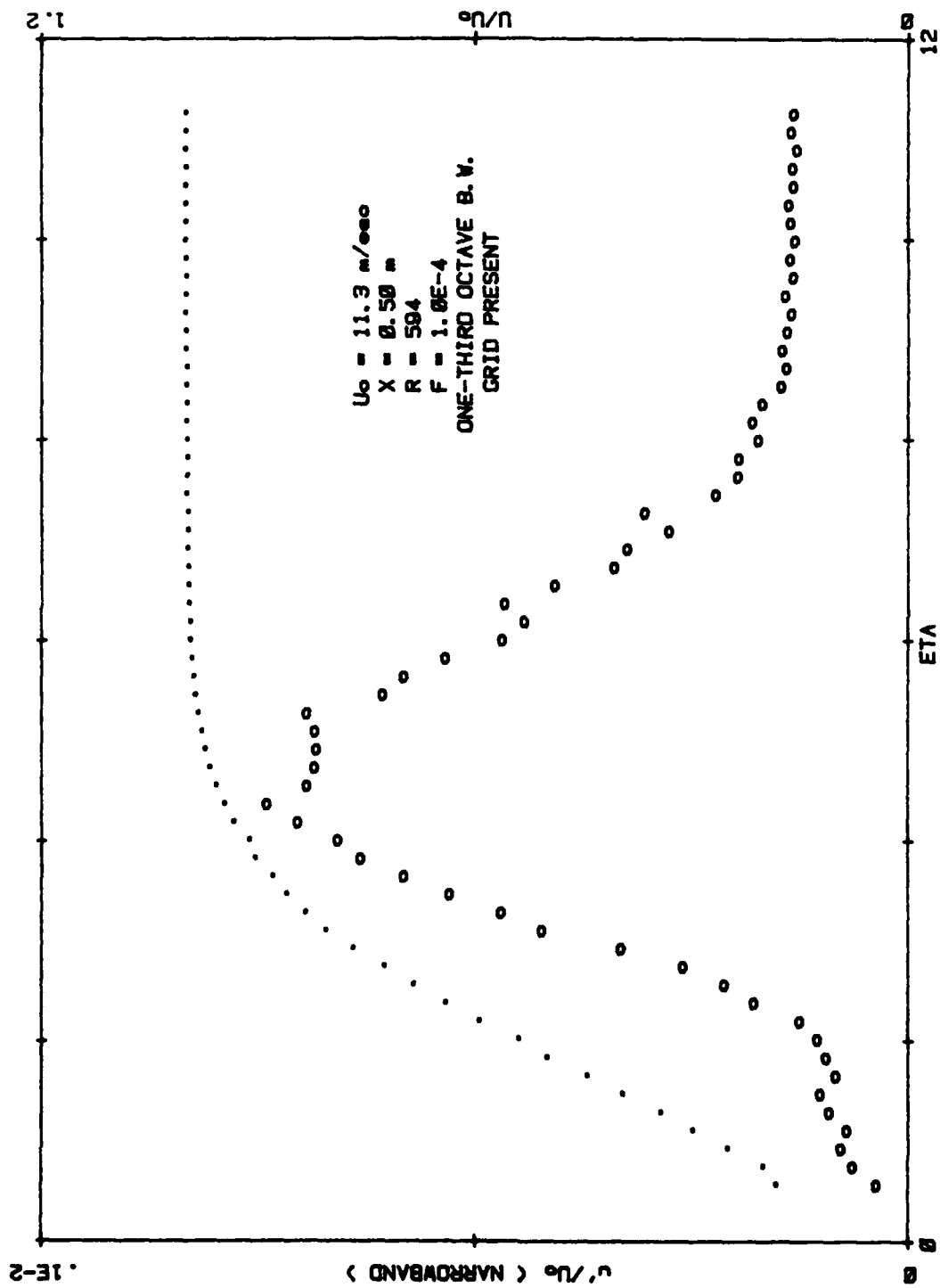


Figure 14c. Narrowband Fluctuation Amplitude in Layer for $R = 594$

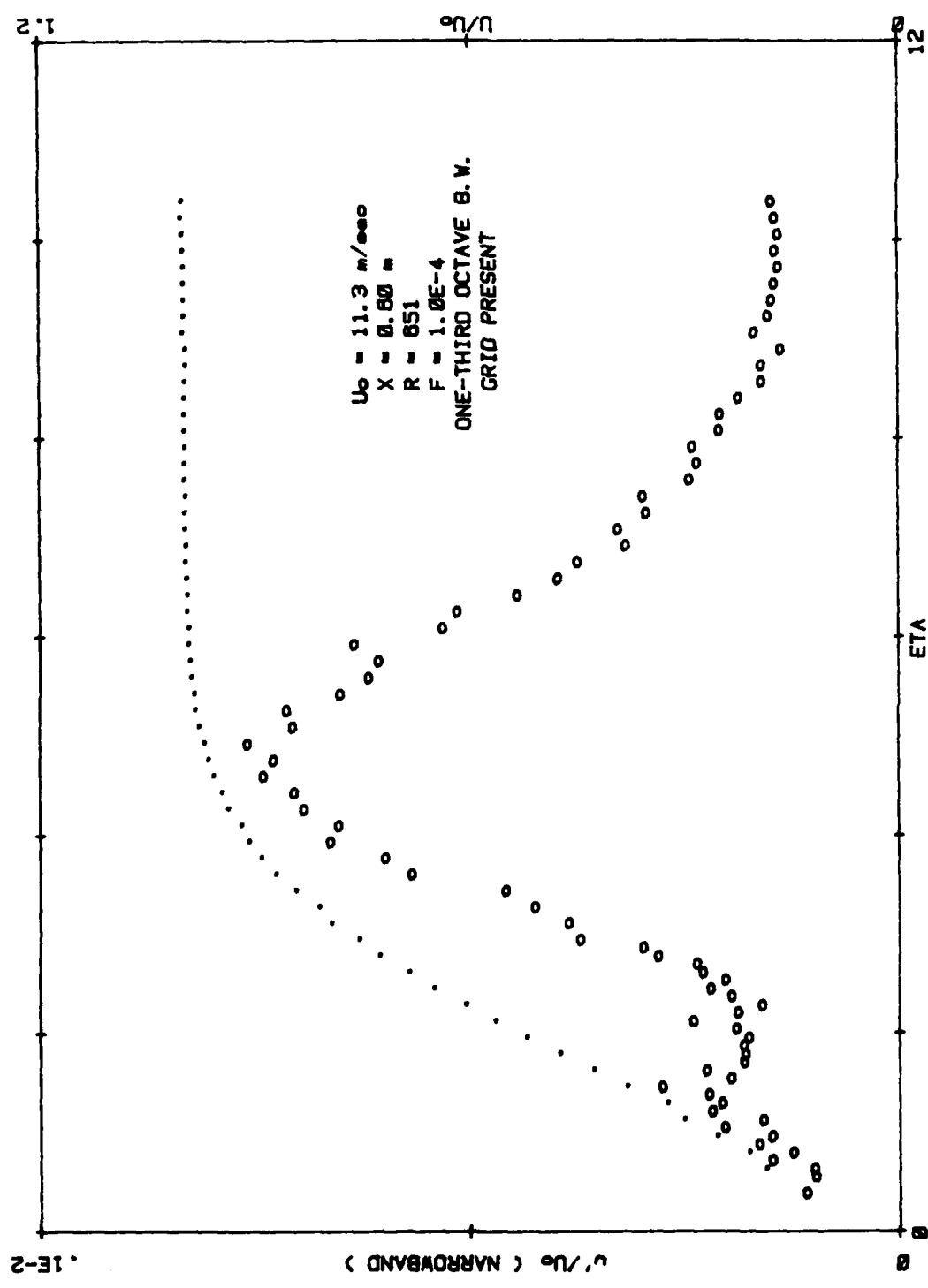


Figure 14d. Narrowband Fluctuation Amplitude in Layer for $R = 651$

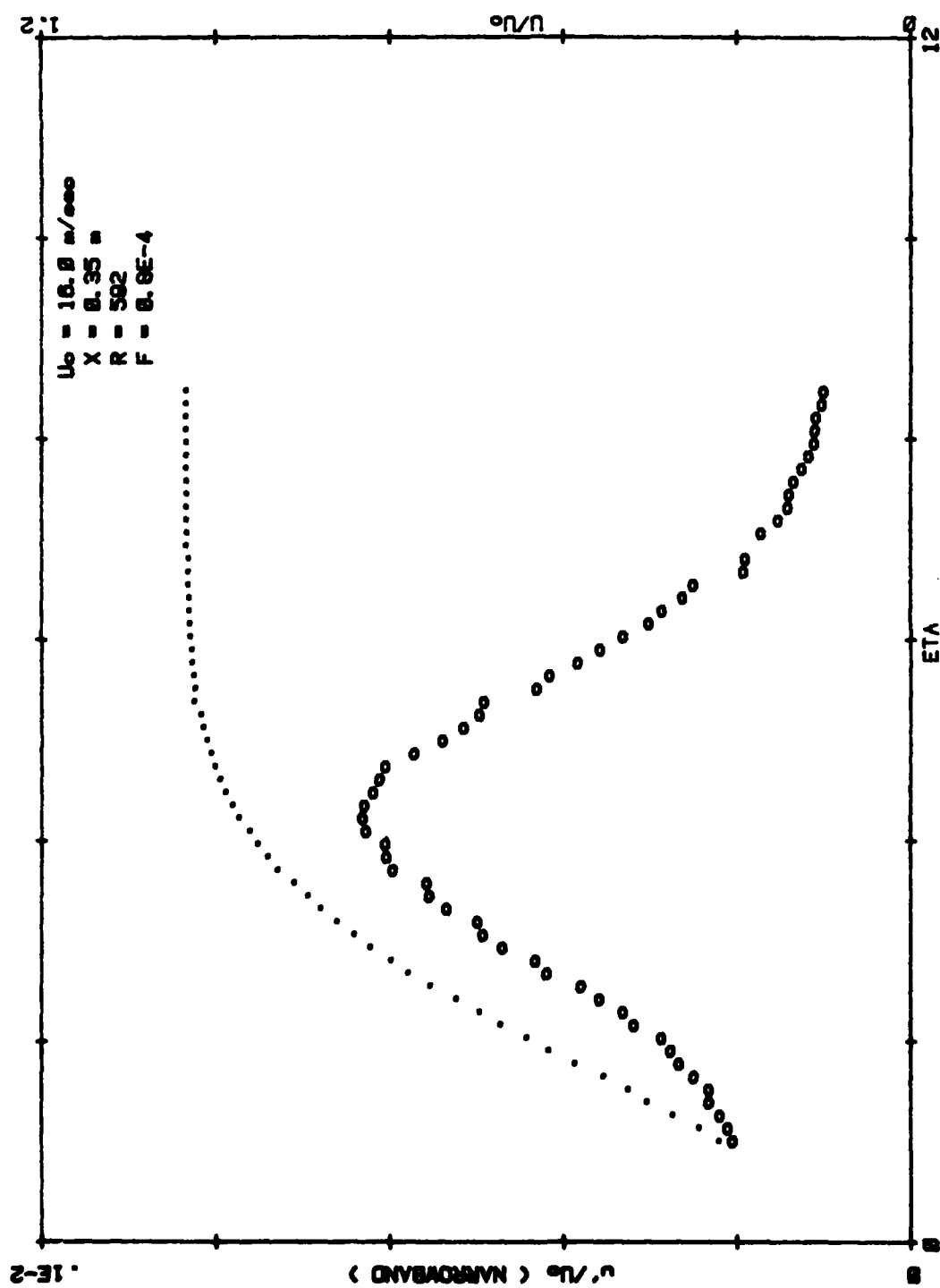


Figure 15a. Narrowband Fluctuation Amplitude in Layer for $R = 592$

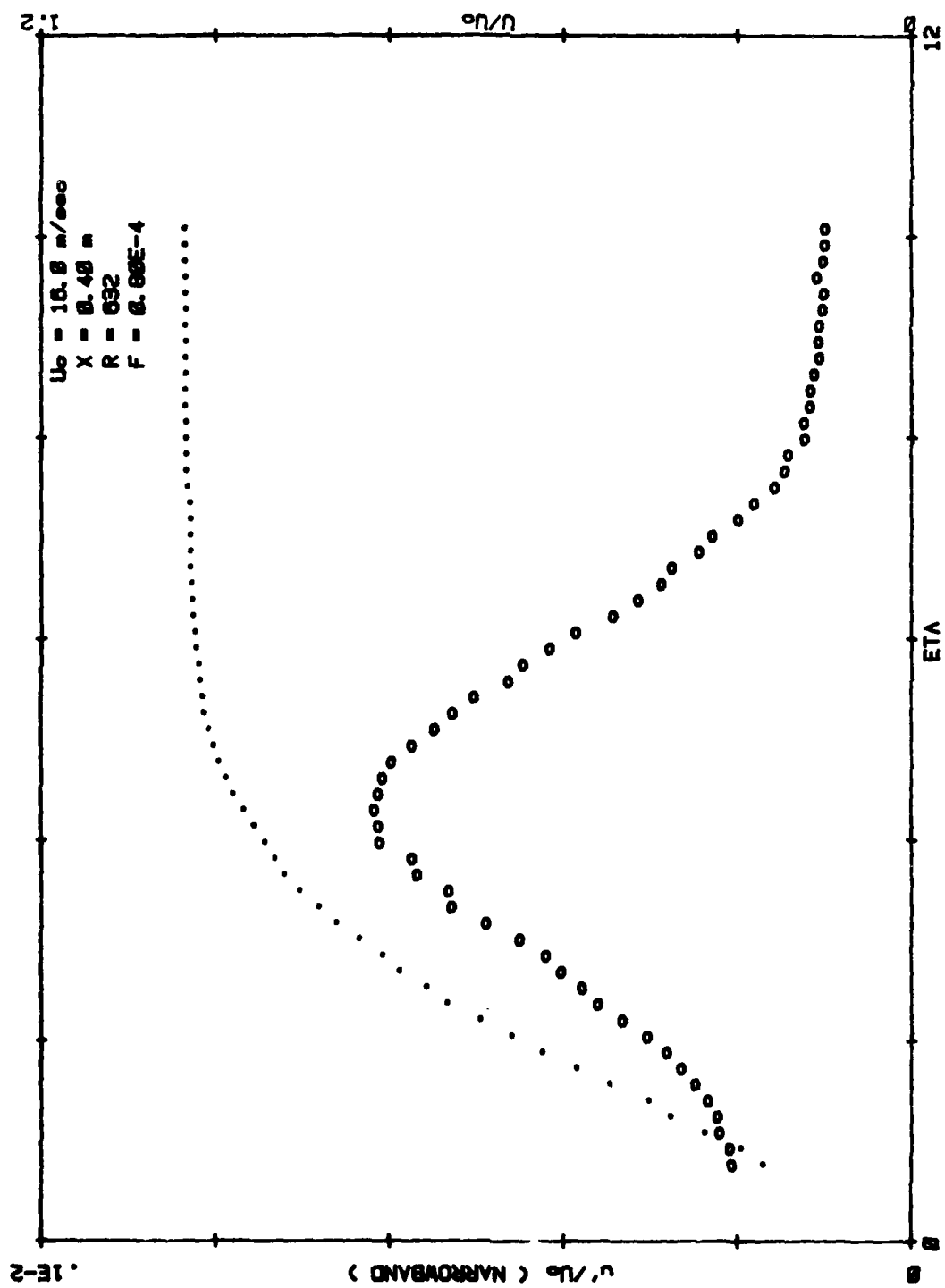


Figure 15b. Narrowband Fluctuation Amplitude in Layer for $R = 632$

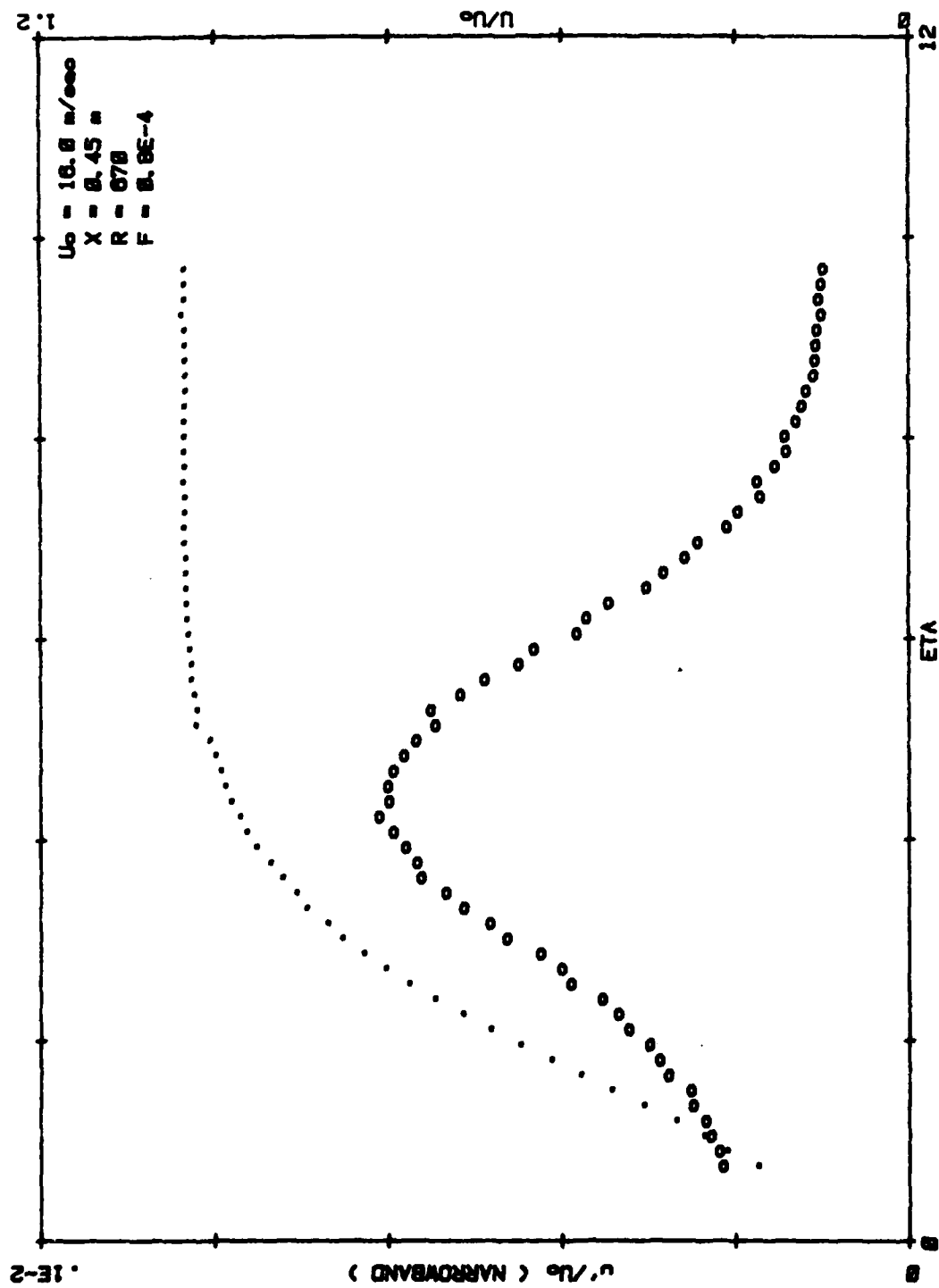


Figure 15c. Narrowband Fluctuation Amplitude in Layer for $R = 670$

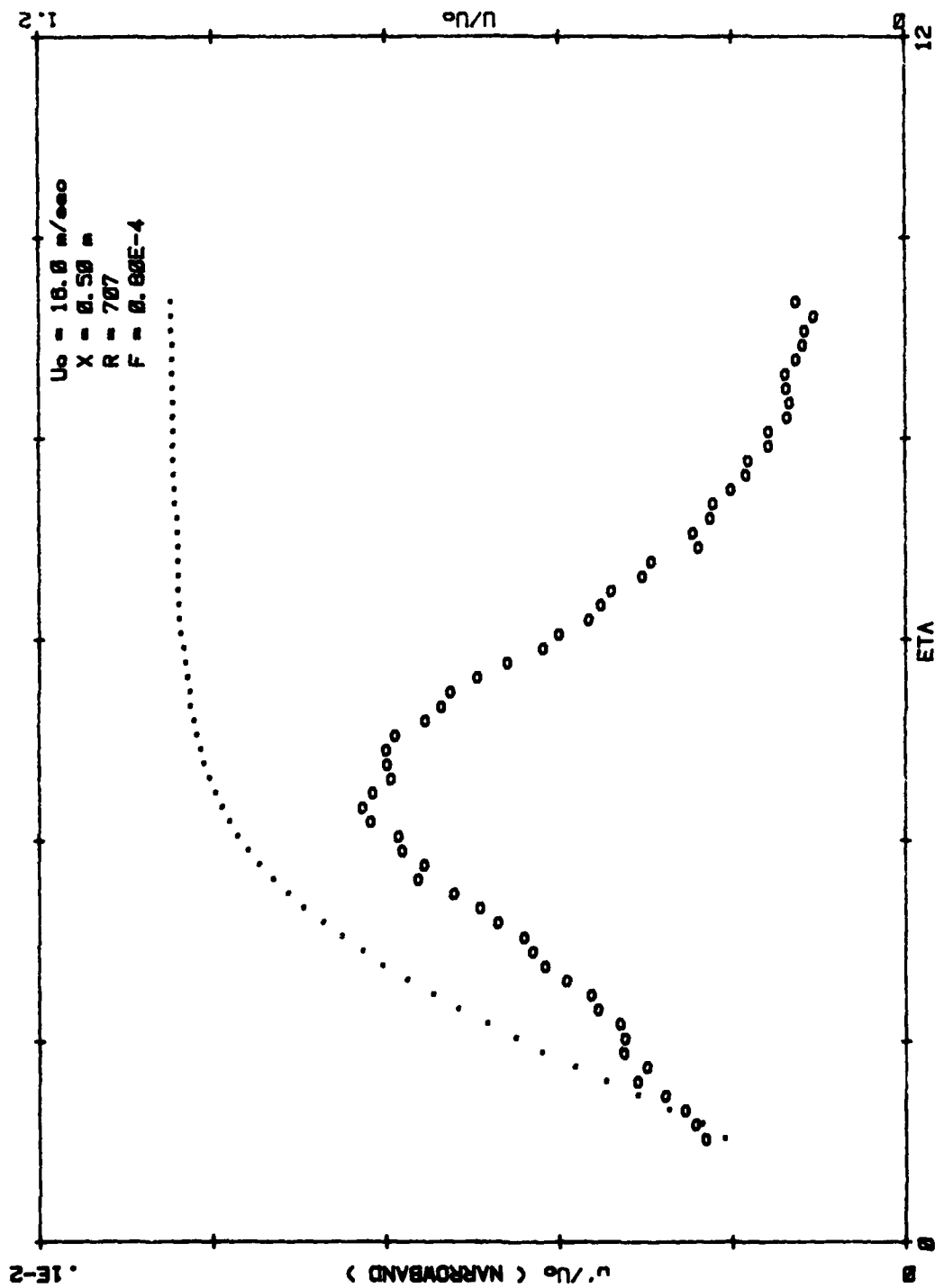


Figure 15d. Narrowband Fluctuation Amplitude in Layer for $R = 707$

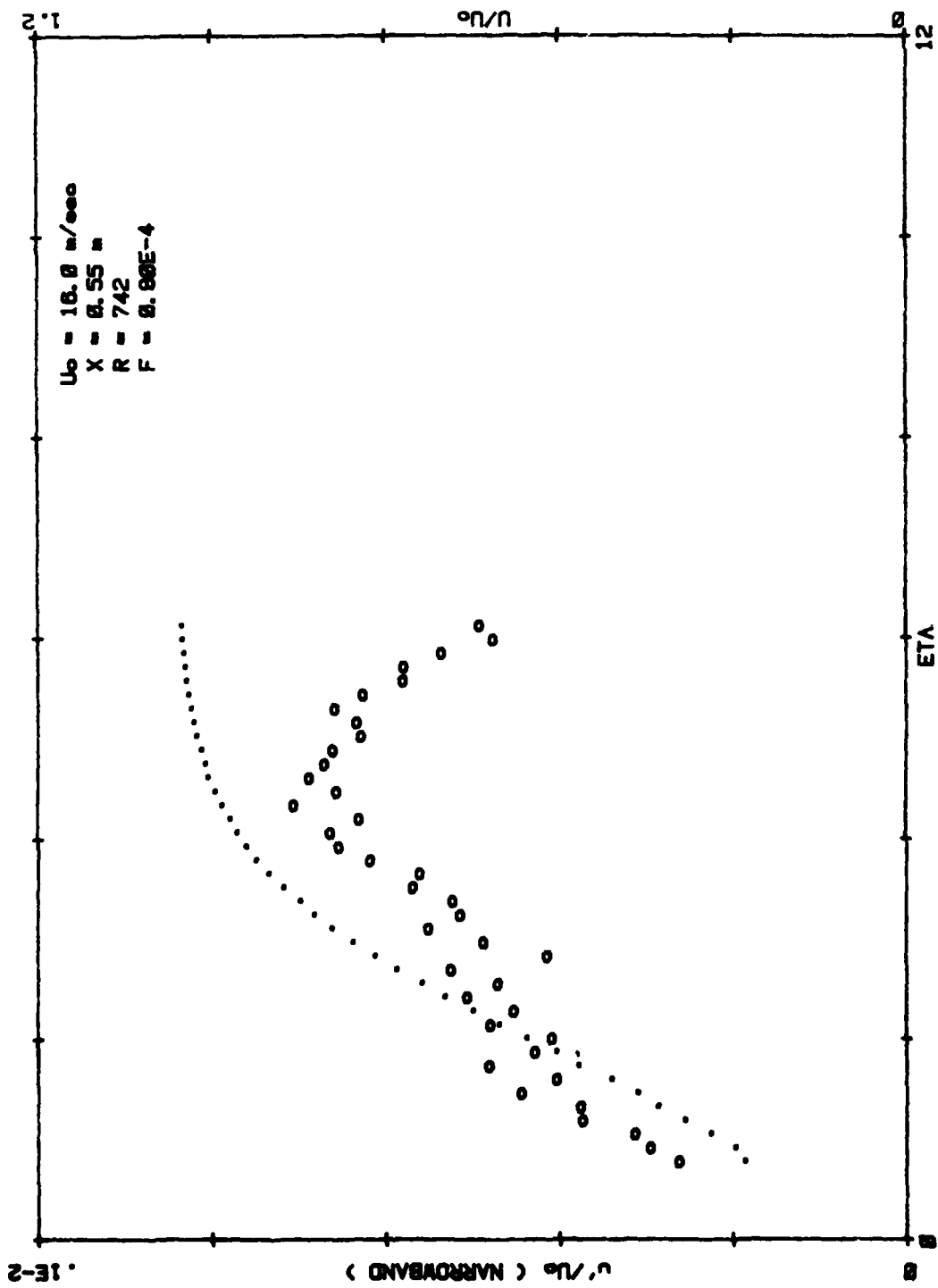


Figure 15e. Narrowband Fluctuation Amplitude in Layer for $R = 742$

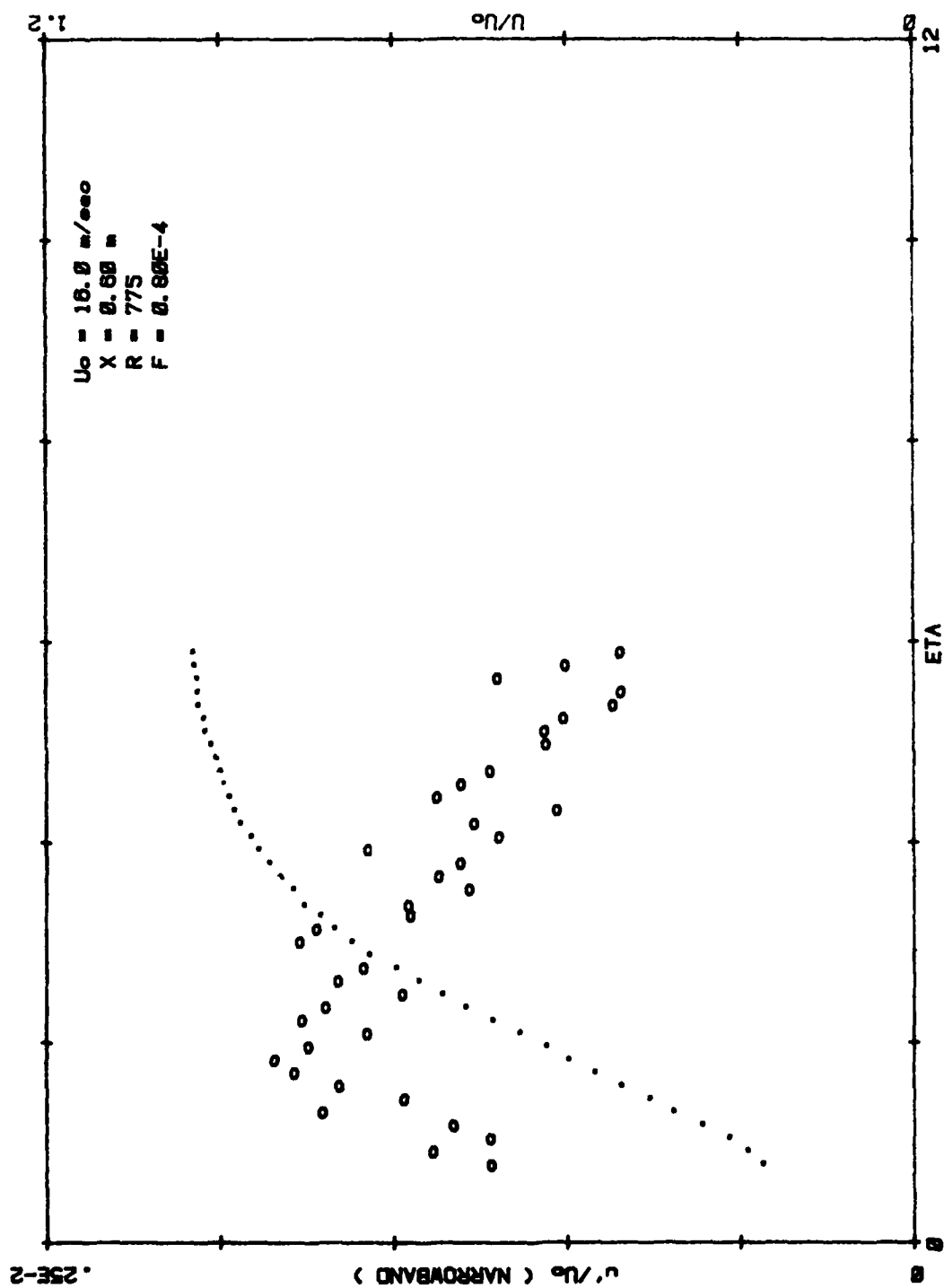


Figure 15f. Narrowband Fluctuation Amplitude in Layer for $R = 775$

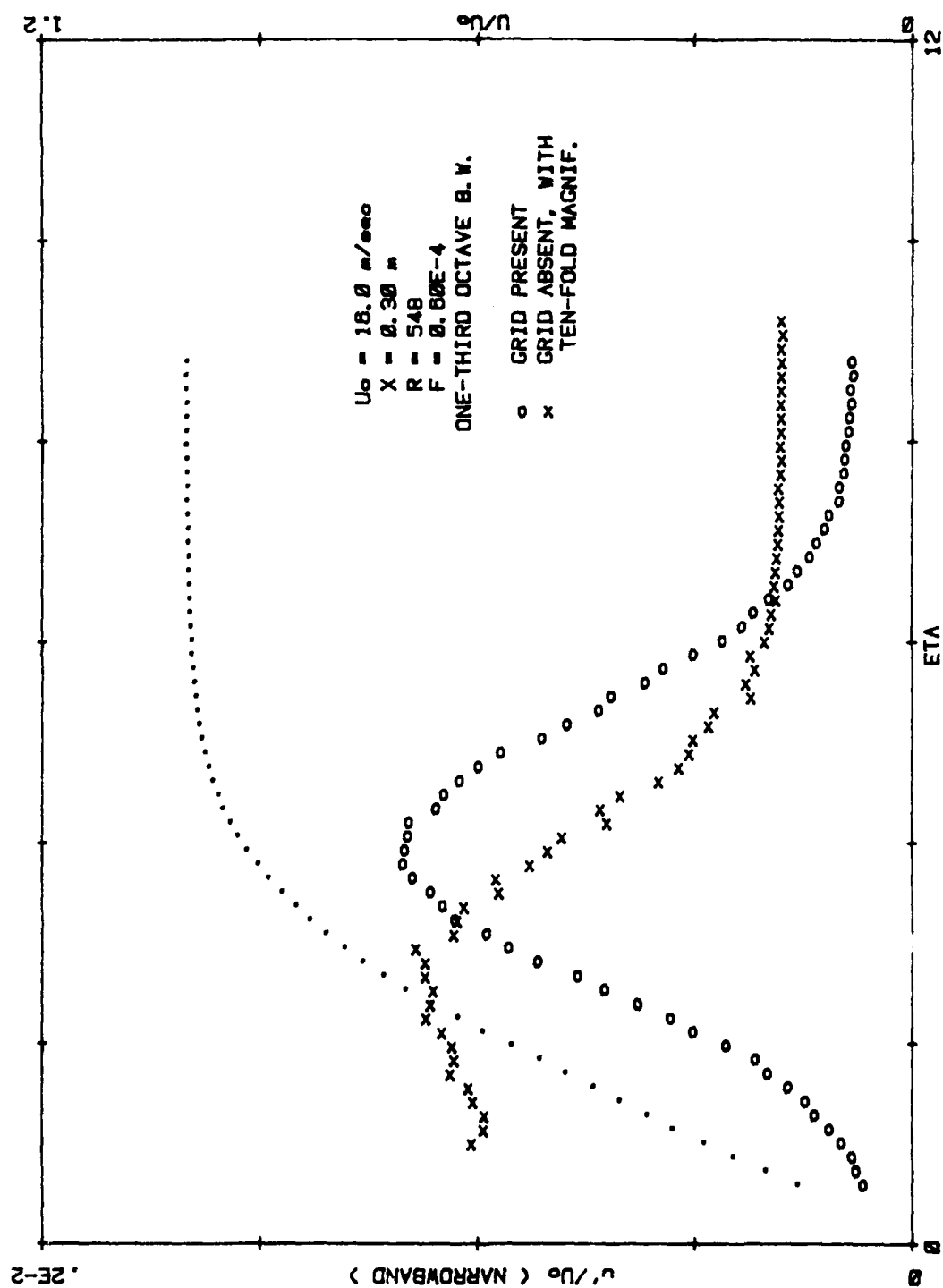


Figure 16. Narrowband Fluctuation Amplitude in Layer with Grid Present and Absent

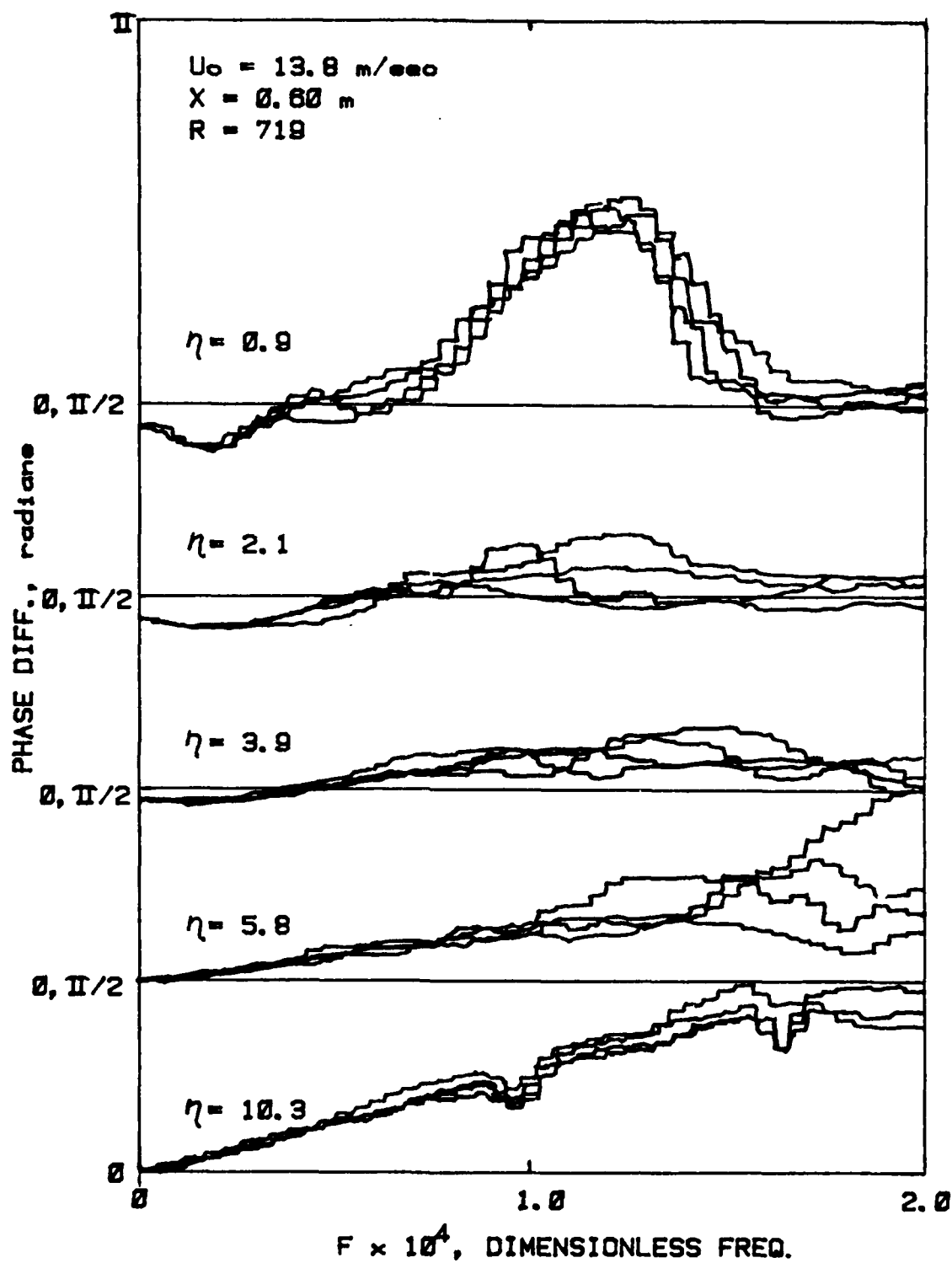


Figure 17. Measured Phase Difference at Several Stations Through the Layer

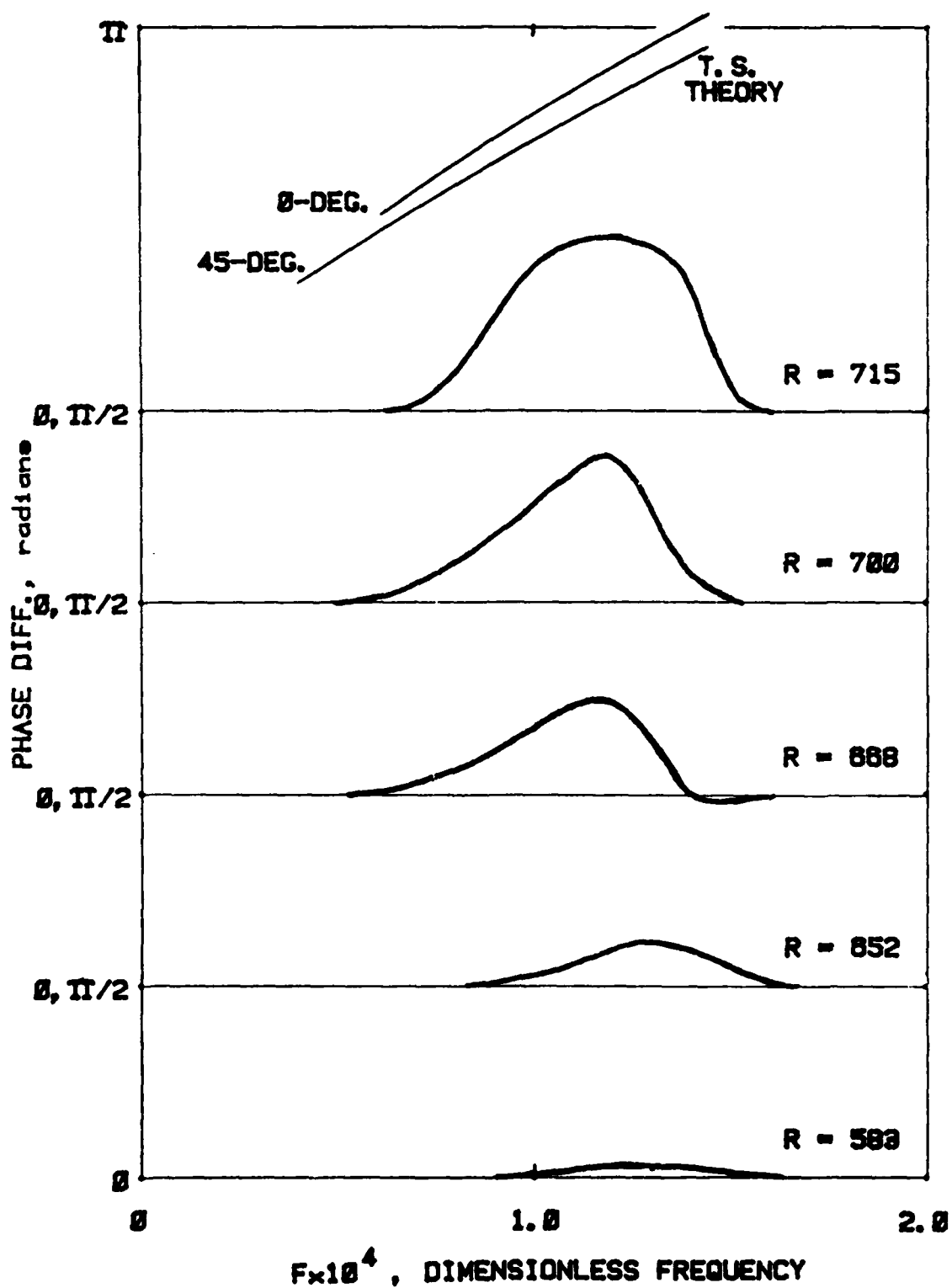


Figure 18. Measured Phase Difference at Vertical Location Near T-S Peak for Several x-Stations

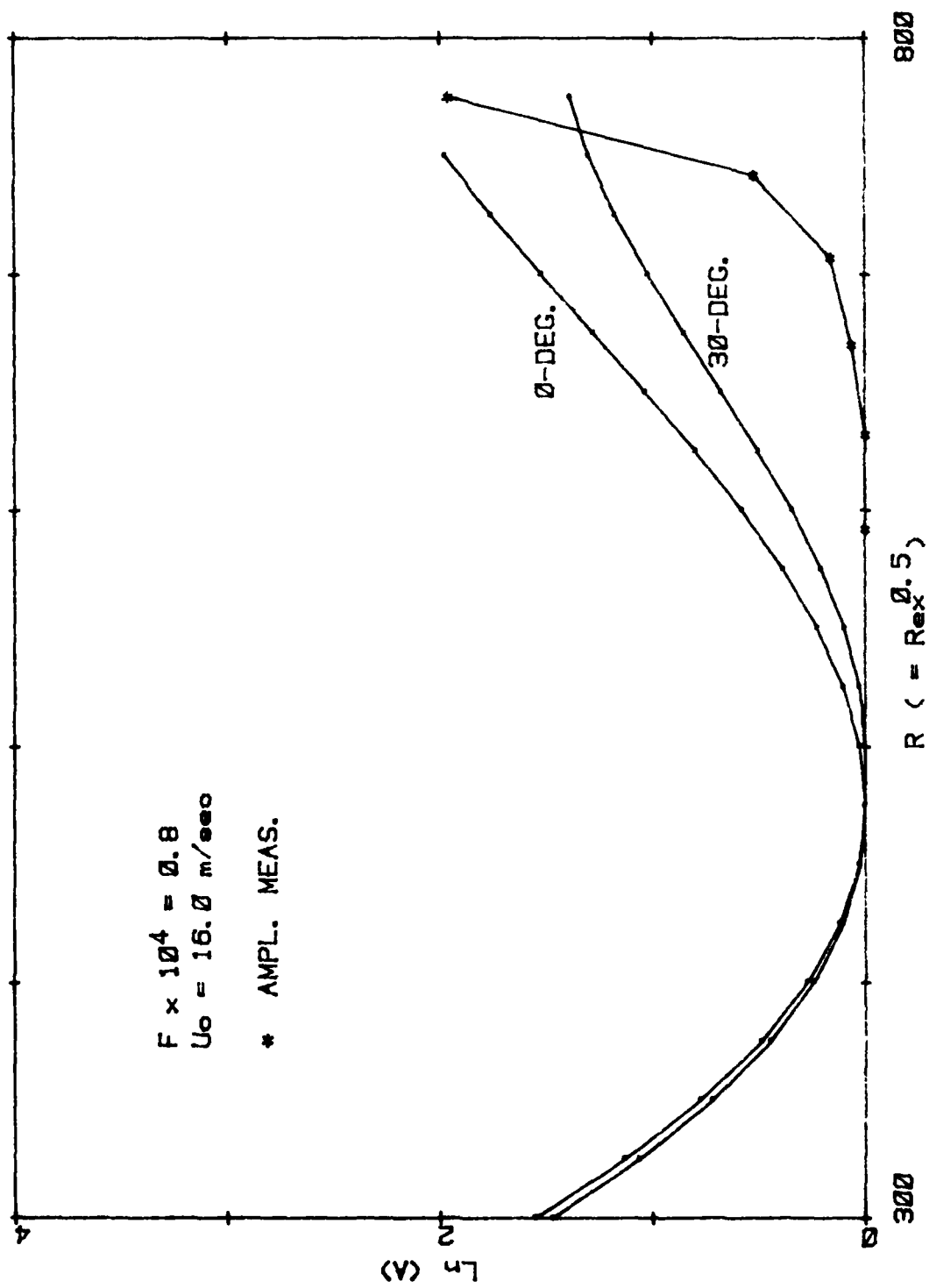


Figure 19a. Theoretical and Measured Narrowband Fluctuation Amplitude Versus R for $F \times 10^4 = 0.8$

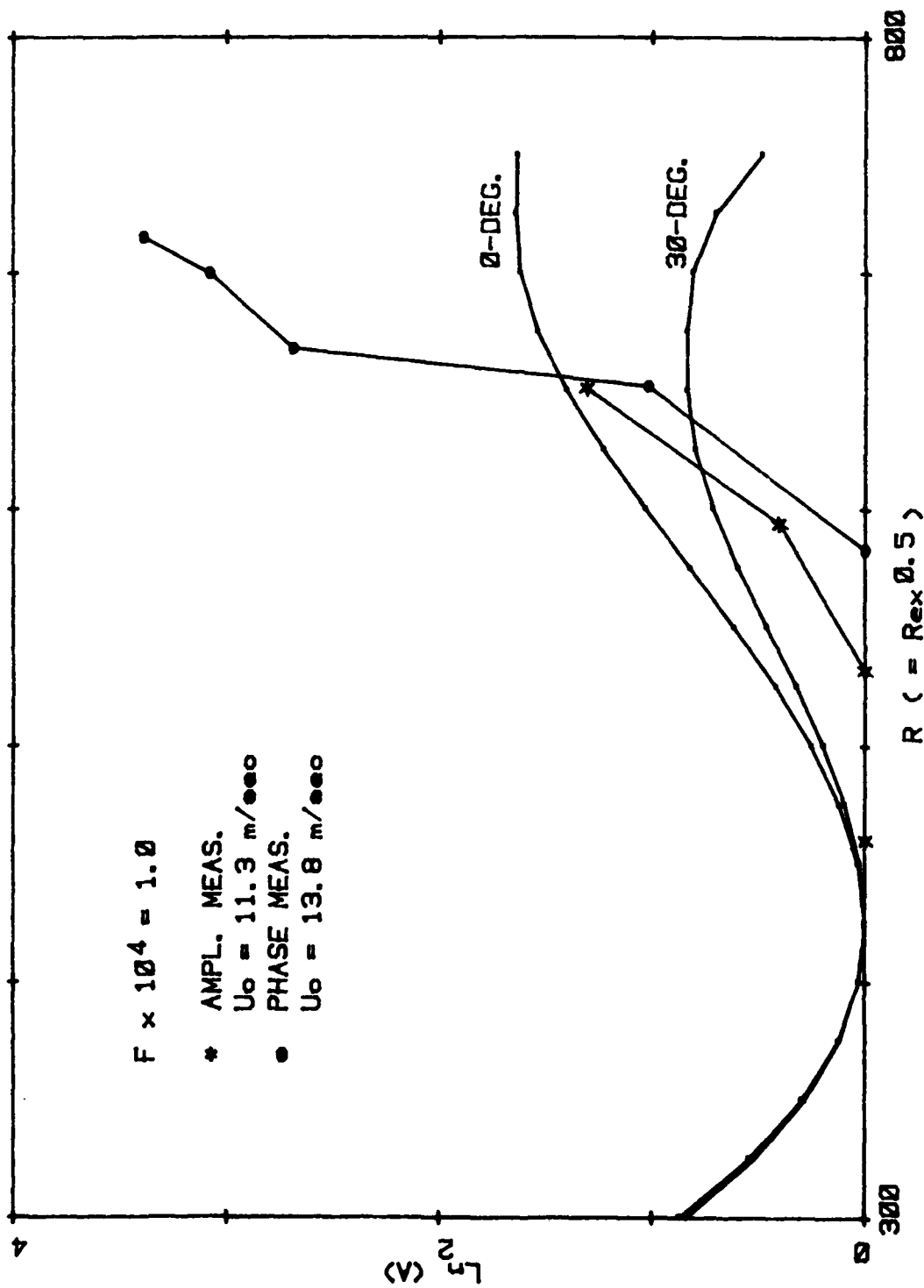


Figure 19b. Theoretical and Measured Narrowband Fluctuation Amplitude Versus R for $F \times 10^4 = 1.0$

PART II: LAMINAR BOUNDARY LAYER DISTORTION BY
SURFACE ROUGHNESS; EFFECT UPON STABILITY

SECTION I

INTRODUCTION

Surface roughness is one of several factors which strongly influence the location of transition to turbulence upon aerodynamic vehicles. With the development of various linear stability theories, together with the growth in computational capability, it has become both usual and worthwhile to attempt to understand transition phenomena in terms of stability results, and to use these, in turn, for prediction. A central requirement of all stability theories is that the mean flow profile of the layer be specified everywhere. While various programs can yield information about the profile and its dependence upon pressure gradient, heat transfer, etc., the ability to predict the effect of roughness upon the flow profile is limited. Neither the experimental results nor the analytical methods presently available are yet adequate.

The present experiments attempt to supply information concerning the effect of distributed roughness for the case where the roughness height, k , is small compared to the layer thickness, and for Reynolds numbers Re_k , based upon k and the velocity at the height $y=k$, which transcend those for which the presence of the roughness alters the transition location. It is to be emphasized at the outset that the present work is neither a stability experiment nor a transition experiment, but rather is a microscopic investigation of the mean velocity within layers where small roughness is present.

Roughness of the scale considered here is likely to exist in high-unit-Reynolds-number flows where boundary layers are exceedingly thin. It might be supposed that small roughness heights would produce small distortion of the flow, and indeed this is the case here to such extent that complex experimental methods were necessary in order to measure the distortion. That such small perturbations are important is illustrated by a stability-theory result provided by L. M. Mack (private communication) who found that specifying a pressure gradient for an initially-Blasius laminar layer such as to increase the wall friction by one percent increased the most-unstable wave amplification rate by five percent. This increase would be expected to diminish a transition Reynolds number considerably, had one been computed, on account of the exponential growth. Thus, even small roughness may be important. Several review articles relating to the effect of surface roughness on the boundary layer mean flow and to the consequent effect of this upon transition have been presented. Preeminent are the ones by Morkovin¹ and by Sedney², both of which include extensive reference lists. From these it is apparent that three distinct categories of roughness have been studied: 2-D isolated elements, 3-D isolated elements, and distributed roughness. It is worth summarising the principal features of each. Two-dimensional roughness, typified by a linear surface irregularity aligned normal to the external flow direction, constitutes the type which is best understood in terms of underlying mechanisms. Klebanoff and Tidstrom³ showed that, for a Blasius layer in which a circular cylinder with diameter of the order of the displacement thickness was immersed, the element itself did not initiate flow fluctuations; rather, it modified the mean flow profile locally to a form more unstable to the preexisting

fluctuations arriving at the station of the element. It was the flow immediately aft of the cylinder, i.e., the finite-length recovery zone, which was particularly unstable, and which provided a net increase of fluctuation level. The flow about isolated, 3-D elements has been studied by Gregory and Walker⁴, by Tani, Komoda, Komatsu and Iuchi⁵, by Mochizuki^{6,7}, and by Gupta⁸. The flow here is rather different from the 2-D case in several ways. When Re_k is sufficiently low that transition does not occur close behind the element, the wake produced by it is very persistent along the downstream dimension, remaining narrow and possessing a substantial velocity defect for many tens of roughness heights. The flow visualization studies of Gregory and Walker⁴ and of Mochizuki^{6,7} reveal the existence of two vortex pairs which extend downstream within the wake. One of the pairs originates upstream of the protuberance in the form of a horseshoe, while the other is induced by the separation zone behind the element. Velocity measurements have been made in the wake by means of hot-wire anemometry by Tani et al⁵, by Mochizuki⁷, and by Gupta⁸. An important consequence of the vortical system evident in these experiments is a vertical transport of momentum. Mochizuki's experiments showed with great clarity that as Re_k was increased beyond about 300, the wake spontaneously became unsteady, and executed a large-amplitude, laminar oscillation. Transition did not then ensue in consequence, but as Re_k surpassed about 600, a wedge of turbulence centered upon the wake formed far downstream, and moved rapidly closer to the element with increasing Re_k . This observation is consistent with the results of the other experiments as well, including the earlier one of Von Doenhoff and Horton⁹, wherein the effect of sandpaper roughness upon transition was determined by means of hot-wire anemometry. There, transition was unaffected for $Re_k < 600$, whereas it moved to the first location of roughness for values above this level. The practical effect of a 3-D protuberance is that transition either is induced at the element, or is not greatly affected by it.

Distributed roughness may be defined as an assemblage of 3-D elements of various heights and spacings disposed about a surface. Although it is not an essential feature, present interest is directed toward the case in which both the height and spacing are small in comparison to the boundary layer thickness. A more essential restriction is that the Re_k of the elements be below that which induces transition at the element, i.e., below about 600. Distributed roughness transition data for incompressible flow are provided by Feindt¹⁰ and by Achenbach¹¹. Feindt's measurements included the effect of a systematic variation of the pressure gradient, including both positive and negative values. For values of the Reynolds number based upon free-stream velocity, rather than upon that at the top of the element, below about 120 the transition location equalled that on the fully smooth surface, while for higher values the location moved progressively forward. A shortcoming of the Feindt experiment was that the turbulence level of the airstream was rather high, and consequently, the zero-pressure-gradient transition Reynolds number was several-fold lower than that achieved in many experiments. A current view provided by this experiment is that a surface must be polished such that Re_k not exceed 50, approximately, if the highest possible high transition Reynolds numbers are sought.

The measurements by Achenbach were made using a circular cylinder in cross-flow as the test model, according to which the pressure gradient was everywhere favorable except near separation. The boundary layer properties for this experiment have been computed by Merkle, Tzou, and Kubota¹², from which it is

learned that the roughness size utilized was for most conditions larger than the momentum thickness of the layer. Owing to the stagnation of the flow at the front of the cylinder, the values of Re_k were low there, and transition occurred no farther forward than 10° from the axis.

A recent experiment which paralleled the present one to some extent has been described by Reshotko and Leventhal¹³. There, the mean profile above a sandpaper-covered surface which supported an initially-Blasius layer was measured, and the flow-fluctuation development was studied. The results indicate that the Blasius profile was displaced outward from the wall without other apparent modification, and that the low-frequency fluctuation growth, rather than the Tollmien-Schlichting frequency growth, was increased substantially. Transition to turbulence was moved forward, as expected.

A number of analyses of the effect of roughness have appeared. The one by Merkle, Kubota, and Ko¹⁴, pertaining to distributed roughness, has attracted considerable attention. A more recent version of this is given in Ref. 12. It is hypothesized that the roughness induces flow unsteadiness near the wall, i.e., produces a turbulent sublayer beneath the laminar flow, and that this alters the momentum transport, thereby enhancing the Tollmien-Schlichting instability. Through suitable adjustment of the free parameters incorporated within the model, predicted transition locations agreed with certain experimental results. A more basic analysis of the distributed roughness problem has been carried out by Singh and Lumley¹⁵. Hoffman and Lumley¹⁶ found an unfavorable comparison between results of this analysis and certain ones obtained by use of the method of Refs. 12 and 14. However, they pointed out that the analysis was not applicable in cases where the wall slope was steep, such as for sand-grain roughness. Finally, Smith, Sykes, and Brighton¹⁷ have employed triple-deck analysis to analyze the flow close behind a low surface protuberance. Merkle *et al*¹² have utilized this analysis to consider the effect of surface waviness on the mean flow profile.

SECTION II

EQUIPMENT AND TECHNIQUES

The experiment was conducted in a low-turbulence wind tunnel 2.0m-long by 0.35m-wide by 0.60m-high which provided a free-stream fluctuation level below 0.1% over the speed range 0 to 30m/sec. The lateral walls of the tunnel were adjusted such as to yield a static pressure which was everywhere equal to the ambient room pressure to within one percent of the dynamic pressure. The turbulence level and pressure gradient of the tunnel are described further in Part One. The test plate, 1.5m-long by 0.6m-wide, was constructed with an elliptical leading edge, and was mounted vertically between the floor and ceiling of the flow channel. It was composed of acrylic plastic in order to allow machinability and to provide a surface finish of optical quality. Hot-wire probes were supported upon a three-axis, computer-controlled traverse mechanism whose resolution was 0.001 inches (0.0025cm). A useful option of the software controlling the traverse provided the ability to maintain the sensor height (the dimension normal to the plate) such as to follow a constant velocity layer as the probe was swept along either the streamwise or lateral direction. The traverse was located below the tunnel; a strut which held the flow sensor extended into the channel through a slot in the tunnel floor.

All flow measurements except those of static pressure were made by use of hot-wire anemometry. Two probes were used principally: the active length of one was 0.25 mm, while that of the other was 1.5 mm. The shank of each was 1.25mm-diam by 5 cm long. The first of these was appropriate for measuring the lateral variation of velocity in the narrow wake behind a 3-D element. The longer sensor length of the second probe formed a lateral average of the velocity when measuring the distortion produced by distributed roughness elements. The probes were operated by means of a Thermo-Systems, Inc. 1050-Series hot wire set. Owing to the close proximity of the sensor to the wall in these tests, a preliminary evaluation of error due to heat loss to the wall was conducted by drilling a 6.35mm-diam. hole in the plate surface and then covering this with 10-micron aluminized Mylar. It was found that for the flow speeds utilized, wall loss was not important.

Hot wire linearization and calibration were carried out with the aid of an Interdata (Perkin-Elmer) Model 70 computer system which was utilized also to control all aspects of the measurement sequence and for data reduction. This system incorporated a 10-bit high-speed ADC (analog-to-digital converter) which digitized the amplified hot-wire signal in bursts of 2048 samples. The digitization rate was typically set to 5000/sec. For calibration, the sensor was placed in the tunnel free-stream, and for each of many flow speed settings the wire output was measured. The response was represented analytically using the least-squares method, and a look-up table was generated. This converted each possible output code of the ADC to the equivalent velocity. The software also formed the mean and the variance of the 2048-sample ensembles. Three types of surface roughness were tested. The first type was a single 3-D element, wherein a 0.75mm-diam cylinder protruded through a hole in the plate into the airstream by a length 0.37mm, designated as the roughness height, k . This "grit" was attached to the armature of a miniature electric solenoid mounted on the rear side of the plate. The activation of the solenoid under program control caused the grit to retract flush with the plate surface. The purpose of this is described below. The second consisted of #80 abrasive which was applied to a surface prepared by coating with water-base adhesive. The surface was held oblique while the grit was sprinkled in order to improve the spatial uniformity of the grit density. The third type of roughness consisted of a two-dimensional array of 0.30mm-diam. glass beads affixed to the plate on a square-grid pattern 0.62mm on a side and aligned 45° to the flow direction. This test surface was prepared by applying contact adhesive to the surface, laying a 40-mesh wire screen over this, brushing a supply of loose beads about the screen such as to admit one bead into each pore, and removing the screen with care. Because the velocity perturbations to be measured in the case of the single roughness-element wake were of very small magnitude, signal averaging techniques were necessary for accuracy. By measuring the velocity at a specific point with the grit alternately present and absent, small differences could be determined reliably. It was necessary, of course, to allow time for the flow to become established after activation of the grit, and tests were conducted to determine such requirements. Four ensembles of 2048 digitizations were obtained for each half of the grit-present/grit-absent cycle. The number of cycles was adjusted as necessary to values between five and 80, the latter number being required for velocity measurements far behind the element. A profile of 50 measurement points of 80 ensembles each, for example, required more than four hours, but involved no operator attention. Signal averaging was also employed in the distributed roughness case, i.e., for the #80 abrasive and for the bead array. This type of roughness could not be

retracted into the plate, but instead was applied to a rectangular area of the surface of a 20cm-diam. turntable which was set into the test plate flush with the surface. Motor-driven rotation of the turntable through 180° under program control caused the grit to be transported away from the area where it could influence the measurement. On account of the larger perturbation caused by this type of roughness, five ensembles sufficed in most cases.

The hot-wire data thus acquired included the mean velocity for both the grit-present and -absent conditions, the variance for each of these velocities, and the standard deviation of the difference of the two mean velocities. These were stored in disk files for analysis and display as appropriate.

SECTION III

RESULTS

1. TYPES OF RESULT; FORMAT OF PRESENTATION

It was reasoned at the outset of the experiment that small roughness would produce a small distortion of the flow, and that it might be possible to describe the perturbation due to distributed roughness as a sum of the contributions of the individual elements which make up the roughness field. That is, that linear superposition might be useful in obtaining an understanding of distributed roughness effects. Accordingly, the measurements to be described consisted of studies of the wake of a single element, of the interaction between the wakes of two elements in proximity, of the interaction of the wake of one element with the wakes of a multitude of other elements, and finally, of the distortion due to distributed roughness.

In carrying out these experiments, it was found that the variance of the velocity with respect to its mean, which represents the flow fluctuation, did not increase significantly in the presence of roughness. This quantity was therefore not analyzed further. All results to be presented pertain to the station $x = 0.6$ or 0.7 m, a region chosen in preference to a more aft one in order to permit the attainment of higher values of Re_x . Preliminary results at $x = 1.3$ m indicated that the profile there was also represented by the Blasius theory, and that transition did not occur on the plate.

In all cases the velocity defect produced by the roughness under test is presented, and, except for the distributed roughness case, the profile of the velocity itself is omitted. The defect is the difference in velocity between the smooth-wall case and that in the presence of roughness. It is to be understood that in the absence of the latter the profile was described accurately by the Blasius theory, so that the defect represents the departure of the profile from this when roughness was present.

2. SINGLE-ELEMENT RESULTS

As explained below, the single-element perturbation field may be classified into near-wake and far-wake regions. Fig. 1 presents the centerline-profile of velocity defect within the inner one-fourth of the layer for four near-wake stations, and for a particular value of Re_x . η is the co-ordinate y/x times the square-root of the x -Reynolds number. It is seen that the defect is everywhere of positive sign, that it increased from a zero value at the wall with positive

second derivative, that it attained a maximal value at a location slightly above the crest of the element, and that it declined to a small proportion of this value at $\eta = 1.5$. The defect continued to decline in the region $\eta = 1.5$ to 6.0, not shown, and was zero at that outer limit. Other near-wake profiles for values of Re_k between 25 and 135, obtained in less detail and not shown, were similar in shape to those given, with the peak defect occurring near the height of the element crest for the near-wake region.

Fig. 2 displays the lateral variation of the normalized velocity defect at four stations which fell within both the near-wake and far-wake regions. Owing to the narrowness of the near wake, a numerical deconvolution program was utilized to estimate the error due to the use of the small, but finite-sized, hot-wire probe in surveying this region. It was found that for the forward-most profile of Fig. 2, the maximum error occurred at the centerline, and that this amounted to less than five percent. This level of accuracy was considered satisfactory, and no correction for probe size was applied to the defect amplitude data, which are given later.

The differing character of the two upstream profiles from the downstream ones constitutes one indication that the boundary separating the two regions lay between the stations $\Delta x = 12$ and 40, where $\Delta x = x - x_k$. The figure shows that the centerline defect became negative beyond this boundary, probably as a consequence of two effects. First, the near-wake amplitude diminished rapidly behind the element, as in Fig. 1, and second, the vortical system mentioned in Section I, and described below, remained of nearly constant strength along the streamwise dimension. This system induced a downward flow of faster-moving fluid at the centerline and an upward flow of slower fluid at off-axis locations.

The profiles of Fig. 2 were obtained in each case by traversing the sensor laterally at the constant height for which the centerline defect was of maximum magnitude, whether positive or negative. The heights of maximum defect for the stations $\Delta x/k = 4$ and 12 are apparent in Fig. 1. Moreover, the η -profiles of defect at all far-wake stations were similar in shape and in height to that shown in Fig. 1 for $\Delta x/k = 20$, and thus the maximum defect and the corresponding height of survey were located near $\eta = 0.7$ to 0.8 for stations $\Delta x/k > 20$ at this value of Re_k . The profiles were non-similar in the intermediate region between the near and far wakes, but were approximately equal in vertical dimension to those found either closer to or farther from the element.

The lateral and vertical profiles obtained throughout the region of survey, which extended to $\Delta x/k = 480$, showed that the wake remained compact in both transverse dimensions in comparison with the boundary layer thickness. For the near wake, both the vertical height and the lateral width were apparently established by the size of the element. In the far-wake region, the height remained relative constant, whereas the lateral width increased somewhat, as in Fig. 2, thereby promoting a measure of two-dimensionality.

Fig. 3 presents the x -variation of the peak velocity defect observed along the centerline within the near-wake and intermediate regions. It can be seen that the defect declined exponentially in the region extending to $\Delta x/k = 25$, and that the decay ceased there, marking the end of the near-wake region. Within a short distance behind this station the centerline defect became negative, denoting the forward boundary of the far-wake region.

Indicated on the ordinate of the figure is the value of the Blasius velocity at the top of the element, $U(k)/U_0$. Because the data may be extrapolated forward to this value, approximately, it seems that the magnitude of the near-wake defect scaled with the velocity there. As the free-stream velocity was varied such as to cover the Re_k range 25 to 135, the near-wake peak defect continued to show the same exponential decay rate as that seen in the figure, while the level of defect, taken as the extrapolated intercept upon the ordinate, varied approximately as the $1/2$ -power of the velocity. This also described the variation of $U(k)/U_0$, thereby supporting the assertion that the initial defect scaled with that quantity.

Fig. 4 presents the amplitude of the peak velocity defect which prevailed along the full extent of the region of survey, except that only those near-wake results which fit within the range of display are included. The far-wake results have been divided into those with a negative defect, i.e., with an increase in velocity in the presence of the element, and those with a positive defect. These two classes lay respectively on the centerline, and at symmetrically disposed locations on either side of the wake, as in Fig. 2. The relative constancy of the two curves seen in Fig. 4 beyond $\Delta x/k = 100$ implies that the wake assumed a rather permanent form, and might have persisted into the transition region, had one existed. The magnitude of the centerline defect near the farthest station of survey was of the order of one-half percent of the free-stream velocity, but because the defect lay close to the wall the local stress there must have been altered by a few percent.

Fig. 5 depicts the general configuration of the defect distribution in the far-wake region as viewed in the streamwise direction. The probe was stepped through the two-dimensional array of points of measurement whose locations upon the plane $\Delta x/k = 80$ are denoted by crosses, and the contours were drawn in accordance. The lateral extent of the figure is approximately one boundary layer thickness and the vertical extent is half a layer. It is evident that most of the perturbation occurred relatively close to the wall, a result which prevailed to the aft limit of survey.

Although the contours do not directly yield the cross-flow streamline pattern, they do give some indication of this. In particular, the far-wake centerline defect was everywhere negative, in accordance with the previous figure, and this means that the horseshoe vortex pair transported fluid toward the plate at the centerline and away from the surface at the two locations of positive defect. The associated momentum transport evidently exceeded that due to viscosity, for the latter was inadequate to diminish the strength of the induced flow during its streamwise translation, as seen in Fig. 4. Attempt has not yet been made to integrate the momentum excess and deficit over the plane of this figure in order to determine the fate of the deficit initially present in the near-wake.

3. MULTIPLE-GRIT INTERACTION STUDIES

Tests were made in which a second, non-actuated, "grit" equal in dimensions to those of the retractable one, was placed in axial proximity to the latter. It was found that the presence of the upwind element reduced the additional defect due to the downwind one by only 30 percent when the center-to-center spacing was two diameters, and that this reduction vanished rapidly with increase of separation. The form of the wake was not altered. However, when the

relative positions of the pair were reversed, keeping the separation at two diameters, the near wake of the upwind member was split in two as it flowed past the aft one. The symmetry of the wake was then critically dependent upon the accuracy of the lateral alignment, and it became difficult to judge the magnitude of the defect. However, at 12 heights behind the aft element, the wake was restored to the approximate form and magnitude of the free-element result.

A second type of interaction study was conducted in which the retractable element was centered within a roughness field 2.0 cm wide by 5.0 cm long, the latter dimension amounting to approximately 100 momentum thicknesses. This field consisted of glass beads in the same arrangement as was used for the distributed roughness studies described below. Here, the wake of one element among more than 10^4 was individually distinguishable. The velocity defect for this case is presented in Fig. 6. There, it is seen that the magnitude of the defect was diminished three-fold, approximately, in comparison to the smooth-wall case, and that the symmetry was altered. However, the shape and dimension of the vertical profiles were unchanged, and it may be seen in the figure that the wake was not widened. Hence, it retained its compactness. The reduction of the defect is believed to have been due to a sheltering of the central element by the wakes of other elements preceeding it in location, while the asymmetry may have resulted from a failure to align the axes of the bead array with the flow direction accurately, as indicated by the sensitivity to lateral alignment in the two-element experiment.

Both the double- and multiple-grit results imply that there may exist a degree of validity to the concept of linear superposition of wakes in describing the distributed roughness velocity profile. However, the usefulness of this may be limited by an uncertainty in the magnitude of the sheltering of each constituent element by those ahead of it.

4. DISTRIBUTED ROUGHNESS MEASUREMENTS

Preliminary experiments concerning distributed roughness composed of #80 abrasive applied to the turntable surface revealed the presence of an effect of some importance. There, the profile above a 7.5 cm-length field was surveyed at several stations, and it was found that, in contrast to the single element case, the defect profile extended to the outer edge of the layer. In the latter case, the defect was mostly confined to the inner one-sixth of the layer at similar Re_k , as in Fig. 1. Here, the defect was observed to have a small but measurable value ahead of the field, to increase in magnitude monotonically along the first two-thirds of the length of roughness, and to decline thereafter, reaching one-half the maximum value at the trailing boundary. The defect was relatively uniform along the lateral dimension except near the edges of the field.

A presently-held view which may serve to explain these findings is that the roughness retarded a quantity of fluid adjacent to the wall, and that this, together with the bulk volume of the roughness, displaced the outer portion of the boundary layer outward from the wall, thereby inducing a pressure field. According to this reasoning, the lower fluid velocity observed within the outer layer was not principally the consequence of retardation by viscosity or by pressure, but rather of the outward translation of the slower-moving fluid of the layer as it passed over the roughness. The pressure field may have

accounted for the defect observed upstream of the forward boundary, and for the decline of defect ahead of the aft boundary. Attempt was made to measure the expected pressure field by means of a wall-contact static pressure probe. The data so-obtained sufficed to prove the existence of such a field, but did not define its value well on account of the small magnitude.

In order to determine the flow response to an outward displacement of the boundary layer through a known distance, and to further assess certain aspects of experimental technique, tests were made in which the abrasive usually applied to the turntable was replaced in succession by Mylar sheets of 0.013 and 0.025 cm thickness. Each was 5.0 cm wide by 16.0 cm long. The velocity defect profiles measured at various stations upstream and downstream of the leading edge were found to be similar in shape and linearly proportional in magnitude to the thickness of the step for the two cases. Fig. 7 displays results for the thinner material. As is to be expected, the defect is seen to approach that corresponding to a simple translation of the layer away from the wall. However, it is apparent that the readjustment process is rather slow, requiring hundreds of step-heights.

The results obtained subsequently pertained to the flow over a bead-array roughness field which extended 8.0 cm in both the upstream and downstream directions from the site of measurement, and 2.5 cm laterally on each side. The 8.0 cm-length amounted to approximately 150 momentum thicknesses in the smooth-wall layer. Fig. 8 shows the mean velocity profiles measured over the rough wall and over the smooth one, with the Blasius theory being given for comparison with the latter. It is evident that in the rough-wall case the outer portion of the layer has retained the shape of the Blasius profile but has been translated outward from the wall. A similar result has been found by Reshotko and Leventhal¹³. As mentioned, the displacement is believed to be due to the presence of the retarded fluid near the wall, and to the volumetric contribution of the elements. The latter was estimated from geometrical considerations to be 0.13 times the bead diameter, or approximately $\eta = 0.04$. The observed displacement was $\eta = 0.25$, and thus greatly exceeded the contribution due to the roughness volume.

The figure shows that the vertical gradient of velocity vanished within a region near $\eta = 0.4$, i.e., near the element crests. Based upon a recognition of the momentum transport mechanism afforded by the vortical wakes of upstream elements, a reduction of gradient was expected in this region, but the apparent absence of a gradient was regarded as surprising. Therefore, two supplementary tests were carried out. The first concerned examination of all aspects of the hot-wire calibration and heat-loss, but revealed no evidence of significant error. The second test, with bead-roughness, verified that the profile was reproduced when the axial station of measurement was varied in steps amounting to one-fourth the bead-array spacing, i.e., that local details of the flow about the elements were not predominant. In consequence of such tests, it is believed that the vanishing of the gradient was not an artifact of the experimental methods.

The velocity defect corresponding to the difference between the smooth and rough-wall profiles is presented in Fig. 9. There, the displacement effect of the outer flow is further verified by the conformity between the measured defect and the gradient of the Blasius profile for the region $\eta > 2.0$, approximately. A departure of the measurement from the relevant theoretical

result is more readily apparent in this figure than in the previous one. Here, such a departure is seen to have occurred at locations within the layer below $\eta = 2.0$, which is also the region of the layer within which the single-element far-wake was present for a similar value of Re_k , as in Fig. 5. The exceedingly steep variation of D/U_0 near $\eta = 0.3$, corresponding to the vanishing of U/U_0 seen in Fig. 8, is evidently a manifestation of the efficiency of the momentum transport provided by the upstream-element wakes.

The results show, therefore, that the roughness produced a substantial distortion of the flow. Although the region of the layer below the element crests could not be surveyed because the experimental technique involved a lateral translation of the roughness field, it is certain that forces of significant magnitude in comparison with the wall stress must have been generated by the pressure-drag of the elements and by the shear stress acting upon their surfaces. For the region of the layer extending from the element crests to an intermediate height near $\eta = 2.0$, the velocity profile, and particularly the vertical gradient of velocity, were altered substantially with respect to the Blasius result. As indicated above, this was evidently one consequence of an enhanced vertical momentum transport generated by the wakes of the upstream elements. However, a certain measure of the profile modification observed here may have been due to the finite extent of the roughness field along the streamwise direction. That is, the transient condition experienced by the layer in its passage over the roughness field may have contributed to the profile development, possibly through the mechanism of the induced pressure field. It is believed that the contribution of this spatial transient was weak because no evidence to the contrary was found in the outer portion of the layer. There, the excellent agreement between the measured profile and a displaced Blasius one showed that little retardation or acceleration of the fluid could have occurred along a particular streamline. In that region, therefore, the observed defect may be thought of as more apparent than real, since it was the consequence of an outward displacement of the flow, and not one of an axial force.

5. STABILITY OF DISTORTED PROFILES

The first results available from the experiment consisted of near-wake profiles similar to those of Fig. 1. Although these did not pertain to a two-dimensional flow, they were utilized as test data during the development of a program to be used for finding suitable analytic representations of the measured profiles. The resultant representations were incorporated into the two-dimensional, parallel-flow, linear stability program by L. M. Mack. Stability calculations showed these profiles to be more stable than the Blasius one, a result not initially expected. This was subsequently attributed to the presence of the inner one of the two inflection points discernable within the profiles of Fig. 1. Because these pertained only to the three-dimensional configuration, the finding was regarded as not significant for present interests.

Unfortunately, distributed roughness flow profiles such as that of Fig. 8 could not be analyzed for stability characteristics because the velocity could not be estimated with confidence in the region extending from the closest point of measurement to the wall. Therefore, a profile measured at a station aft of the #80 abrasive field described earlier was utilized for such purpose. The defect profile and an analytic function which represents the data well are

given in Fig. 10. This profile possessed but one inflection point, and this was of such type as to destabilize the flow. Mack found that, for the most unstable frequency of the Blasius layer at the appropriate Reynolds number, the amplification rate was 6.24×10^{-3} . In contrast, waves of the same frequency in the profile behind roughness showed an amplification rate 16.55×10^{-3} . This increase represents a drastic destabilization of the layer, but it is to be noted that this effect extended over a limited streamwise region because of an eventual return of the profile to the Blasius form. Nevertheless, even small roughness of the type considered here may have an important effect on stability and transition.

6. CONCLUSIONS

a. The wake of a single 3-D element at values of Re_k between 25 and 135 was classified into near-wake and far-wake regions. The velocity defect within the near wake scaled with the velocity at the element crest, and the spatial dimensions apparently scaled with the element size.

b. The far-wake of the single element remained compact in comparison with the boundary layer thickness and lay close to the plate surface. This wake was persistent along the streamwise coordinate.

c. A characteristic feature of the far wake was the occurrence of a negative velocity defect at the lateral centerline. This excess velocity was induced by the trailing vortex system of the element. This system, by its form and by its persistence, probably constituted in general an important mechanism for the transport of momentum in the direction normal to the plate in the case of distributed roughness.

d. The interaction between two elements in proximity was weak; sheltering was not large for separation distances exceeding two diameters, approximately. The wake of one element surrounded by a multitude of others was readily distinguishable, and remained compact in both cross-flow dimensions.

e. The most readily apparent effect of distributed roughness upon the boundary layer flow was an upward displacement of a major portion of the Blasius profile without alteration of form. The magnitude of the displacement substantially exceeded the volumetric average thickness of the roughness itself. The displacement was therefore caused by flow retardation within the roughness field.

f. The profile form within the region of the layer extending from the element crests to $\eta = 1.5$ showed evidence of a momentum transport mechanism of high efficiency. The vortical wakes of the upstream elements are believed to have provided the transport.

g. The profile measured above distributed roughness was inadequate to permit estimation of the velocity in the region of the layer below the element crests, rendering inappropriate an analysis of the stability characteristics of the layer. Instead, a profile measured downstream of a distributed roughness field was analyzed and shown to be highly unstable to Tollmein-Schlichting waves.

h. The value of Re_k for this latter case was only ten. Thus, even small-scale roughness might affect transition if it had similar characteristics, in terms of spatial density and steepness of slope, to that tested here.

REFERENCES

1. M. V. Morkovin, "Instability, Transition to Turbulence and Predictability", AGARD-AG-236, May 1977.
2. R. Sedney, "A Survey of the Effects of Small Protuberances on Boundary-Layer Flows", AIAA Journal, Vol. 11, pp. 782-792, 1973.
3. P. S. Klebanoff and K. D. Tidstrom, "Mechanism by Which a Two-Dimensional Roughness Element Induces Boundary-Layer Transition", Physics of Fluids, Vol. 15, July 1972, pp. 1173-1188.
4. N. Gregory and W. S. Walker, "The Effect on Transition of Isolated Surface Excrescences in the Boundary Layer", Aeronautical Res. Council, England, R. & M. 2779, 1955.
5. I. Tani, H. Komoda, Y. Komatsu, and M. Iuchi, "Boundary-Layer Transition by Isolated Roughness", Report No. 375, Aeronautical Research Institute of Tokyo, Nov. 1962.
6. M. Mochizuki, "Smoke Observation on Boundary Layer Transition Caused by a Spherical Roughness Element", Journal of the Physical Society of Japan, Vol. 16, pp. 995-1008, May 1961.
7. M. Mochizuki, "Hot-Wire Investigations of Smoke Patterns Caused by a Spherical Roughness Element", Natural Science Report, Ochanomizu University, Tokyo, Japan, 1961.
8. A. K. Gupta, "Some Observations in the Wake of a Small Vertical Cylinder Attached to a Flat Plate", Phys. Fluids, Vol. 23, Part 1, pp. 221-223, Jan. 1980.
9. A. Von Doenhoff and E. A. Horton, "A Low-Speed Experimental Investigation of the Effect of a Sand-Paper Type of Roughness on Boundary-Layer Transition", NACA Tech. Note No. 3858, 1956.
10. E. G. Feindt, "Untersuchungen uber die Abhangigkeit des Umschlages Laminar-Turbulent von der Oberflächenrauigkeit und der Druckverteilung", Jahrbuch 1956 der Schiffbautechnischen Gesellschaft, Vol. 50, pp. 180-203, 1957.
11. E. Achenbach, "Influence of Surface Roughness on the Cross-Flow around a Circular Cylinder", J. Fl. Mech. Vol. 46, Part 2, pp. 321-335, 1971.
12. C. L. Merkle, K. T. S. Tzou, and T. Kubota, "An Analytical Study of the Effect of Surface Roughness on Boundary-Layer Stability", Dynamics Technology, Inc., Torrance, CA., Report DT-7606-4, 1977.

13. E. Reshotko and L. Leventhal, "Preliminary Experimental Study of Disturbances in a Laminar Boundary Layer Due to Distributed Surface Roughness," AIAA Paper 81-1224, Palo Alto, CA, June 1981.
14. C. L. Merkle, T. Kubota, and D. R. S. Ko, "An Analytical Study of the Effects of Surface Roughness on Boundary-Layer Transition", AFOSR TR 75-0190, Oct. 1974.
15. K. Singh and J. L. Lumley, "Effects of Roughness on the Velocity Profile of a Laminar Boundary Layer", Appl. Sci. Res., 24, p. 168-186, 1977.
16. G. H. Hoffman and J. L. Lumley, "The Laminar Velocity Profile in a Flat Plate Boundary Layer with Surface Roughness", TM 77-150, Pennsylvania State University, Applied Research Lab, 1977.
17. F. T. Smith, R. I. Sykes, and P. W. M. Brighton, "Two-Dimensional Boundary Layer Encountering a Three-Dimensional Hump", J. Fluid Mech., Vol. 83, part 1, pp. 163-176, 1977.

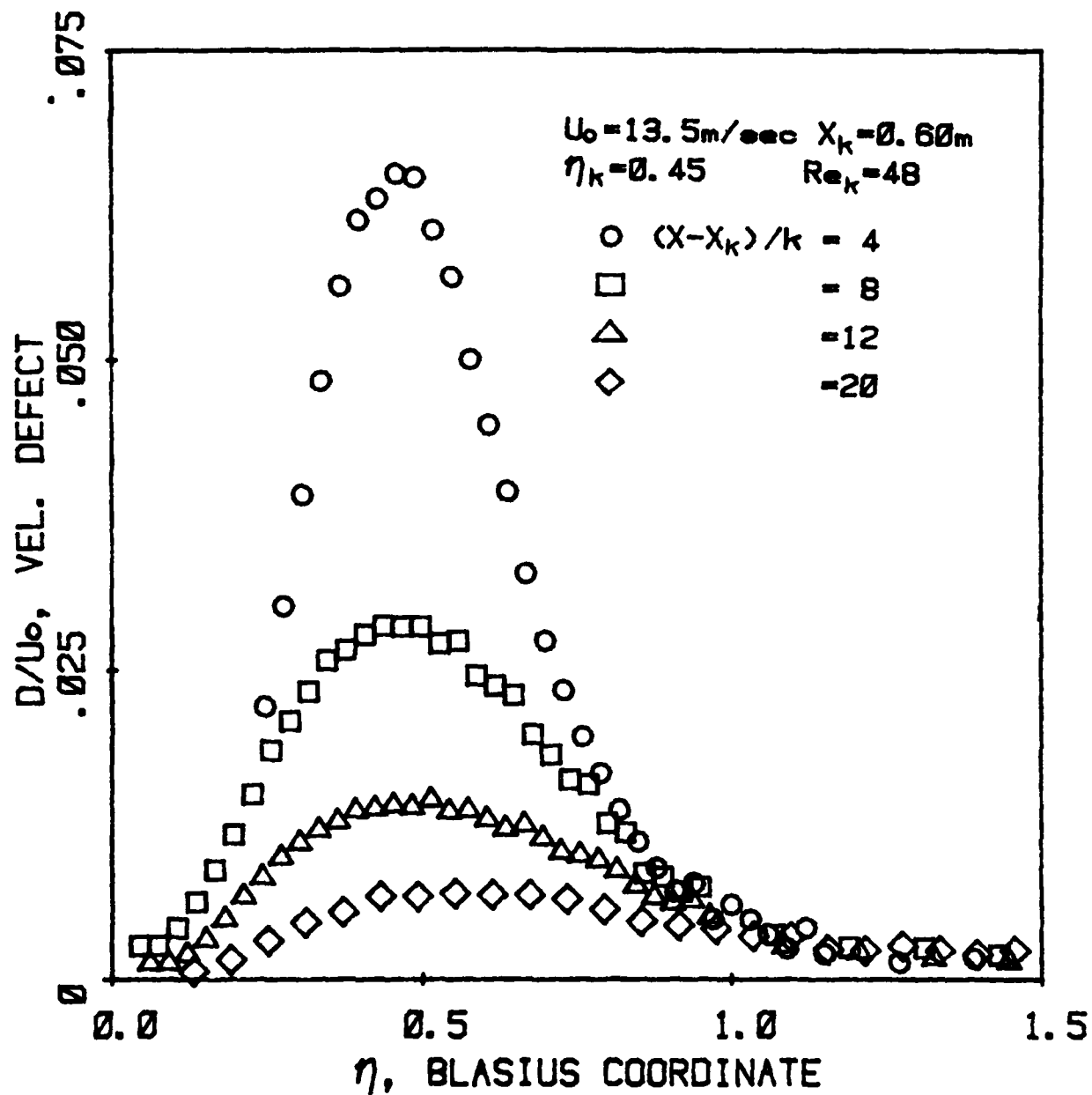


Figure 1. Vertical Profiles of Velocity Defect at Lateral Centerline Behind a Single Roughness Element

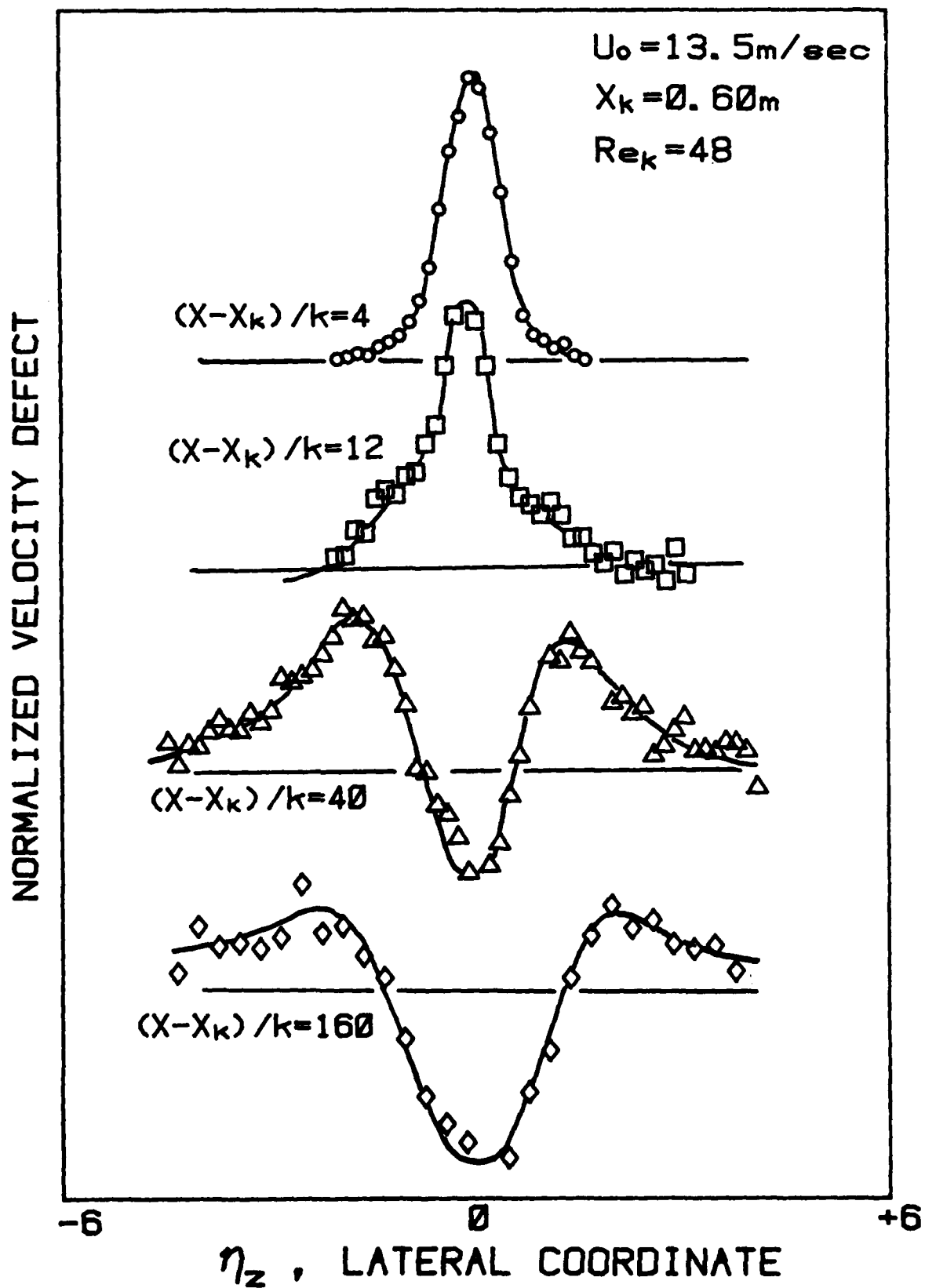


Figure 2. Lateral Variation of Velocity Defect at Four Stations Behind a Single Roughness Element. Measurements Made at Height of Peak Defect. Baselines Are Zero Defect

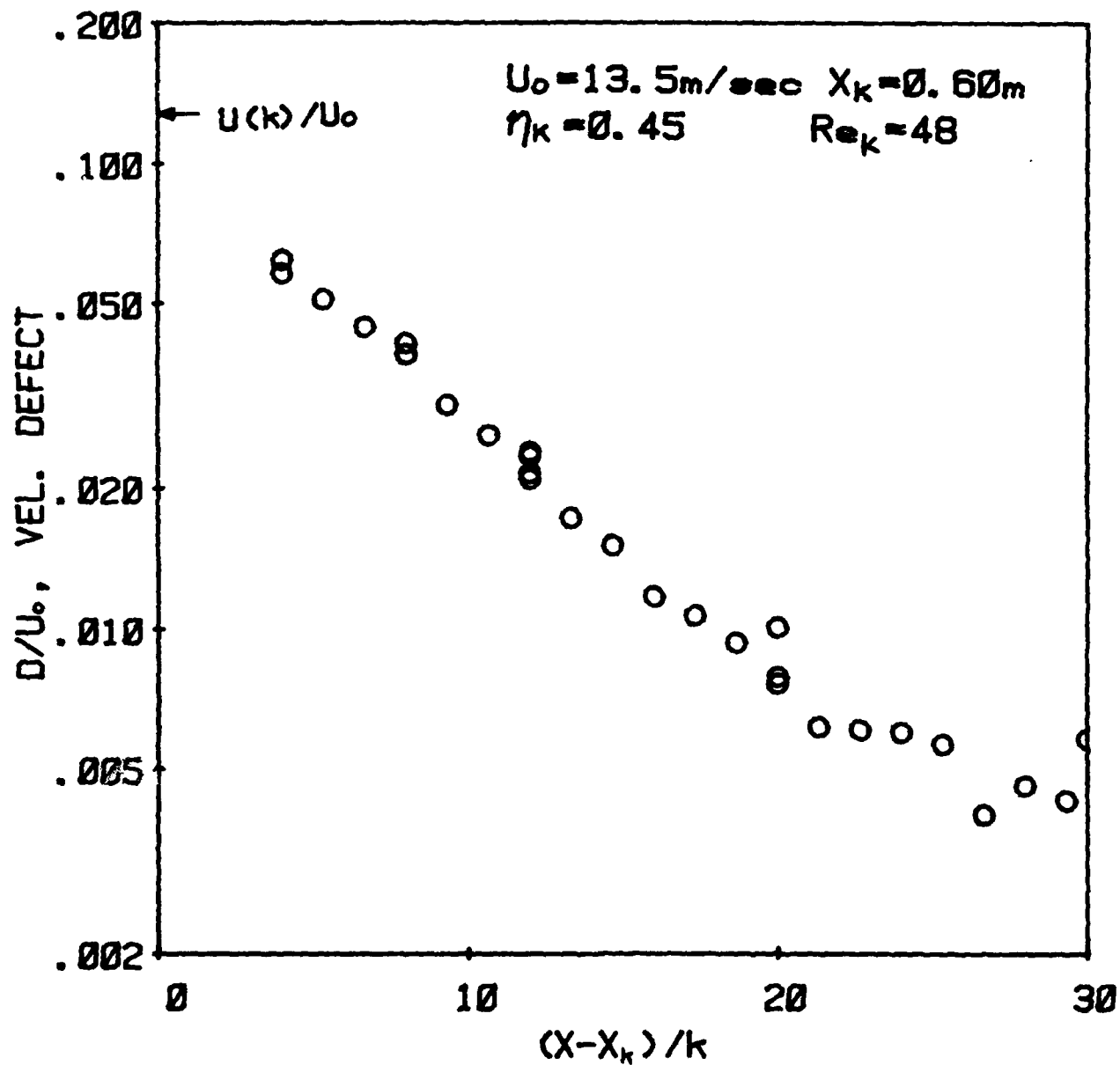


Figure 3. Streamwise Variation of Peak Velocity Defect in Near-Wake Behind a Single Roughness Element. Measurements Made at Lateral Centerline. Blasius Velocity at $y = k$ is Indicated by Arrow

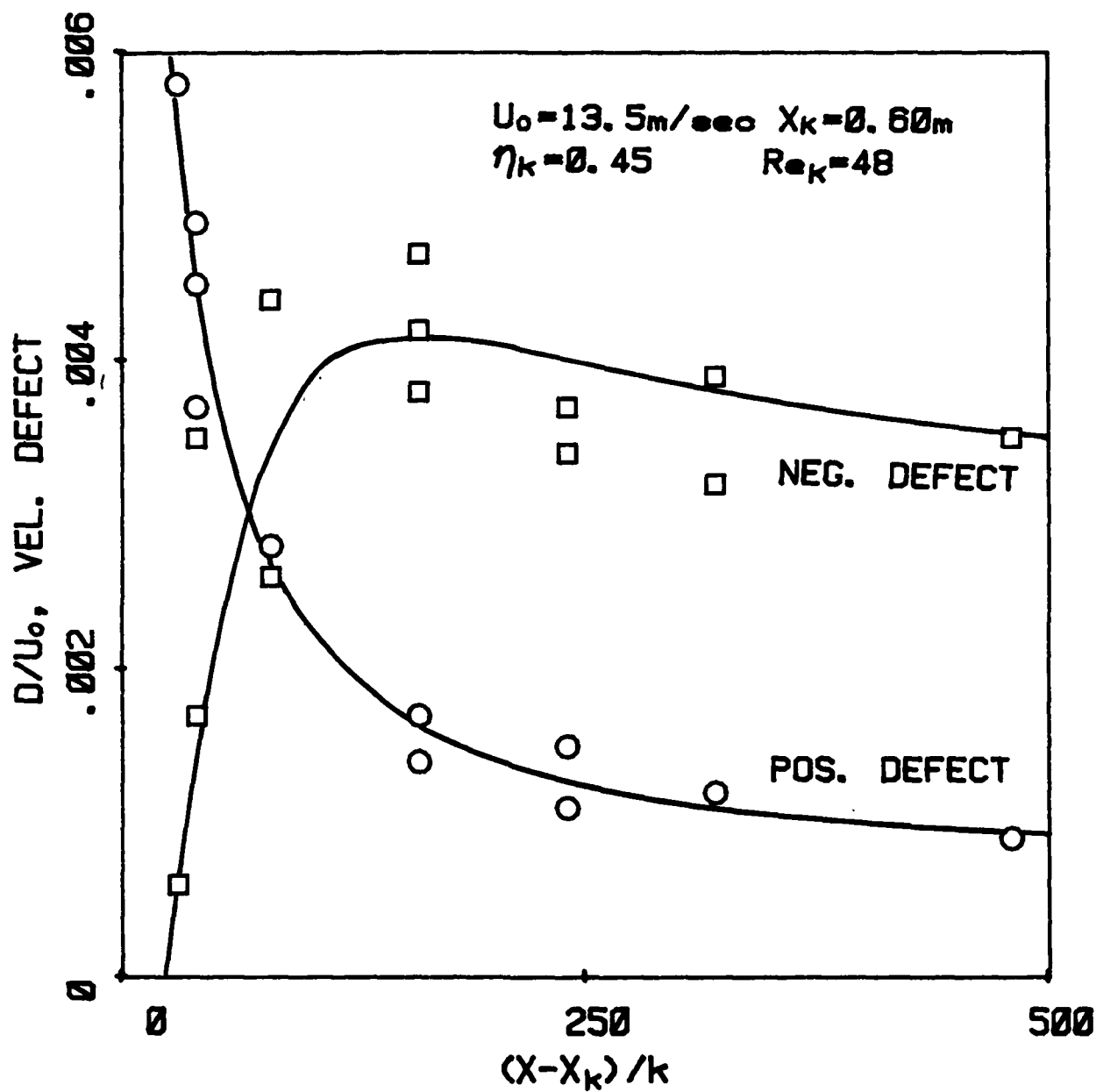


Figure 4. Streamwise Variation of Peak Velocity Defect Magnitude in Far-Wake Behind a Single Roughness Element. Negative Defect Occurred on Lateral Centerline; Positive Defects Appeared on Each Side of Centerline for $x/k > 50$

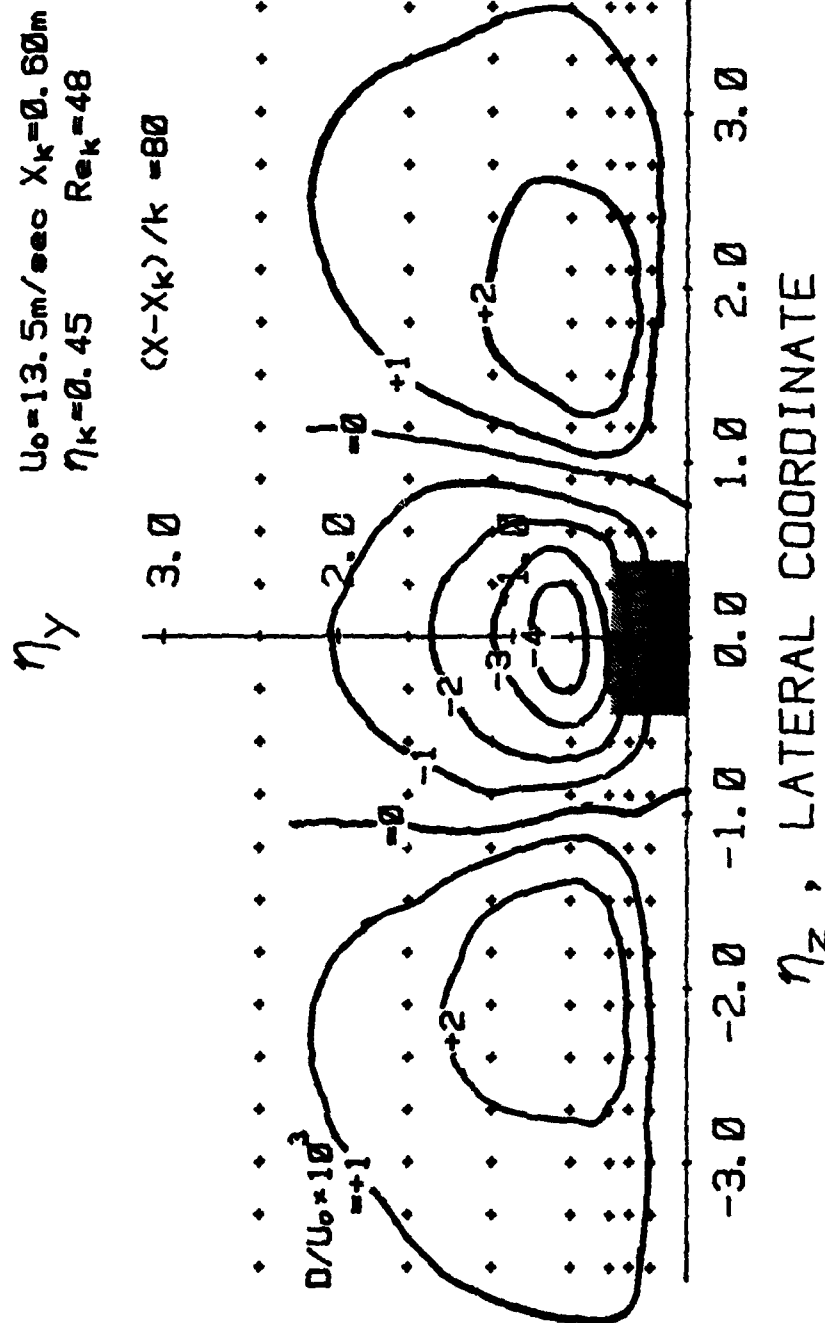


Figure 5. Iso-Defect Contours at a Station 80 Roughness-Heights Behind a Single Element. Positions of Measurement Denoted by Small + Symbols. Element Shown to Scale in Gray

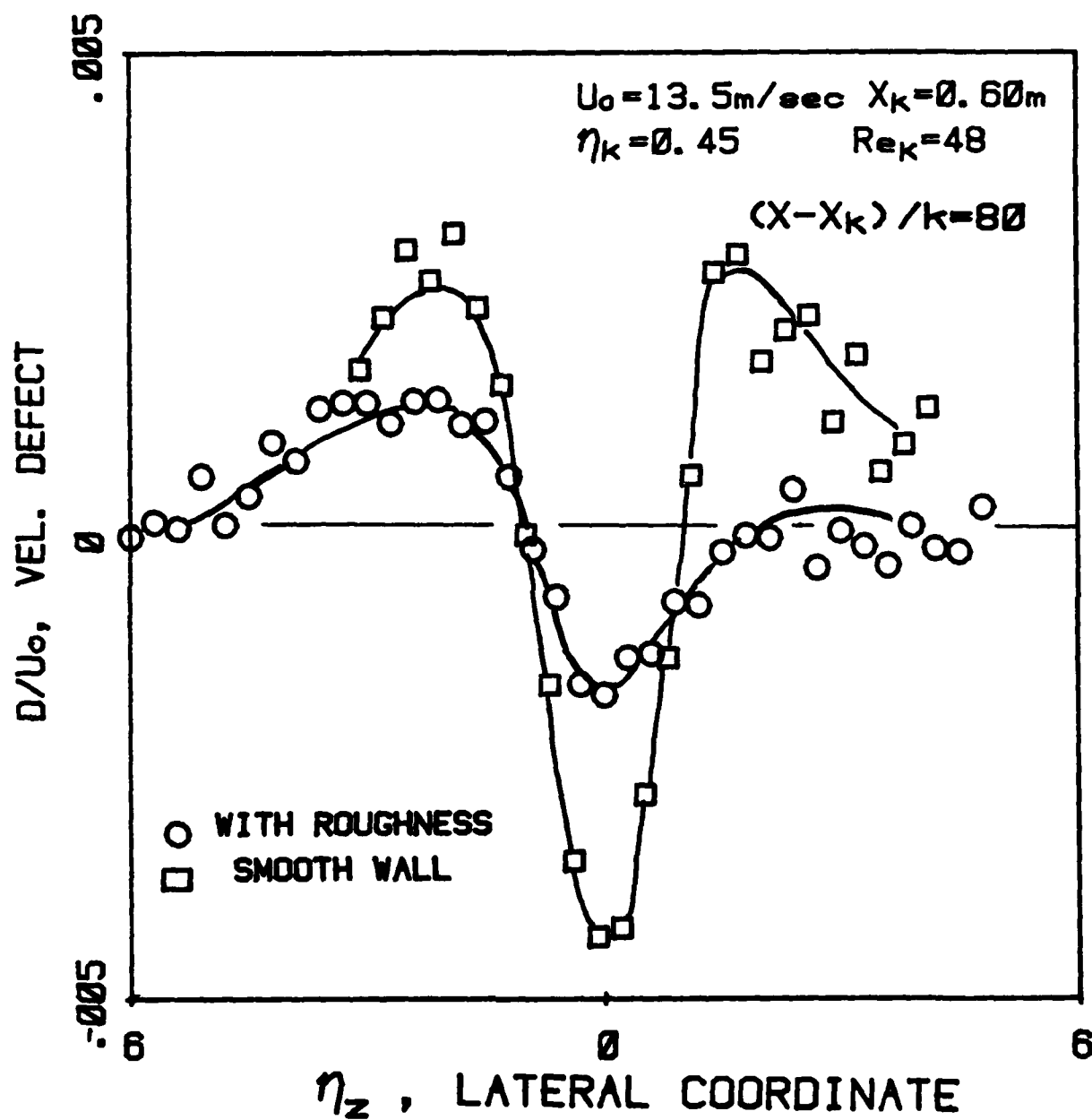


Figure 6. Lateral Variation of Velocity Defect Due to a Single Roughness Element Amid a Field of Other Elements (Circles), and Same Results in Absence of Field (Squares)

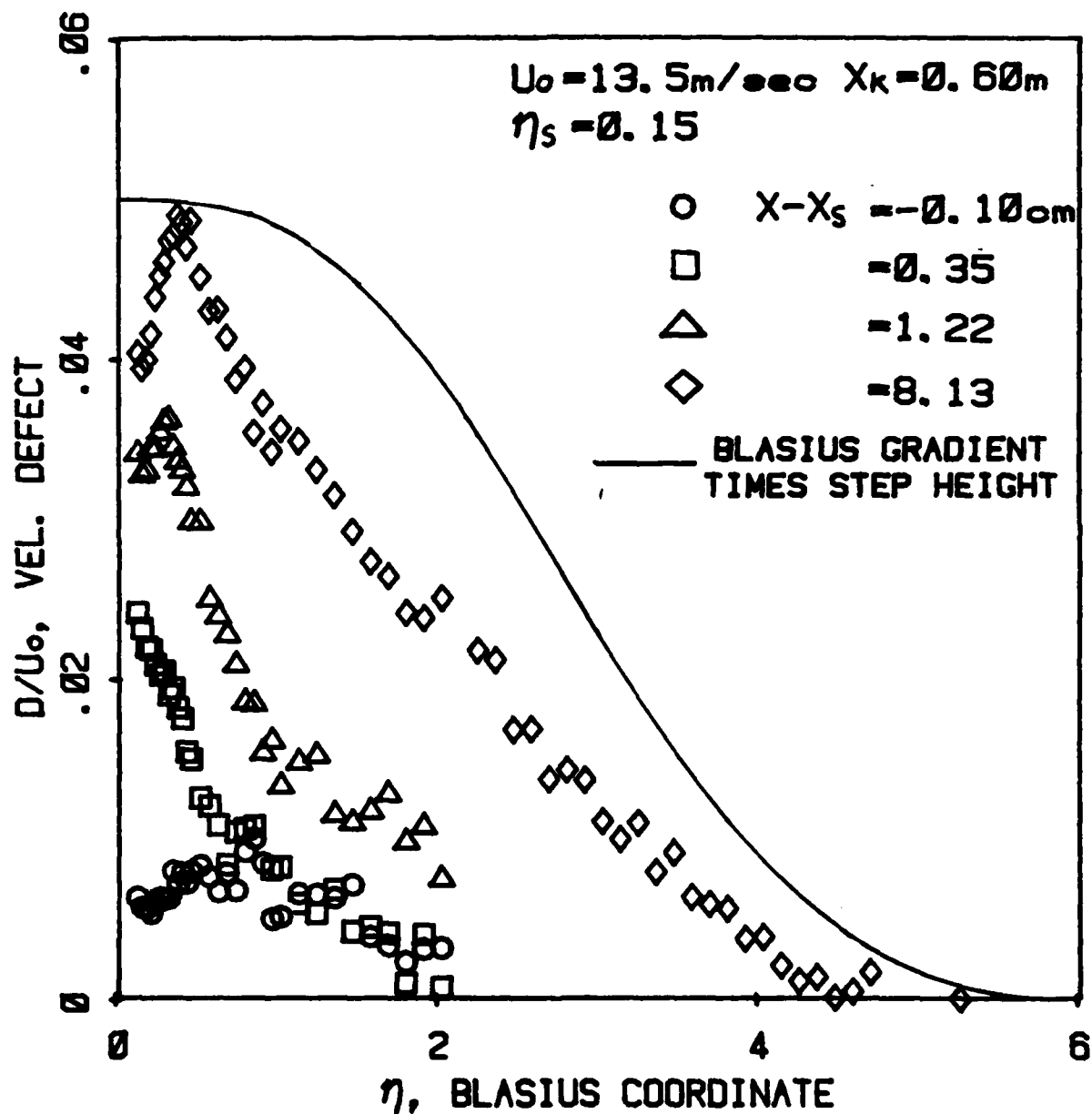


Figure 7. Velocity Defect Induced by Flow Over a Forward-Facing Step of Small Height Located at $x = x_s$

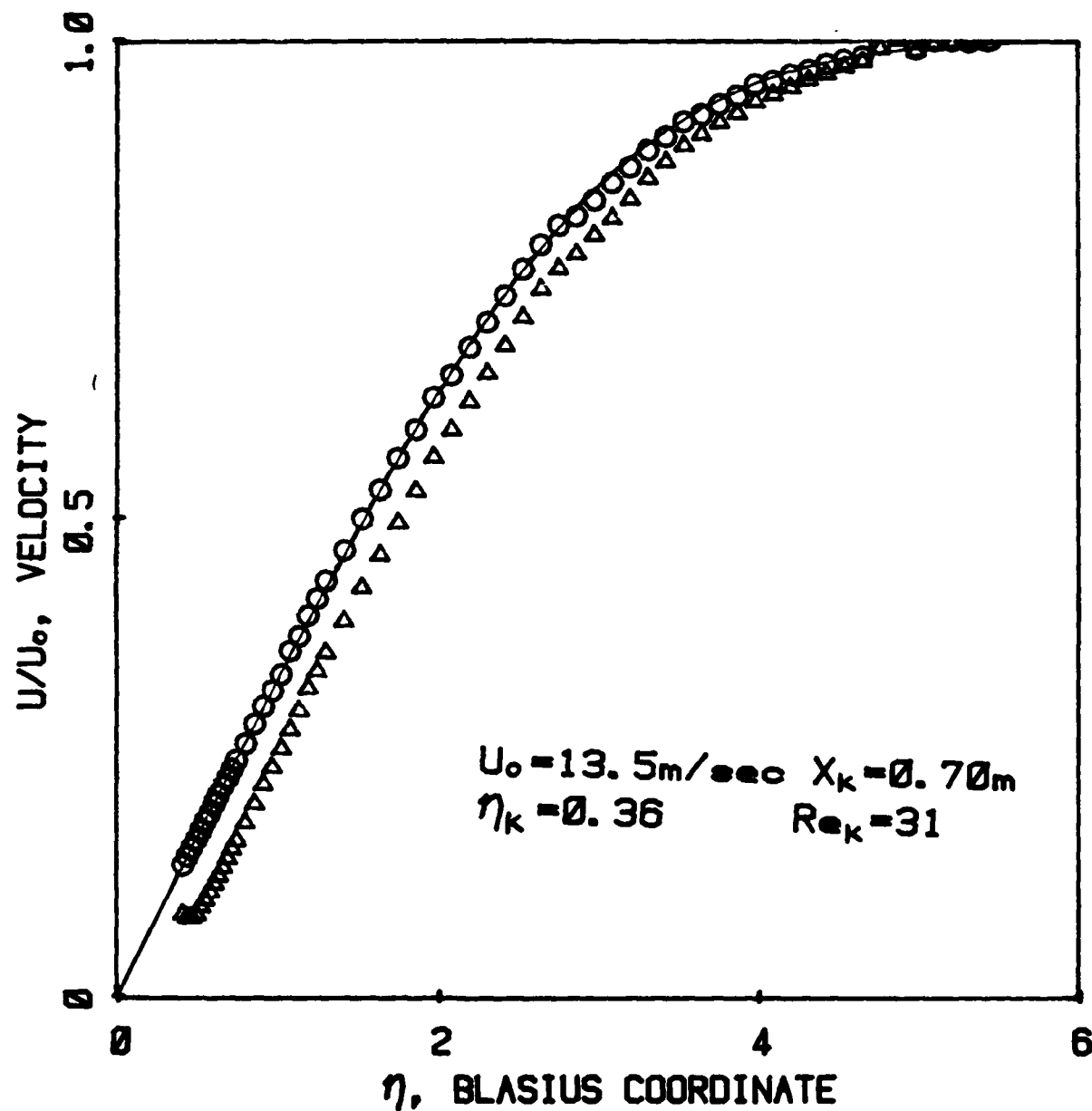


Figure 8. Velocity Profiles Above Distributed Roughness (Triangles) and Above Smooth Surface (Circles) at Same Station. Blasius Profile is Shown

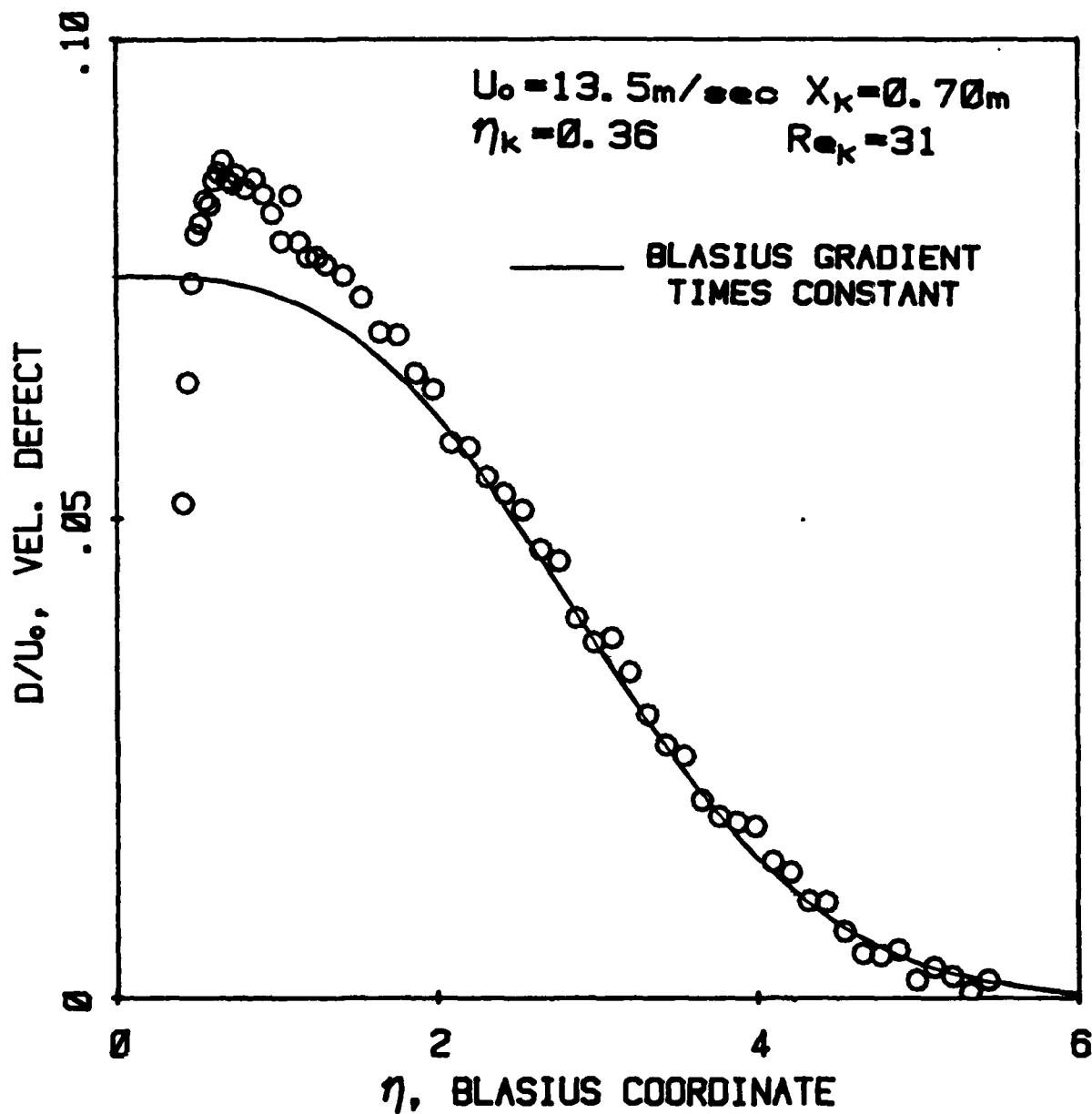


Figure 9. Velocity Defect Due to Distributed Roughness Corresponding to Data of Fig. 8. Curve Has Been Fitted to Data in Region $n > 1.5$

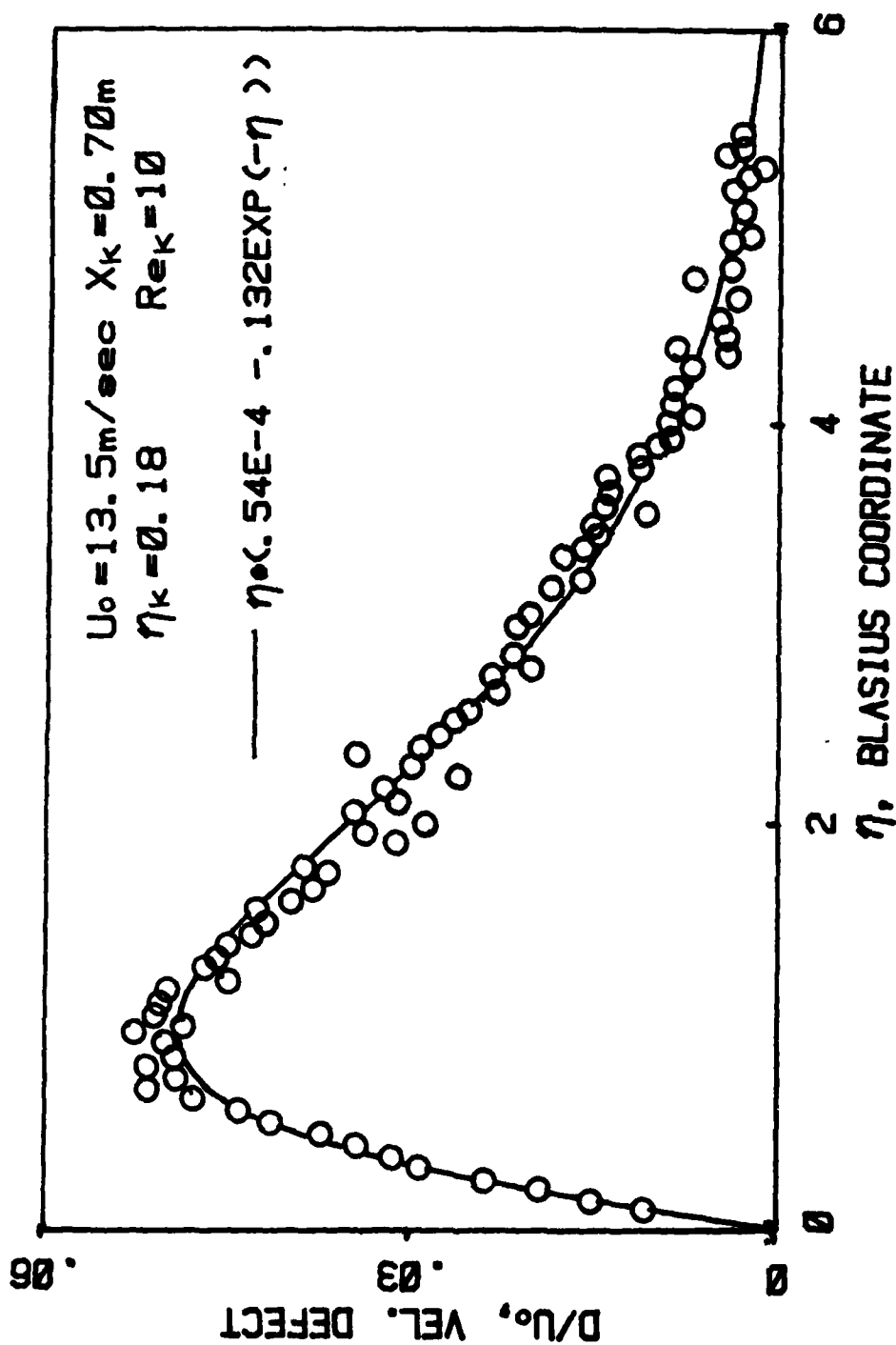


Figure 10. Velocity Defect Downstream of Distributed Roughness (#80 Abrasive) and an Analytic Representation Intended for Use in Stability Analysis

**DA
FILM**